

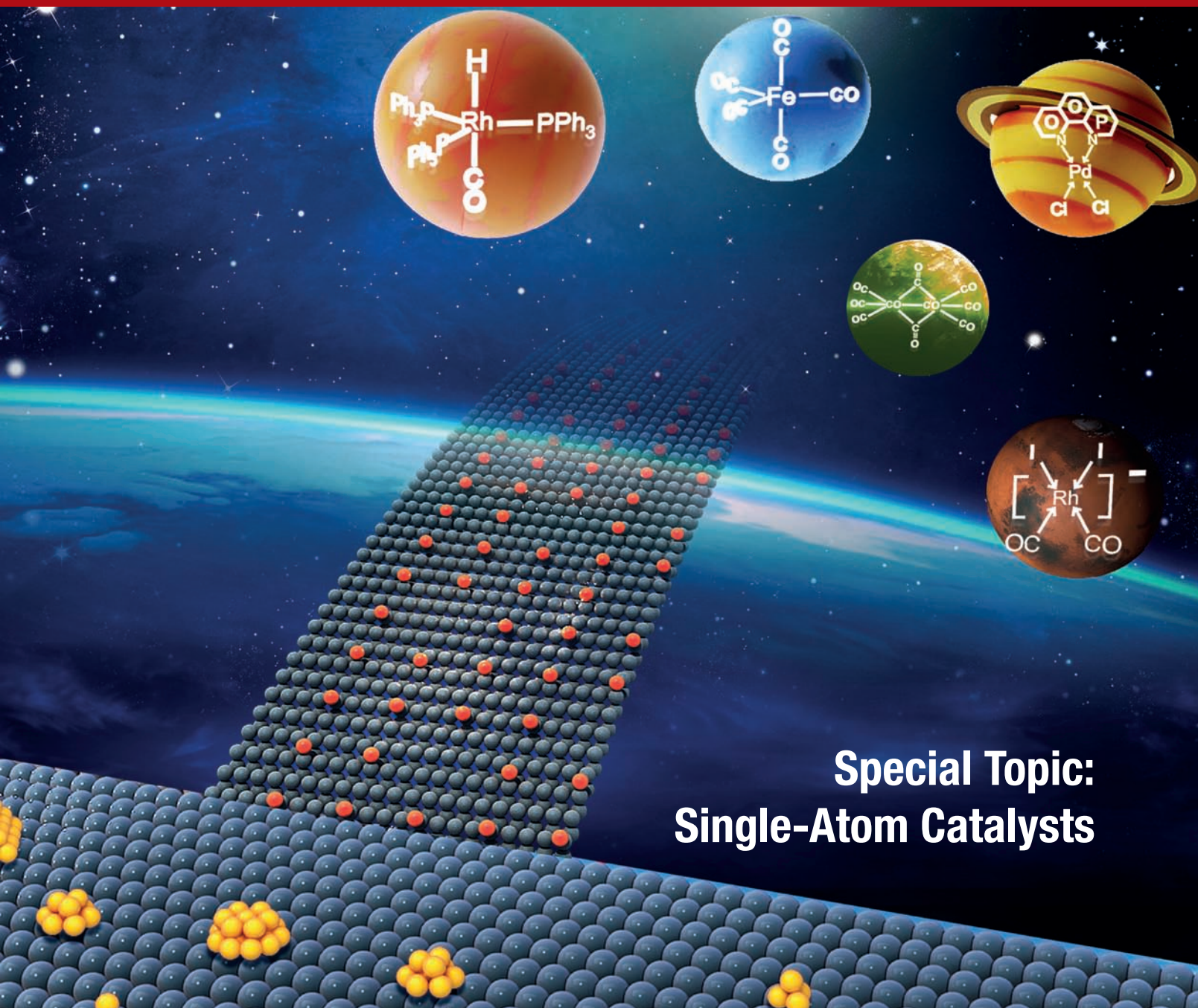
# NCSR

国家科学评论  
National  
Science  
Review



PRINT ISSN 2095-5138  
ONLINE ISSN 2053-714X  
CN 10-1088/N  
academic.oup.com/nsr

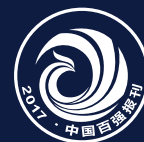
VOLUME 5 • ISSUE 5 • SEPTEMBER 2018



Special Topic:  
Single-Atom Catalysts

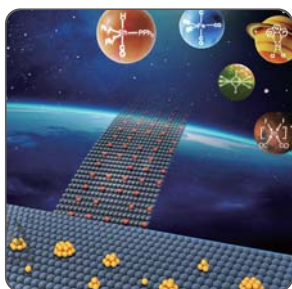
Science Press | OXFORD  
UNIVERSITY PRESS

Project for Enhancing International  
Impact of China STM Journals



# Special Topic: Single-Atom Catalysts

## GUEST EDITORIAL



*Guest Editors: Nanfeng Zheng and Tao Zhang*

Preface: single-atom catalysts as a new generation of heterogeneous catalysts

625

## RESEARCH HIGHLIGHT



*Yao Zheng and Shi-Zhang Qiao (pictured)*

Metal-organic framework assisted synthesis of single-atom catalysts for energy applications

626

## PERSPECTIVES



*Lei Zhang, Mohammad Norouzi Banis and Xueliang Sun (pictured)*

Single-atom catalysts by the atomic layer deposition technique

628



*Abhaya Datye (pictured) and Yong Wang*

Atom trapping: a novel approach to generate thermally stable and regenerable single-atom catalysts

630

## PERSPECTIVES



*Jean-Marie Basset (pictured) and Jérémie D.A. Pelletier*

Predictive approach of heterogeneous catalysis

633



*Pengxin Liu and Nanfeng Zheng (pictured)*

Coordination chemistry of atomically dispersed catalysts

636



*Jin-Cheng Liu, Yan Tang, Yang-Gang Wang, Tao Zhang and Jun Li (pictured)*

Theoretical understanding of the stability of single-atom catalysts

638

## RESEARCH ARTICLE

---



Zupeng Chen, Evgeniya Vorobyeva, Sharon Mitchell (left), Edvin Fako, Núria López, Sean M. Collins, Rowan K. Leary, Paul A. Midgley, Roland Hauert and Javier Pérez-Ramírez (right)

Single-atom heterogeneous catalysts based on distinct carbon nitride scaffolds

642

---

## REVIEW

---



Leilei Zhang, Yujing Ren, Wengang Liu, Aiqin Wang (left) and Tao Zhang (right)

Single-atom catalyst: a rising star for green synthesis of fine chemicals

653

---

## REVIEW

---



Zhijun Li, Dehua Wang, Yuen Wu (left) and Yadong Li (right)

Recent advances in the precise control of isolated single-site catalysts by chemical methods

673

---

## INTERVIEW

---



Jean-Marie Basset  
(Reporter: Philip Ball)

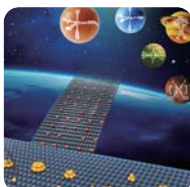
Single-atom catalysis: a new field that learns from tradition

690

---

## COVER IMAGE

---




Single-atom catalysts (SACs) with well-defined mononuclear active sites on a solid support are expected to bridge homogeneous and heterogeneous catalysis. See the section of Special Topic (pages 625–693).

Image credit: Leilei Zhang, Yujing Ren, Aiqin Wang and Xiaoling Yu.

Special Topic: Single-Atom Catalysts

## Preface: single-atom catalysts as a new generation of heterogeneous catalysts

Nanfeng Zheng <sup>1,\*,\dagger</sup> and Tao Zhang<sup>2,\*,\dagger</sup>

Heterogeneous catalysis plays a leading role in the chemical industry. Creating heterogeneous catalysts with minimal use of metals but well-defined catalytic sites is highly desired for developing cost-effective and green chemical processes. With single metal atoms dispersed on supports, single-atom catalysts are featured in their optimized usage of metal and also the similar chemical environments of metal sites. It has been long believed that the single-atom catalysts should not be stable enough to be prepared via conventional catalyst-preparation techniques. However, in 2011, Tao Zhang's group in Dalian Institute of Chemical Physics, cooperating with Jun Li from Tsinghua University and Jingyue Liu from Arizona State University, successfully demonstrated the feasibility to fabricate stable and efficient single-atom Pt catalysts using a simple co-precipitation method. The research also presented a systematic methodology to investigate single-atom catalysts using advanced characterization techniques. During the past several years, the work has greatly stimulated the rapid development of the field. There are now numerous studies demonstrating that single-atom catalysts serve as an excellent catalyst system to bridge homogeneous catalysts with well-defined molecular structures and heterogeneous catalysts with structural complexity. With more and more contributions to this rapidly growing field, single-atom catalysts have been emerging as next-generation heterogeneous catalysts for various applications.

This special topic aims at highlighting the latest research advances in the field of single-atom catalysts. The research highlight by Shi-Zhang Qiao *et al.* focuses on how to use metal-organic framework materials to assist the synthesis of single-atom catalysts for energy applications, which has been recently studied extensively by many research groups in China. The review article by Tao Zhang and Aiqin Wang *et al.* summarizes the developments of single-atom catalysts for green synthesis of fine chemicals. Yadong Li and Yuen Wu *et al.* reviewed the recent advances in the precise control of single-atom catalysts by chemical methods. The perspective articles in this special topic cover several issues of single-atom catalysts ranging from preparation techniques, catalytic mechanisms and also theoretical understanding. Xueliang Sun *et al.* discuss the development of the

atomic layer deposition technique as an effective method to prepare single-atom catalysts for various applications. In the perspective article by Abhaya Datye *et al.*, atom trapping is demonstrated as a viable method for the synthesis of oxide-supported single atoms of platinum-group metals. Jean-Marie Basset *et al.* discuss the research advances to design single-atom catalysts based on surface organometallic chemistry. From the viewpoint of coordination chemistry, Nanfeng Zheng *et al.* discuss in their perspective article different roles of supports in single-atom catalysts. The stability of single-atom catalysts is a critical issue for their industrial applications. The perspective article by Jun Li *et al.* focuses on the theoretical understanding of the stability issue of single-atom catalysts. This special topic also offers a research article contributed by Javier Pérez-Ramírez and Sharon Mitchell *et al.* which demonstrates that palladium atoms can be effectively isolated on carbon nitride scaffolds beyond graphitic heptazine-based polymers for creating stable and efficient single-atom Pd catalysts for selective hydrogenation. An interview with Jean-Marie Basset is also included in this special topic to share his personal views on the development and prospects of the field of single-atom catalysts.

As guest editors, we would like to express our sincere appreciation to all the authors, reviewers and also the editorial office of NSR for their efforts to make this special topic possible. We hope that this special topic will gain broad attention from chemistry, physics, materials science and other related fields.

Nanfeng Zheng<sup>1,\*,\dagger</sup> and Tao Zhang<sup>2,\*,\dagger</sup>

<sup>1</sup>State Key Laboratory for Physical Chemistry of Solid Surfaces, Collaborative Innovation Center of Chemistry for Energy Materials, and Department of Chemistry, College of Chemistry and Chemical Engineering, Xiamen University, China

<sup>2</sup>State Key Laboratory of Catalysis, iChEM (Collaborative Innovation, Center of Chemistry for Energy Materials), Dalian Institute of Chemical Physics, Chinese Academy of Sciences, China

\*Corresponding authors.

E-mails: nfzheng@xmu.edu.cn; taozhang@dicp.ac.cn

<sup>\dagger</sup>Guest Editor of Special Topic

## CHEMISTRY

Special Topic: Single-Atom Catalysts

**Metal-organic framework assisted synthesis of single-atom catalysts for energy applications**Yao Zheng<sup>1</sup> and Shi-Zhang Qiao<sup>1,2,\*</sup>

Metal single-atom catalysts (M-SACs) are emerging as a new research frontier because of their low-coordination metal atoms and uniform structures. As a representation of maximum atom utilization efficiency, M-SACs demonstrate unique properties in a wide variety of heterogeneous catalysis and electrocatalytic processes [1,2]. Metal-organic frameworks (MOFs) are composed of metal-containing nodes and organic linkers, and are typically characterized as atomically dispersed metal sites. With the versatility of metal ions and ligands, the direct pyrolysis of MOFs serves as an ideal route for preparing various M-SACs. However, this seemingly simple strategy is still highly challenging due to the drastic reactive processes that occur at high temperature that rapidly convert metal ions into aggregated nanoparticles. Very recently, Yadong Li *et al.* developed a general synthetic strategy for M-SAC preparation by utilizing particular zeolitic imidazolate frameworks (ZIFs)—a kind of MOF that are topologically isomorphic with zeolites [3–5]. The resultant M-SACs (M = Fe, Co, Ni) demonstrated excellent activities for energy-related electrocatalytic reactions.

The most important principle of this methodology is the utilization of low-boiling-point atoms, such as Zn (mp 420°C, bp 907°C), in ZIF-8 and Zn/Co bimetallic ZIF-67, which evaporated at high temperature, leaving abundant N-rich defects. As a result, the isolated metal ions were closely anchored through N-coordination, avoiding their

aggregation during pyrolysis. For the synthesis of Fe and Ni single atoms in an N-carbon matrix (Fe-SAs/CN and Ni-SAs/CN), Fe(acac)<sub>3</sub> and Ni(NO<sub>3</sub>)<sub>2</sub> were selected as metal sources, respectively, and were confined in the molecular-cages of ZIF-8 (Fig. 1) [3,4]. Co-SAs/CN was synthesized from a partially Zn-replaced ZIF-67 with a Zn/Co = 1:1 (Zn/Co-ZIF-67) precursor (Fig. 1) [5]. After pyrolysis at 900–1000°C in an Ar atmosphere, the metal ions were thermally reduced and atomically dis-

persed in the N-carbon matrix. This was directly observed by high-angle annular dark-field scanning transmission electron microscopy. The precise molecular structures of these isolated metal atoms were well identified by extended X-ray absorption fine structure and X-ray absorption near-edge structure. As shown in Fig. 1, the ZIF-8-derived Fe-SAs/CN and Ni-SAs/CN, and Zn/Co-ZIF-67-derived Co-SAs/CN, show a 4, 3 and 2 metal coordination number with surrounding N atoms, respectively.

With precise N-coordination and high metal loadings of 1.5–4 wt. %, all M-SACs showed superior electrocatalytic activities. For example, Fe-SAs/CN demonstrated a half-wave potential of 0.9 V for the oxygen-reduction reaction in alkaline electrolyte—a key cathodic step for proton exchange membrane fuel cells, even outperforming commercial Pt/C and most non-precious-metal catalysts [3]. Ni-SAs/CN exhibited an excellent turnover frequency for the electroreduction of CO<sub>2</sub> (5273 h<sup>-1</sup>), with a Faradaic efficiency for CO generation of 71.9% [4].

In summary, Yadong Li *et al.* developed a general and well-designed method for the simple preparation of M-SACs with the assistance of ZIFs. Due to the wide variety of metal atoms in versatile MOFs, this accurately controlled methodology may present some guidelines for the rational design and modulation of M-SACs for broader applications.

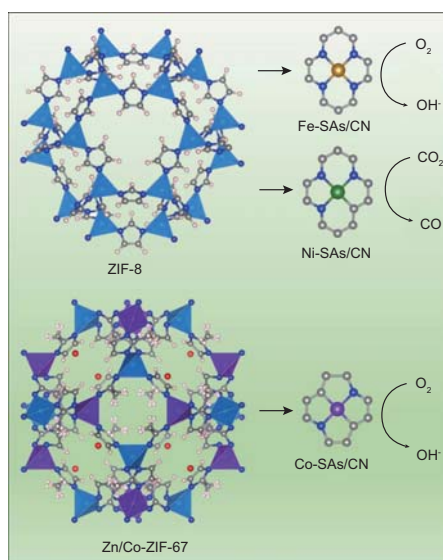


**Figure 1.** Schematic illustration of the precursor and structures of Fe, Ni and Co single atoms supported in N-carbon matrices. Color code: grey: carbon; royal blue: nitrogen; white: hydrogen; red: oxygen; light blue: zinc; brown: iron; green: nickel; purple: cobalt.

Yao Zheng<sup>1</sup> and Shi-Zhang Qiao<sup>1,2,\*</sup>

<sup>1</sup>School of Chemical Engineering, The University of Adelaide, Australia

<sup>2</sup>School of Materials Science and Engineering, Tianjin University, China

\*Corresponding author.

E-mail: s.qiao@adelaide.edu.au

## REFERENCES

1. Yang X, Wang A and Qiao B *et al. Acc Chem Res* 2013; **46**: 1740–8.
2. Liu P, Zhao Y and Qin R *et al. Science* 2016; **352**: 797–800.
3. Chen Y, Ji S and Wang Y *et al. Angew Chem Int Ed* 2017; **56**: 6937–41.
4. Zhao C, Dai X and Yao T *et al. J Am Chem Soc* 2017; **139**: 8087–91.
5. Yin P, Yao T and Wu Y *et al. Angew Chem Int Ed* 2016; **55**: 10800–5.

Special Topic: Single-Atom Catalysts

## Single-atom catalysts by the atomic layer deposition technique

Lei Zhang, Mohammad Norouzi Banis and Xueliang Sun\*

Noble metal nanocatalysts have been widely applied in the petrochemical industry, medicine, environmental protection and energy sectors. To decrease the cost and maximize the utilization efficiency, single-atom catalysts (SACs), as a new frontier in heterogeneous catalysis, have attracted considerable attention due to their unique catalytic properties. Unlike traditional nanocatalysts, the catalytic performance of single-atom catalysts is highly dependent on their low-coordination environment, quantum size effects and metal–support interaction. Recently, several methods have been developed for the preparation of single-atom catalysts, including the impregnation method [1], co-precipitation method [2], photo-reduction method [3] and atomic layer deposition (ALD) method [4–6]. Among these, the ALD process is a powerful approach for studying the relationship between the catalysts' structure and their catalytic performances, as it has a great capability to precisely control the deposition of single atoms and nanoclusters. In this perspective, we will briefly discuss the recent progress in the rational design of single-atom catalysts through atomic layer deposition. In addition, we will summarize the key issues for the development of ALD methods and the outlook for future research trends.

Generally, one complete ALD cycle contains two main processes (Fig. 1a) [7]. Taking the deposition of single Pt atoms on graphene as an example, the first step is the reaction of the Pt precursor with the adsorbed oxygen on the surface of the graphene. The second step

is an oxygen pulse to convert the precursor ligands to Pt–O species to form a new adsorbed oxygen layer on the Pt surface (Fig. 1b). During the ALD process, Pt catalysts with atomically precise design and control can be synthesized by adjusting the ALD cycles. In 2013, Sun and co-workers fabricated single Pt atoms on graphene nanosheets by ALD for the first time [3]. The graphene substrate exhibited many carbon vacancies and defects, which were favorable for anchoring Pt precursors. Up to now, single-atom Pt catalysts have also been achieved on nitrogen-doped graphene and CeO<sub>2</sub> supports [4,5]. When single Pt atoms are deposited on CeO<sub>2</sub>, the atoms tend to deposit on the Ce rows of the CeO<sub>2</sub>(110) and (100) facets, instead of the (111) facet [5]. In addition to single Pt atoms, single Pd atom catalysts have also been successfully deposited on graphene by alternately exposing Pd(hfac)<sub>2</sub> and formalin at 150°C [6]. Although several types of single-atom catalysts have been obtained through the ALD method, large-scale production of single-atom catalysts using the ALD process is still challenging, and optimization of the ALD process is required. For example, the use of the spatial atomic layer deposition technique could greatly improve the industrialization process [8].

Atomic-resolution transmission electron microscopy (TEM), scanning tunneling microscopy (STM) and radiation-ray absorption spectroscopy investigations are three typical characterization methods for detecting SACs. We can directly observe the single atoms through atomic-resolution TEM and

STM images while the synchrotron-based X-ray absorption spectrum can provide information on the overall structure of the catalysts. The formation of SACs can be concluded by studying the extended X-ray-absorption fine-structure (EXAFS) spectrum of the corresponding catalysts. Local atomic structure information including coordination number and atomic distances can be derived from the fitted EXAFS spectra in *R* space. The reduction of peak intensity of metal–metal peaks in these spectra can be a good indicator for the formation of SACs. Though we can conclude the formation of single-atomic catalysts through these methods, it remains a great challenge to identify the accurate binding site between the single atoms and the support. As a result, the development of advanced characterization methods is essential for widespread synthesis and application of SACs. In addition, to attain physical insights into the reactions, advanced *in situ/operando* characterization techniques would be necessary. A systematic understanding of the reaction mechanisms will be crucial for discovering the growth behavior of single atoms on different substrates and its practical applications.

The SACs obtained through ALD have extremely high atom-utilization efficiency, which makes them highly active catalysts for several catalytic reactions. The SACs have been proven to be highly efficient catalysts for several electrochemical reactions, including methanol oxidation, the hydrogen evolution reaction and the oxygen reduction reaction (ORR) [3,4,9,10]. Sun and

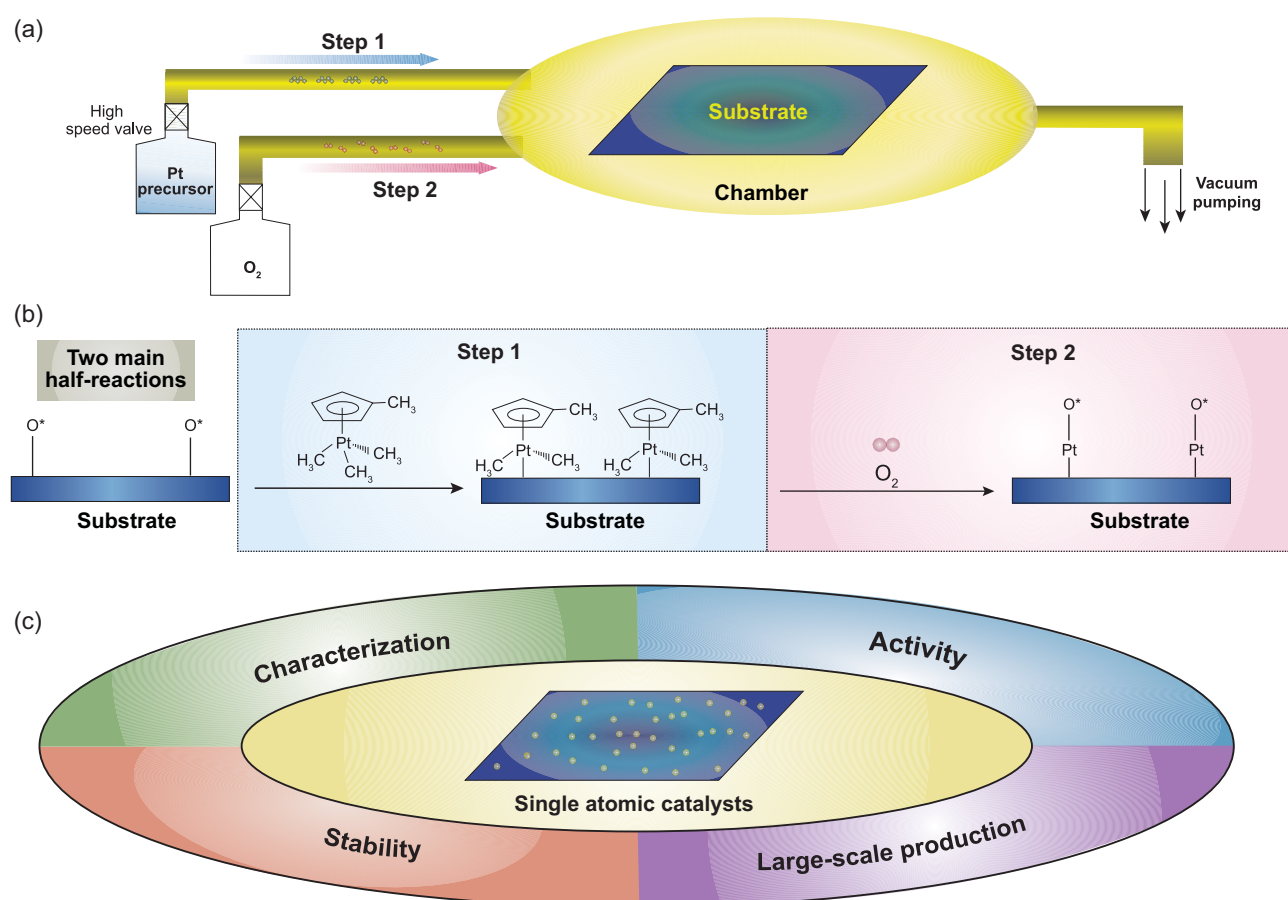


**Figure 1.** (a) Schematic illustrations of the deposition of single-atomic Pt on substrates through the ALD method. (b) The detailed two main half-reactions during a whole ALD cycle. (c) Four key research areas for the development of the ALD technique for single-atom catalysts.

co-workers reported that the single-atom Pt catalysts on graphene showed 10 times higher activity for methanol oxidation and superior CO tolerance compared to conventional Pt/C catalysts [3]. In addition, they found that the mass activity of single-atom Pt catalysts on nitrogen-doped graphene was around 37.4 times greater than that of the Pt/C catalyst [4]. Thanks to the strong bonding energy between Pt and nitrogen-doped graphene, the activity of the catalysts dropped only 4% after 1 000 cycles, indicating a high durability. For the oxygen reduction reaction, two different pathways were demonstrated on single-atom Pt catalysts [9,10]. The support plays a significant role in the selective catalytic reaction route and final product. For instance, single Pt atoms on a sulfur-doped zeolite-templated carbon support could selectively transfer the O<sub>2</sub> to H<sub>2</sub>O<sub>2</sub> through a two-electron pathway [9], while single Pt atoms on nitrogen-doped carbon black exhibited

great performance for highly efficient four-electron ORR [10]. Up till now, the initial active sites for the enhanced mechanism are still unclear. More fundamental studies should focus on the influence of the support on the performance of single-atom catalysts, which might provide a systematic understanding of the interactions between the SAC and substrates. In addition to electrochemical catalytic reactions, the SACs also exhibited superior performance as heterogeneous catalysts in several traditional catalytic reactions. For example, Pt/FeOx and Pt/CeO<sub>2</sub> catalysts exhibited a remarkable activity towards both CO oxidation and preferential oxidation of CO in H<sub>2</sub> [2,5]. The single-atom Pd/graphene catalysts obtained through ALD showed 100% butene selectivity in selective hydrogenation of 1,3-butadiene [6]. The adsorption mode of 1,3-butadiene and the enhanced steric effect induced by single Pd atoms played key roles in improv-

ing the butene selectivity. To further increase the activity, the rational design of SACs with multiple compositions should be explored in the future, because bimetallic catalysts can exhibit improved performance compared to pure metals. The area-selective ALD method provides an effective way to fabricate catalysts with multi-compositions. Elam and co-workers synthesized several types of bimetallic nanoparticles by precisely controlling the ALD conditions [11]. Recently, Pt<sub>2</sub> dimers have been fabricated through selective deposition of a secondary Pt atom onto the preliminary one [12]. Based on the above points, we can infer that, under certain ALD conditions, the fabrication of bimetallic dimers is feasible through deposition of the secondary metal atom on the first single-atomic metal. With the formation of dimer structures, the electronic structure of SACs could be tuned, which would further increase the activity of SACs to a new level.



However, the metal loading is usually very low due to the problems associated with agglomeration during the preparation process. Further Pt deposition during the ALD process tends to adsorb on the existing Pt atoms, which will also result in the formation of clusters. As a result, the development of ALD techniques to achieve high loading of SACs is still a challenge for their future commercial application. Furthermore, the selectivity of substrates is important for the dispersion of single atoms [3,11]. Recently, Zeng *et al.* found that the mass loading of single Pt atom catalysts can reach up to 7.5% on MoS<sub>2</sub> [13]. In addition to the low loading issues, another key parameter for the SACs is the durability of the catalysts during the catalytic reactions. Single-atom catalysts are highly mobile and tend to aggregate during the catalytic reactions due to the high surface energy of SACs. The interaction between SAC and substrate plays an important role in their stability. Several studies have shown that nitrogen-doped carbon black, graphene and nitrogen-doped graphene can form strong coordination sites with metal, thus observably improving their stability [3,4,10]. However, the single atoms still tend to aggregate on traditional substrates. More studies should focus on the development of effective

routes to stabilize the catalysts. The ALD deposition of metal oxide around Pt catalysts has been proven to be an effective way to stabilize the Pt clusters. For example, the ORR stability of Pt clusters was significantly increased by selective deposition of ZrO<sub>2</sub> around Pt clusters to form a cage structure [14]. This method of stabilization may also be applied in single-atom systems. In addition, the fabrication of porous structures to pin the atoms in the hole might also increase the stability of single-atom catalysts. We believe that the ALD method might open up new opportunities in fabrication and optimization of SACs for improved activity and durability in heterogeneous reactions.

## FUNDING

This work was supported by the Natural Sciences and Engineering Research Council of Canada (NSERC), Canada Research Chair (CRC) Program, Canada Foundation for Innovation (CFI) and the University of Western Ontario.

Lei Zhang, Mohammad Norouzi Banis and Xueliang Sun\*

Department of Mechanical and Materials Engineering, The University of Western Ontario, Canada

\*Corresponding author.

E-mail: xsun@eng.uwo.ca

## REFERENCES

1. Yang S, Kim J and Tak YJ *et al. Angew Chem Int Ed* 2016; **55**: 2058–62.
2. Qiao B, Wang A and Yang X *et al. Nat Chem* 2011; **3**: 634–41.
3. Liu P, Zhao Y and Qin R *et al. Science* 2016; **352**: 797–800.
4. Cheng N, Stambula S and Wang D *et al. Nat Commun* 2016; **7**: 13638.
5. Wang C, Gu XK and Yan H *et al. ACS Catal* 2017; **7**: 887–91.
6. Yan H, Cheng H and Yi H *et al. J Am Chem Soc* 2015; **137**: 10484–7.
7. Sun S, Zhang G and Gauquelin N *et al. Sci Rep* 2013; **3**: 1775.
8. George SM. *Chem Rev* 2010; **110**: 111–31.
9. Choi CH, Kim M and Kwon HC *et al. Nat Commun* 2016; **7**: 10922.
10. Liu J, Jiao M and Lu L *et al. Nat Commun* 2017; **8**: 15938.
11. Lu J, Low K-B and Lei Y *et al. Nat Commun* 2014; **5**: 3264.
12. Yan H, Lin Y and Wu H *et al. Nat Commun* 2017; **8**: 1070.
13. Li H, Wang L and Dai Y *et al. Nat Nanotechnol* 2018; **13**: 411–7.
14. Cheng N, Banis MN and Liu J *et al. Adv Mater* 2015; **27**: 277–81.

National Science Review

5: 628–630, 2018


doi: 10.1093/nsr/nwy054

Advance access publication 22 May 2018

## CHEMISTRY

Special Topic: Single-Atom Catalysts

# Atom trapping: a novel approach to generate thermally stable and regenerable single-atom catalysts

Abhaya Datye <sup>1,\*</sup> and Yong Wang<sup>2,3</sup>

An important goal of heterogeneous catalyst synthesis is the dispersion of the active metal uniformly on a catalyst support, ideally achieving atomic dispersion. Isolated single atoms dispersed on oxide supports provide efficient utilization of scarce platinum group metals (PGMs). The enhanced reactivity of Pt<sub>1</sub>/FeO<sub>x</sub> by

Qiao *et al.* [1] generated a lot of excitement in this field and helped set in motion the field of single-atom catalysis (SAC). Since then, we have seen numerous reports of higher reactivity and better selectivity for SACs in a range of catalytic reactions. Synthesis methods for depositing transition metals,

through strong electrostatic adsorption (SEA), ion exchange, co-precipitation, grafting, impregnation or deposition-precipitation, are well developed. To generate and maintain single-atom catalysts using these currently available methods, it is necessary to use low metal loading and to limit the operating

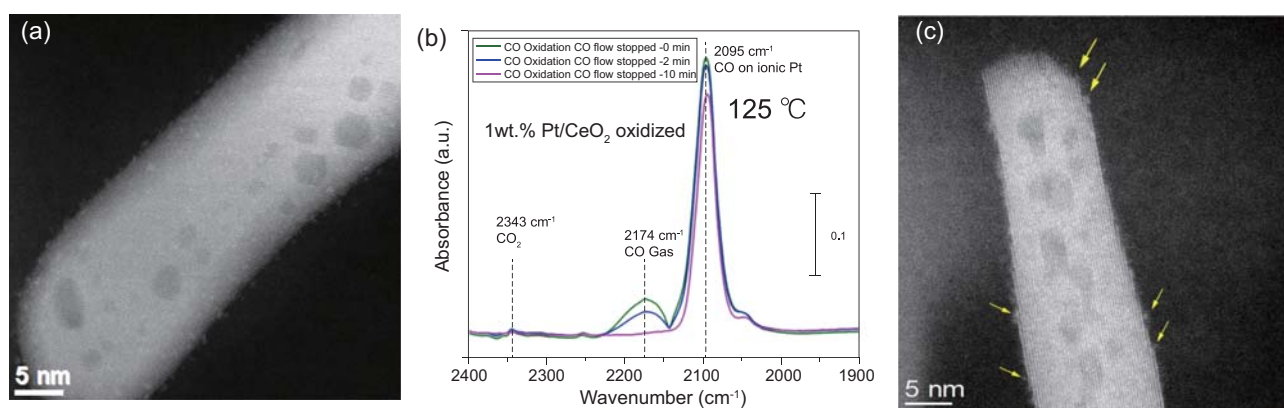


**Figure 1.** (a) AC-STEM of Pt/CeO<sub>2</sub> nanorods, prepared via atom trapping, (b) DRIFTS of adsorbed CO after 30 min of reaction and with flowing O<sub>2</sub> while CO flow was stopped and (c) AC-STEM image of the catalyst after multiple cycles of CO oxidation showing that the single-atom species are stable under lean conditions. Adapted from [9].

temperatures to prevent agglomeration of single atoms into nanoparticles [2]. For industrial applications, it would be desirable to achieve high metal loadings and stable performance at high temperatures, which can be achieved by the methods of atom trapping that we describe here.

One of the earliest reports on the stabilization of isolated metal atoms came from the work of Kwak *et al.* [3] on Pt atoms on penta coordinated Al<sup>3+</sup> in gamma alumina and a similar mechanism was also invoked for amorphous mesoporous alumina [2]. Aberration-corrected STEM images provided evidence for single-atom Pt species and the specific sites on the alumina were identified using NMR spectroscopy [3]. In later work, it was reported that the key parameter helping to prevent sintering of Pt was the formation of a stable coherent interface with the support, such as Pt(111) with MgAl<sub>2</sub>O<sub>4</sub>(111) helping to stabilize Pt against sintering [4]. However, on both of these supports, alumina and MgAl<sub>2</sub>O<sub>4</sub>, heating the Pt catalyst to high temperatures (800°C) in air leads to growth of large Pt metal particles that yield sharp XRD peaks. The reason for the rapid growth of Pt particle size is the high vapor pressure of PtO<sub>2</sub> when Pt is heated in air [5]. Since a number of PGMs form volatile metal oxides [5], it is important to develop methods to stabilize PGMs under oxidative conditions.

In the course of our work on diesel oxidation catalysts, we discovered [6] that

mobile Pt oxides reacted with PdO forming metallic Pt–Pd alloy particles. The reaction of PtO<sub>2</sub> with PdO is thermodynamically favored even in flowing air, forming metallic alloy Pt–Pd alloys. Sintering of Pt is slowed down considerably in the presence of Pd. But excess PdO is needed to provide the sites for capturing mobile Pt species. The mechanism by which PdO helps to slow the sintering of Pt was termed ‘Regenerative Trapping’ [7], analogous to the self-regenerating perovskite catalyst reported previously [8]. When applying this approach to other oxides, we discovered that CeO<sub>2</sub> can effectively trap the PtO<sub>2</sub> vapor, yielding stable isolated single atoms of Pt<sup>2+</sup> on the surface of ceria [9].

Figure 1a shows aberration-corrected HAADF images of the Pt/CeO<sub>2</sub> catalyst as prepared by heating the Pt precursor with ceria at 800°C in flowing air [9]. The sample was used for multiple runs of CO oxidation under lean conditions, with 1% CO, 1.5% O<sub>2</sub> and the balance He, and temperatures up to 300°C. DRIFTS spectra of this catalyst during CO oxidation are shown in Fig. 1b indicating a single prominent band at ~2100 cm<sup>-1</sup> that is characteristic of Pt<sup>2+</sup> on the ceria. When the CO flow was stopped and O<sub>2</sub> flow continued, the CO band did not decrease significantly in intensity, indicating that this CO is strongly bound to ionic Pt. Figure 1c shows the image after reaction, showing that the isolated single atoms of Pt are stable and there is no change in the catalyst after

multiple reaction cycles. These results confirm that the atom-trapping approach is successful in generating atomically dispersed Pt catalysts that are thermally stable at 800°C in air. However, these catalysts are not very reactive for CO oxidation due to strong CO adsorption on ionic Pt. We therefore explored various methods of activation to enhance the reactivity. For example, treatment in steam at 750°C activated the ceria by creating oxygen vacancies and hydroxyls in the vicinity of Pt single sites that were stable at high temperatures and allowed the catalyst to achieve high reactivity for CO oxidation at low temperatures [10].

Atom trapping is not restricted to ceria supports. It was previously reported that heating a Pd/La-alumina catalyst at 700°C in air also forms isolated Pd<sup>2+</sup> on the alumina support [11]. Similarly, the regeneration of Pt–Sn/Al<sub>2</sub>O<sub>3</sub> catalysts was assisted by the presence of atomically dispersed Sn on the alumina support [12]. It is evident then that, in the case of Al<sub>2</sub>O<sub>3</sub> supports, it is necessary to provide trapping sites, such as La or Sn, to help create atomically dispersed species. In contrast, the ceria support is unique in its ability to trap Pt species. We further studied Pt–Sn/CeO<sub>2</sub> catalysts for propane dehydrogenation, where they show stable performance with high selectivity [13]. Due to the reducing conditions, the Pt atoms become mobile and alloy with the Sn, forming bimetallic nanoparticles in the working catalyst (Fig. 2a). However, the catalyst can be readily

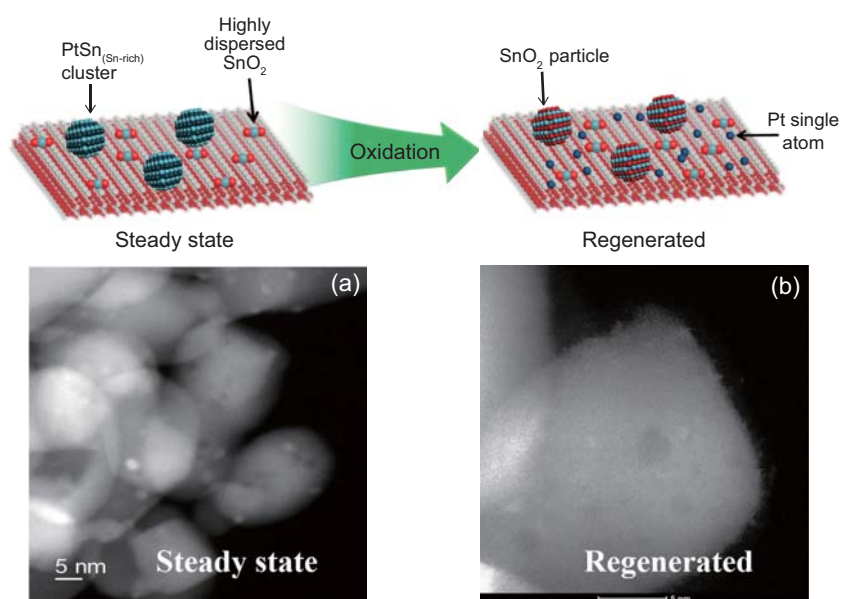


**Figure 2.** (a) AC-STEM image of the working catalyst, after 6 h at 680°C in  $C_3H_8$  and  $H_2$  and (b) after oxidative regeneration in flowing air at 580°C. Adapted from [13].

regenerated under oxidizing conditions, with the Pt forming single-atom species while the Sn remains in the form of  $SnO_2$  particles (Fig. 2b). These results demonstrate the ease with which ceria supported catalysts can be regenerated to recreate the single-atom species.

In summary, high-temperature vapor phase synthesis is demonstrated as a viable method for synthesis of atomically dispersed PGM catalysts. There are other reports of transformation of noble metal nanoparticles into thermally stable single atoms using high temperatures [8,14]. Oxidizing conditions are always used for catalyst regeneration [15], since this represents the most common approach to remove carbonaceous deposits (coke) that lead to catalyst deactivation. PGMs can form mobile oxides in most cases [5]. Even when the oxide has a low vapor pressure, as in the case of  $PdO$ , it is

possible to emit mobile Pd species under oxidizing conditions as demonstrated by the regeneration of  $Pd/La-Al_2O_3$  creating single-atom Pd species [11]. Therefore, understanding the sites for atom trapping could pave the way for broader application of this approach for synthesis single-atom catalysts.

## FUNDING

This work was supported by the US Department of Energy (DOE) (DE-FG02-05ER15712).

*Conflict of interest statement.* None declared.

Abhaya Datye <sup>1,\*</sup> and Yong Wang<sup>2,3</sup>

<sup>1</sup>Department of Chemical and Biological Engineering and Center for Micro-Engineered Materials, University of New Mexico, USA

<sup>2</sup>The Gene & Linda Voiland School of Chemical Engineering and Bioengineering, Washington State University, USA

<sup>3</sup>Institute for Integrated Catalysis, Pacific Northwest National Laboratory, USA

\*Corresponding author.

E-mail: datye@unm.edu

## REFERENCES

1. Qiao B, Wang A and Yang X *et al. Nat Chem* 2011; **3**: 634–41.
2. Zhang Z, Zhu Y and Asakura H *et al. Nat Commun* 2017; **8**: 16100.
3. Kwak J, Hu J and Mei D *et al. Science* 2009; **325**: 1670–3.
4. Li W-Z, Kovarik L and Mei D *et al. Chem Mater* 2014; **26**: 5475–81.
5. McCarty J, Lau K and Hildenbrand D *et al. Studies in Surface Science and Catalysis*. Amsterdam: Elsevier, 1997, 601–7.
6. Carrillo C, Johns T and Xiong H *et al. J Phys Chem Lett* 2014; **5**: 2089–93.
7. Carrillo C, DeLaRiva A and Xiong H *et al. Appl Catal B-Environ* 2017; **218**: 581–90.
8. Nishihata Y, Mizuki J and Akao T *et al. Nature* 2002; **418**: 164–7.
9. Jones J, Xiong H and Delariva A *et al. Science* 2016; **353**: 150–4.
10. Nie L, Mei D and Xiong H *et al. Science* 2017; **358**: 1419–23.
11. Peterson E, DeLaRiva A and Lin S *et al. Nat Commun* 2014; **5**: 4885.
12. Pham H, Sattler J and Weckhuysen B *et al. ACS Catal* 2016; **6**: 2257–64.
13. Xiong H, Lin S and Goetze J *et al. Angew Chem Int Ed* 2017; **56**: 8986–91.
14. Wei S, Li A and Liu J-C *et al. Nat Nanotechnol* 2018; **13**: 856–61.
15. Sattler J, Ruiz-Martinez J and Santillan-Jimenez E *et al. Chem Rev* 2014; **114**: 10613–53.

National Science Review

5: 630–632, 2018

doi: 10.1093/nsr/nwy093

Advance access publication 5 September 2018

## CHEMISTRY

## Special Topic: Single-Atom Catalysts

## Predictive approach of heterogeneous catalysis

Jean-Marie Basset\* and Jérémie D.A. Pelletier

'Predictive catalysis' or 'catalysis by design' has recently advanced heterogeneous catalysis by using the conceptual tool of surface fragments [1] such as 'surface organometallic fragments' (SOMF) or 'surface coordination fragments' (SCF) to achieve and understand a presumed catalytic cycle (see Fig. 1). One or several fragments of the molecule are linked to one metal atom linked to the surface ( $[M]-H$ ,  $[M]-R$ ,  $[M]=CR_2$ ,  $[M]\equiv CR$ ,  $[M]=O$ ,  $[M]=NR$ ,  $[M]-O-OH$  in which  $[M]$  is a surface metal atom linked to an oxide by one, two or several sigma or pi bonds). Surface fragments are the logical continuation of the abundant work published in the field of Surface Organometallic Chemistry (SOMC). In this paradigm based on molecular understanding of surface catalytic sites, one 'single' metal atom is surrounded by ligands and linked to the surface of an oxide via covalent or ionic bonds [2]. It is a continuation of classical heterogeneous catalysis in the direction of single-atom catalysis (SAC). In SAC, single metal atoms are also linked to an oxide by coordination, covalent or ionic bonds but are at the other extreme of catalysis by metal nanoparticles because SAC is the result of a conceptual evolution from metal nanoparticles to a single atom by size reduction of the nanoparticle. It is a continuation of homogeneous catalysis but with a rigid surface as a ligand.

SOMC has allowed the discovery of new catalytic reactions (e.g. Ziegler-Natta depolymerization [3], alkane metathesis [1], non-oxidative methane coupling [1], cyclo-alkane metathesis [4], etc.) and has improved the activity, the selectivity or the lifetime of known ones. The concepts of molecular chemistry (organic, organometallic, coordination chemistry) are the keys to explaining how bonds can be broken and formed [2]. In this context, the reactivity

of SOMF or SCF and their sequence in the cycle are pivotal to the overall outcome of catalysis.

SOMC can generate catalytic sites that are *in principle* identical (single-site or close to single atom) by grafting transition metal atoms onto highly dehydroxylated metal oxide support handled under a controlled atmosphere. This strategy, limited to metal-oxides or metallic surfaces, presents considerable advantages over traditional heterogeneous catalysts in which various populations of potentially active metallic sites coexist. All the steps of the preparation are carefully controlled using the methods of organometallic and coordination chemistry. Hence, the coordination sphere of the grafted metal can be accurately determined (well-defined catalytic site) by modern solid/surface characterization techniques (elemental analysis, *in situ* IR, *in situ* UV, Solid State Nuclear Magnetic Resonance spectroscopy (SS NMR), Extended X-ray absorption fine structure (EXAFS) and *in operando* EXAFS, etc.) [2]. The surface should be considered as a bulky rigid ligand preventing most undesired interferences between catalytic sites (e.g. leading to bimolecular deactivation). The relationship between structure and activity become possible to establish; with the addition of the SOMF tools, it is now a predictable discipline.

The various steps of the catalytic cycle are monitored to understand deactivation, to increase activity and/or selectivity by changing the support or ligand environment of the 'active site' (Fig. 2). The existing gap between heterogeneous catalysis and homogeneous catalysis has almost completely disappeared, because the elementary steps of molecular chemistry are applicable to 'single-atom catalysis'. We shall review here some of

the recent catalytic results obtained on oxides.

Metal hydrides are the simplest and most frequent surface fragments, yet do not belong to 'organometallic' classification *stricto sensu*. ( $[M]-H$ ) are mostly generated by hydrogenolysis of metal-alkyl ( $[M]-R$ ) and generally promote low-temperature C-H bond activation of alkanes (i.e. methane activation) [5]. ( $[M]-H$ ) and ( $[M]-R$ ) can convert into each other by  $\beta$ -hydride elimination of the metal-alkyl and CH insertion. This has been evidenced in alkane depolymerization [3] (polyethylene is transformed into diesel-range gasoline by group 4 metal-based catalysts under hydrogen).

( $[M]-R$ ) SOMF have numerous examples as polymerization catalysts [6,7]. Another case is the bis-alkyl SOMF with dual ( $[M]-R$ ) SOMF for propane homologation to higher alkanes [8].

Surface carbenes were first evidenced with Nb [9] ( $[(\equiv Si-O)_2 Nb(=CH)]$ ), Mo Mo ( $[(\equiv Si-O) Mo(=CH) Me_3]$ ) ( $=NH$ )Np [10] and Re ( $[(\equiv Si-O) Re(Np) (\equiv C-CMe_3) (=CH) Me_3]$ ) [10]. They were eventually successfully employed as catalysts for olefin metathesis. This reactivity is specific to the ( $[M]=CR_2$ ) SOMF, consistently with the metallacyclobutane intermediate proposed by Chauvin [11]. Variation of activity and selectivity had been linked to both the nature of the metal employed and that of the spectator ligands (i.e. oxo, imido, amido, alkyl, etc.) [12,13].

The first multifunctional SOMF fragments  $[M](H) (=CR_2)$  were identified following the discovery of alkane metathesis using tantalum, tungsten and then molybdenum hydride [14] catalysts supported on alumina or silica in 1997 [15]. In this reaction, saturated hydrocarbons, linear and branched, were rearranged to longer or shorter paraffins. For example, n-propane can be converted

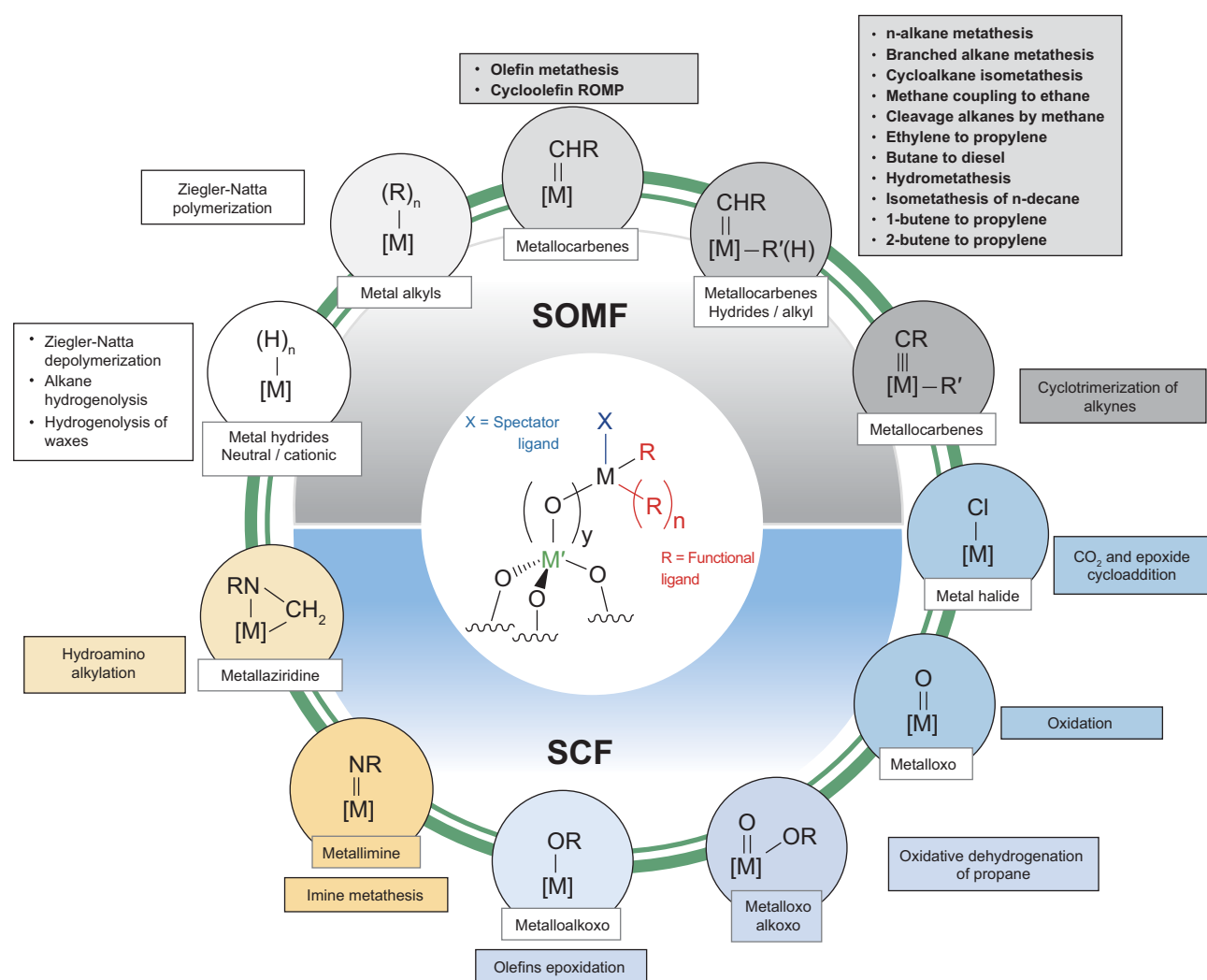


**Figure 1.** Overview of surface fragments: surface organometallic fragments (SOMF) and surface coordination fragments (SCF). Revised version from the figure published by Pelletier and Basset, in *Acc Chem Res* 2016; **49**: 664–77.

into (C<sub>1</sub>, C<sub>2</sub>, C<sub>4</sub>, C<sub>5</sub> ...) paraffins under mild conditions. It was a chemical breakthrough taking into account the inertness of the sp<sup>3</sup> carbon-hydrogen or C–C bonds.

The multifunctional character of the W(=CH<sub>2</sub>)(H) was at the origin of the first cascade reaction on a single metal atom leading from ethylene to propylene by a succession of dimerization of ethylene to butene-1, isomerization of butene-1 to butene-2 and cross-metathesis between butene-2 and ethylene to give propylene.

Another notable application of [M](H)(=CR<sub>2</sub>) was cyclooctane metathesis [16] to produce both ring contraction and ring dimerization

using [(≡Si-O)WMe<sub>5</sub>] as a precursor. Again we have a cascade reaction with [M](H)(=CR<sub>2</sub>) that allows Ring Opening Metathesis (ROM) dimerization or double bond migration followed by a ring-closing metathesis step.

Another ‘polyfunctional’ fragment ([M](H)(≡CR)) explains catalytic terminal alkyne cyclotrimerization. Silica-supported tungsten carbyne complexes have shown high Turn Over Numbers (TONs) without generating significant alkyne metathesis products [4].

The first example of ([M] η<sup>-2</sup>(N(R)CH<sub>2</sub>)) SOMF was obtained with the isolation of silica-supported zirconiaaziridine in 2013 [16]—an active

catalyst for the hydroamino-alkylation of olefins [17].

The first example of ([M]=N) SCF was evidenced by being the first heterogeneous catalyst for imine metathesis using [(≡Si-O)Zr(=NEt)NEt<sub>2</sub>] [18]. Treatment with an imine substrate resulted in imido/imine (=NR<sub>i</sub>, R: Et, Ph) exchange (metathesis) with the formation of [(≡Si-O)Zr(=NPh)NEt<sub>2</sub>]. ([M]=N) effectively catalyse imine/imine cross-metathesis.

([M]-OR) SCF were involved in olefin catalysed by silica-supported titanium complexes [2]. Various (≡SiO)<sub>n</sub>Ti(OCap)<sub>4-n</sub> (OCap =OR, OSiR<sub>3</sub>, OR; R=hydrocarbyl) supported on MCM-41 have been evaluated as

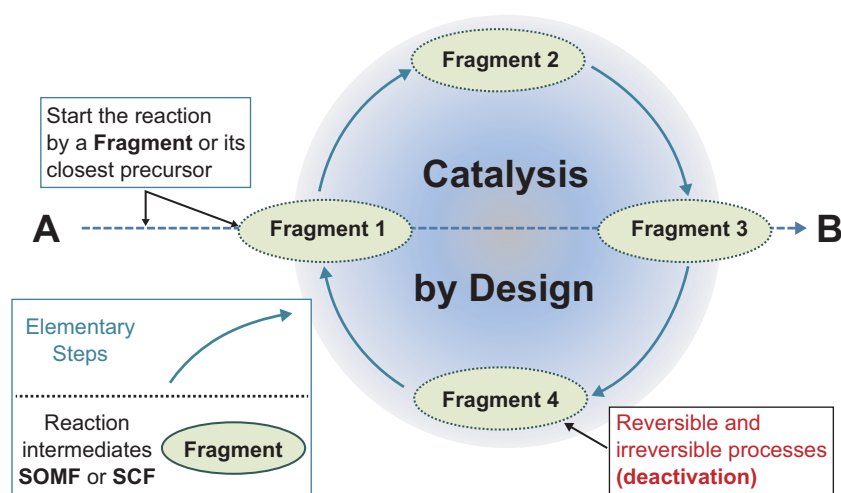


**Figure 2.** Typical schematic to build ‘catalysis by design’ mechanism. Version from the figure published by Pelletier and Basset, in *Acc Chem Res* 2016; **49**: 664–77.

catalysts for 1-octene epoxidation by *tert*-butylhydroperoxide.

Although [M]-Cl are not *stricto sensu* reaction intermediates in CO<sub>2</sub> reaction with epoxides to give cyclic carbonates, the work below is a rare example of cooperating surface bimetallic catalysis. CO<sub>2</sub> and epoxide are each activated by two separate Lewis acid centers ( $\equiv\text{Si-O-NbCl}_4\cdot\text{OEt}_2$ ) maintained in very close proximity by silica [19].

SOMC, alongside surface fragments, allow the prediction of catalysis by determination of the sequence of intermediates and to control the coordination sphere of the metal to achieve targeted reactions. In SAC, the atom grafted onto the surface depends on the reagents/substrates to adopt the right coordination sphere. The SOMC strategy may be seen as the result of a molecular understanding of the elementary steps necessary to achieve a given reaction. One of the questions raised could be the advantage of using SOMC rather than classical heterogeneous catalysis. It is true that ‘classical catalysis’, mostly

based on a ‘trial and error approach’, could be considered as easier in terms of practical advantages, but the SOMC approach offers several competitive advantages: prediction of new catalytic reactions, never observed in classical heterogeneous catalysis; a reliable structure activity relationship because we are dealing with well-defined structures where the physicochemical tools are used with maximum efficiency; and the possibility to control the activity and selectivity with a careful choice of ‘ligands’, ‘spectators ligands’ and supports. This strategy progressively removes the existing gap between heterogeneous and homogeneous catalysis mainly because the concepts of molecular chemistry (in particular the elementary steps) are easily applied to heterogeneous catalysis.

Jean-Marie Basset\* and Jérémie D.A. Pelletier  
King Abdullah University of Science and  
Technology, Saudi Arabia

\*Corresponding author.

E-mail: jeanmarie.basset@kaust.edu.sa

## REFERENCES

- Pelletier JDA and Basset JM. *Acc Chem Res* 2016; **49**: 664–77.
- Basset JM, Psaro R and Roberto D *et al.* *Modern Surface Organometallic Chemistry* 2009, 23–135.
- Dufaud VR and Basset JM. *Angew Chem Int Ed* 1998; **37**: 806–10.
- Riache N, Dery A and Callens E *et al.* *Organometallics* 2015; **34**: 690–5.
- Corker J, Lefebvre F and Lecuyer C *et al.* *Science* 1996; **271**: 966–9.
- Millot N, Soignier S and Santini CC *et al.* *J Am Chem Soc* 2006; **128**: 9361–70.
- Williams LA, Guo N and Motta A *et al.* *Proc Natl Acad Sci USA* 2013; **110**: 413–8.
- Thieuleux C, Maraval A and Veyre L *et al.* *Angew Chem Int Ed* 2007; **46**: 2288–90.
- Asakura K, Nishimura M and Iwasawa Y. *J Mol Catal* 1989; **55**: 159–69.
- Lesage A, Emsley L and Chabanas M *et al.* *Angew Chem Int Ed* 2002; **41**: 4535–8.
- Herisson JL and Chauvin Y. *Makromol Chem* 1971; **141**: 161–76.
- Mazoyer E, Merle N and de Mallmann A *et al.* *Chem Commun* 2010; **46**: 8944–6.
- Basset JM, Coperet C and Soulvong D *et al.* *Acc Chem Res* 2010; **43**: 323–34.
- Blanc F, Coperet C and Thivolle-Cazat J *et al.* *Angew Chem Int Ed* 2006; **45**: 6201–3.
- Vidal V, Theulier A and ThivolleCazat J *et al.* *Science* 1997; **276**: 99–102.
- Hamzaoui B, El Eter M and Abou-Hamad E *et al.* *Chem Eur J* 2015; **21**: 4294–9.
- Hamzaoui B, Pelletier JDA and El Eter M *et al.* *Adv Synth Catal* 2015; **357**: 3148–54.
- Hamzaoui B, Pelletier JDA and Abou-Hamad E *et al.* *Chem Commun* 2016; **52**: 4617–20.
- D’Elia V, Dong HL and Rossini AJ *et al.* *J Am Chem Soc* 2015; **137**: 7728–39.

National Science Review

5: 633–635, 2018

doi: 10.1093/nsr/nwy069

Advance access publication 12 July 2018

## CHEMISTRY

## Special Topic: Single-Atom Catalysts

## Coordination chemistry of atomically dispersed catalysts

Pengxin Liu and Nanfeng Zheng \*

The last decade has witnessed the rapid development of atomically dispersed catalysts. With every active metal atom anchored on the surface of supports, atomically dispersed catalysts offer the maximum atom efficiency, helping to create cost-effective catalysts, particularly those based on earth-scarce metals. While it is still in intense debate whether single metal atoms can provide better catalytic activities than surface atoms of metal nanoparticles, an increasing number of studies have been revealing that the subtle chemical environment surrounding the catalytic metal atoms plays a critical role in determining the overall catalytic performance of an atomically dispersed catalyst. To make single-atom catalysts stable during catalytic reactions, metal atoms thereon are often chemically anchored on the surface of supports through strong metal–metal bonds or coordination bonds with O, N, S or other atoms on supports. This perspective focuses on how the binding sites from supports are involved in the catalytic mechanisms of atomically dispersed catalysts. As shown in Fig. 1a, similarly to the important roles of ligands in homogenous catalysts, changing the binding sites in the first coordination shell surrounding the metal centers of atomically dispersed catalysts is expected to alter their electronic structures and thus catalytic properties. What is even more interesting is that, beyond the first coordination shell, metal cations on supports readily serve as the second coordination shell and are involved in catalytic reactions together with the primary catalytic metal atoms.

With the same binding atoms on supports, lowering the coordination number would alter the electronic and geometric structure of single metal centers, thus changing the adsorption behavior of reactants. For instance, in an atomically

dispersed Fe catalyst system, four Fe-N<sub>x</sub> ( $x = 4-6$ ) coordination environments gave different catalytic activities in the oxidation of alkanes (Fig. 1b). The Fe<sup>III</sup>N<sub>5</sub> structure showed over 1 order of magnitude more active than the high-spin and low-spin Fe<sup>III</sup>N<sub>6</sub> structures and three times more active than Fe<sup>II</sup>N<sub>4</sub> in the selective oxidation of the C–H bond [1]. In the electroreduction of CO<sub>2</sub>, Co-N-C

catalysts with a lower Co-N coordination number showed much higher activity and selectivity to CO (Fig. 1c) [2]. In both cases, the fabrication of active centers of different coordination environments was achieved by thermal treatment at different temperatures. The delicate design of surface defects on carbon supports was also recently demonstrated as an effective method to fabricate Ni single-atom

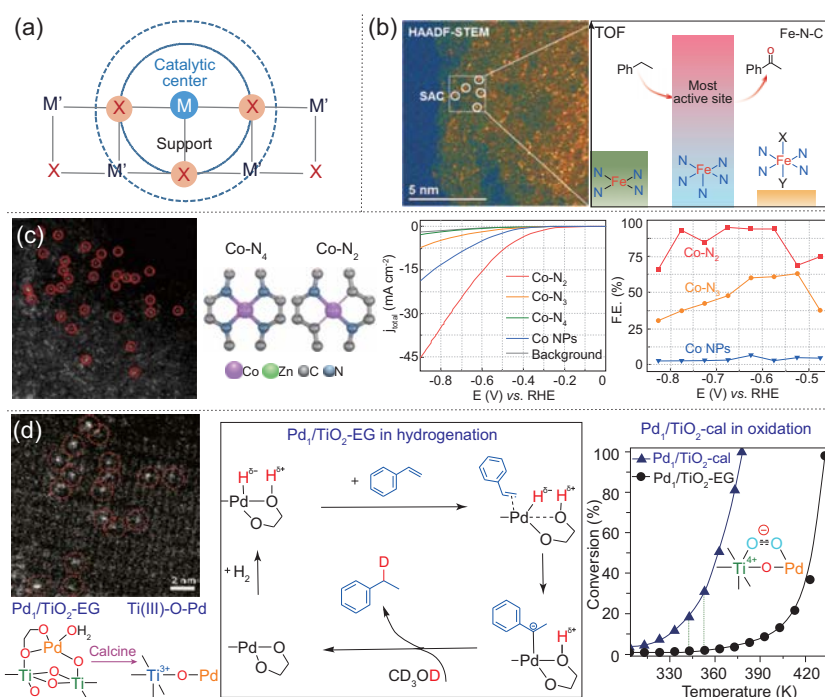


**Figure 1.** Important roles of vicinal coordination environments in determining the catalysis of atomically dispersed metal catalysts. (a) Scheme of the first and second coordination shells of atomically dispersed catalysts that determine the overall catalytic performances. The binding atoms and metal cations from supports are located in the first and second shells, respectively. (b) Compared with other structures, Fe<sup>III</sup>N<sub>5</sub> showed the highest activity in the selective oxidation of the C–H bond (adapted with permission from Ref. [1], ACS). (c) Lower N-coordinated Co showed better performances in electroreduction of CO<sub>2</sub> (adapted with permission from Ref. [2], Wiley). (d) Two atomically dispersed Pd catalysts showed distinct catalytic properties due to the different coordination structures of their Pd atoms. Pd<sub>1</sub>/TiO<sub>2</sub>-EG activated H<sub>2</sub> heterolytically with the assistance of EG ligands, showing a homogeneous-like performance in hydrogenation (adapted with permission from Ref. [4], AAAS). Pd<sub>1</sub>/TiO<sub>2</sub>-cal activated O<sub>2</sub> into superoxide ions due to Ti(III)-O-Pd interfaces, boosting oxidation reactions of CO and VOCs (adapted with permission from Ref. [7], Elsevier).

catalysts with excellent electrocatalytic performance in hydrogen evolution reaction under acidic conditions [3].

Besides the anionic components (e.g.  $O^{2-}$ ,  $N^{3-}$ ,  $S^{2-}$ ) of supports, organic ligands on the surface of supports have potentially important roles in shaping the catalytic performances of atomically dispersed catalysts. For instance, the surface EG (ethylene glycolate) ligands on the photochemically prepared  $Pd_1/TiO_2$ -EG catalyst played a crucial role in catalysing hydrogenation reactions [4]. As shown in Fig. 1d, the EG ligands not only served as binding sites to anchor and thus stabilize Pd atoms onto the  $TiO_2$  support, but also helped to activate  $H_2$  heterolytically into ' $H^+ - H^-$ ' pairs. Such a unique activation pathway makes it possible to precisely control the transfer of activated H atoms during hydrogenation reactions. Such a control results in a perfect homogeneous catalyst-like catalytic selectivity, which is hardly achieved by other Pd-based heterogeneous catalysts.

The second coordination shell of atomically dispersed metals are metal cations from supports, which can also make a significant contribution to their overall catalytic performances through electronic effect and/or oxygen donation. For example, both MgO and HY zeolite-supported single-site Ir complex  $[Ir(C_2H_4)_2(acac)]$  have the identical first-shell coordination environment. Each Ir is coordinated by two O atoms from the supports and two  $C_2H_4$  ligands. However, the electron density of zeolite-supported Ir was lower than MgO-supported Ir due to the electron withdrawal effect of Al in zeolite. Such an electron effect led to a much higher activity of the MgO-supported Ir catalyst than the zeolite-supported one in the hydrogenation of ethylene [5]. In this case, local electron distribution of catalytic atoms depends on the electron affinity of metal cations in supports.

When the metal cations in supports have variable oxidation states, their surrounding O atoms can participate in reactions. Thus, the reactivity depends on the reducibility of the metal cations in supports. For example, a surface science

study on  $Au_1/CuO$  demonstrated that the charge transfer from CuO to Au makes the Au atoms negatively charged, making them active for CO oxidation [6]. Lattice  $O^{2-}$  anions adjacent to the Au atoms can then react with CO to generate  $CO_2$  and  $O^{2-}$  vacancies, leaving the Au atoms neutralized and inactive.  $O^{2-}$  vacancies can then be fixed by reacting with  $O_2$  to make up the complete catalytic cycle. Another nice example on the direct involvement of metal cations in supports is the vicinal effect for promoting oxidation catalysis of  $Pd_1/TiO_2$ -cal, which was made from  $Pd_1/TiO_2$ -EG by removing EG through thermal treatment in air [7]. Although Pd sites in both  $Pd_1/TiO_2$ -cal and  $Pd_1/TiO_2$ -EG catalysts were present as atomically dispersed species in the oxidation state +2, they exhibited distinct catalytic behaviors. While  $Pd_1/TiO_2$ -cal exhibited a dramatically decreased activity in hydrogenation catalysis, the catalyst displayed a significantly increased activity in catalytic CO oxidation, five times higher than that by  $Pd_1/TiO_2$ -EG. As revealed by atomic-resolution electron energy-loss spectroscopy (EELS), a well-defined atomic Ti(III)-Pd-O interface was created after the thermal removal of EG. As shown in Fig. 1d, the exposed  $Ti^{3+}$  sites facilitated the activation of  $O_2$  into superoxide ions ( $O_2^-$ ) and thus suppressed the CO poisoning effect, resulting in a significant enhancement in low-temperature CO oxidation. The direct involvement of metal cations on oxide supports in the catalysis suggests that the real active sites of atomically dispersed metal catalysts can be far beyond isolated metal atoms themselves. Supports of atomically dispersed catalysts play multiple roles than simply serving as ligands.

The active involvement of a support's metal cations that are vicinal to the primary catalytic metal sites may answer the long-debated issue of why atomically dispersed catalysts of the same metal show different activities over different supports. While  $Pt_1/FeO_x$  exhibited high activity in CO oxidation at 27°C [8],  $Pt_1/SiO_2$  and  $Pt_1/HZSM-5$  showed no activity below 100°C [9]. Vapor-phase-synthesized  $Pt_1/CeO_2$  started to show activity over 150°C [10]. More-

over, the preparation and application conditions (e.g. annealing temperature, pre-reduction) of atomically dispersed catalysts are expected to have a significant influence on the local coordination environments of their catalytic metal centers.

Although there have been a large number of reports showing the superior catalytic performances of atomically dispersed metal catalysts over their nanoparticulate counterparts, pictures of the coordination structures around catalytic metal atoms are still blurry in many pieces of work. However, the atomic resolution of the chemical structure of the dispersed metal atoms is crucial to decode the catalytic mechanisms of atomically dispersed metal catalysts, which is currently limited by the lack of effective characterization techniques. Together with the development of atomic-resolution spectroscopy techniques (e.g. electron energy-loss spectroscopy) and high-resolution scanning tunneling microscopy, creating atomically dispersed catalysts that are easy to be characterized is a promising solution. For instance, using ultrathin 1D or 2D nanomaterials as supports for the synthesis of atomically dispersed metal catalysts not only increases the loading amount of single atoms and thus promotes spectroscopic signal-noise ratio, but also decreases the background intensity in microscopy. Meanwhile, the ultrathin feature of the supports allows simplification of the creation of structural models for theoretical calculations to gain molecular understanding on the structure-property relationships that are crucial to the rational design of practical catalysts.


In summary, from the viewpoint of coordination chemistry, the supports not only serve as ligands to stabilize single atoms, but also help to tune the electronic and/or geometric structures of the atomically dispersed metal species. In some cases, metal cations from the support in the second coordination shell of single atoms directly participate in the catalytic reactions as well. It is thus important to understand the catalytic mechanism of atomically dispersed catalysts at the atomic level. We believe the fundamental understanding on the coordination chemistry of atomically dispersed



catalysts will promote the development of the whole field and push them into industrial applications.

## FUNDING

This work was supported by the National Key R&D Program of China (2017YFA0207302) and the National Natural Science Foundation of China (21731005, 21420102001). Dr. P. X. Liu thanks the National Postdoctoral Program for Innovative Talents (BX201600093) and the China Postdoctoral Science Foundation Project (2017M610392).

Pengxin Liu and Nanfeng Zheng \*  
Collaborative Innovation Center of Chemistry for Energy Materials, State Key Laboratory for Physical Chemistry of Solid Surfaces, and

Department of Chemistry, College of Chemistry and Chemical Engineering, Xiamen University, China

\*Corresponding author.  
E-mail: nfzheng@xmu.edu.cn

## REFERENCES

1. Liu W, Zhang L and Liu X *et al. J Am Chem Soc* 2017; **139**: 10790–8.
  2. Wang X, Chen Z and Zhao X *et al. Angew Chem Int Ed* 2018; **57**: 1944–8.
  3. Zhang L, Jia Y and Gao G *et al. Chem* 2018; **4**: 285–97.
  4. Liu PX, Zhao Y and Qin RX *et al. Science* 2016; **352**: 797–800.
  5. Lu J, Serna P and Aydin C *et al. J Am Chem Soc* 2011; **133**: 16186–95.
  6. Zhou X, Shen Q and Yuan K *et al. J Am Chem Soc* 2018; **140**: 554–7.
  7. Liu PX, Zhao Y and Qin RX *et al. Sci Bull* 2018; doi: 10.1016/j.scib.2018.03.002.
  8. Qiao B, Wang A and Yang X *et al. Nat Chem* 2011; **3**: 634–41.
  9. Ding K, Gulec A and Johnson AM *et al. Science* 2015; **350**: 189–92.
  10. Jones J, Xiong H and DeLaRiva AT *et al. Science* 2016; **353**: 150–4.
- National Science Review  
5: 636–638, 2018  
doi: 10.1093/nsr/nwy051  
Advance access publication 30 April 2018

## CHEMISTRY

Special Topic: Single-Atom Catalysts

# Theoretical understanding of the stability of single-atom catalysts

Jin-Cheng Liu<sup>1</sup>, Yan Tang<sup>1</sup>, Yang-Gang Wang<sup>1,2</sup>, Tao Zhang<sup>3</sup> and Jun Li<sup>1,\*</sup>

As a new frontier, the rapid development of single-atom catalysts (SACs) in heterogeneous catalysis has attracted extensive attention since the concept of single-atom catalysis was first coined in 2011 [1,2]. Supported metal single atoms usually possess unique chemical and physical properties and have a special local chemical environment that is distinctly different from conventional supported nanoparticles and metal catalysts. Studies in the past several years have shown four main advantages of SACs: high selectivity, possibly high stability, high atomic efficiency and tunable high activity, as shown in Fig. 1. For efficiency, SAC maximizes the utilization of expensive metals by exposing each single metal atom to reactants. The local configurations of the active centers of an ideal SAC can be highly identical, leading to excellent selectivity compared to supported nanoparticles and metal surfaces that often have multiple yet rather diverse active sites. Unique coordination of single metal atoms with neighboring atoms of support

may lead to high activity for specific reactions. All the above merits are on the basis of the stability of catalysts that people are most concerned about. To avoid aggregation under catalytic reaction conditions, single metal atoms can be stabilized by anchoring at specific sites on the support, including embedding and surface-adsorbing. Considering the complex realistic conditions, the stability of SACs may also depend on the surface condition, support type, reactant species, and finite temperature and pressure, which are difficult to ascertain and vary from one system to another. It remains a grand challenge to guide the prediction and design of highly stable and reactive SACs today.

Four types of single atoms on an oxide surface are shown in Fig. 2b. The single atom can be adsorbed on perfect or defective surfaces and can also be embedded (doped) into cation or oxygen vacancy. Most fabricated SACs from experiments are the embedded type, with strong covalent metal–support interaction (CMSI),

while the sintering of single atoms and dispersion of nanoparticles should involve the diffusion of supported zerovalent single atoms. Therefore, both the supported and embedded single-atom active centers are possible under realistic conditions and worth thorough investigation.

The intrinsic stability of SAC arises from the support-assisted lower chemical potential when compared to nanoparticles. When the free-energy change from nanoparticles to single atoms is negative, nanoparticles can be dispersed to single atoms spontaneously, which leads to thermodynamic stability of SACs (Fig. 2a, black curve). However, even if the free-energy change is positive, single atoms can also be stable when the aggregation barrier is high enough to prevent sintering, which is the kinetic stability of SACs (Fig. 2a, red curve). Following the principles of the atomistic theory of Ostwald ripening developed by W-X Li and coworkers, we have achieved a quantitative

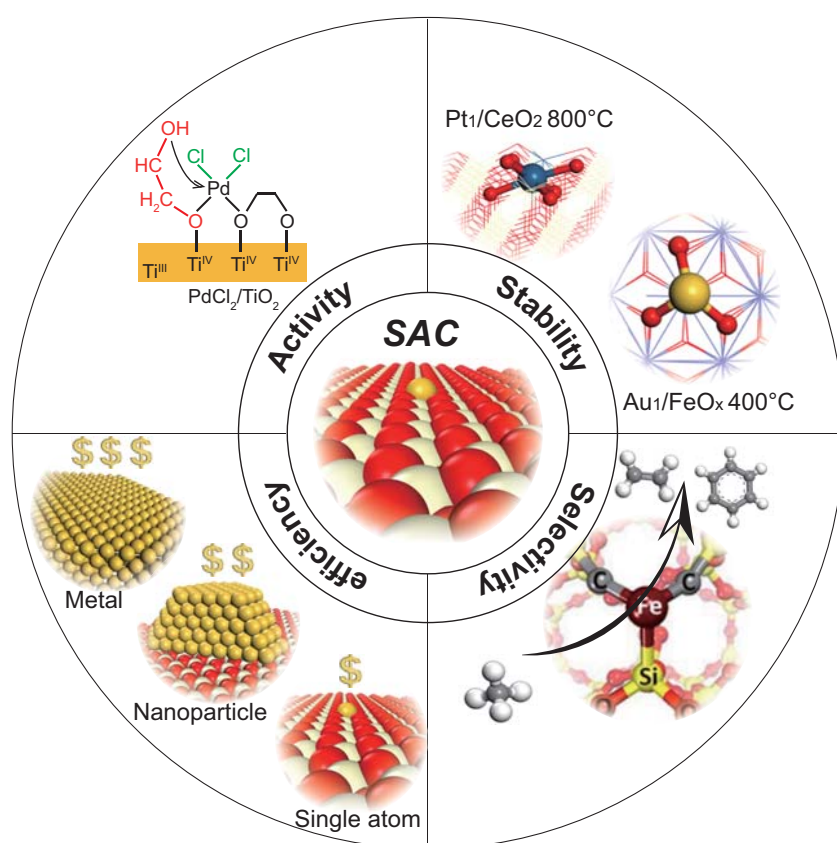


**Figure 1.** Examples illustrating the advantages of single-atom catalysts (SACs) include activity, stability, selectivity and atomic efficiency. (a) High loadings of palladium atoms on  $\text{TiO}_2$  exhibit high catalytic activity in hydrogenation of  $\text{C}=\text{C}$  bonds [3]. (b)  $\text{Pt}_1/\text{CeO}_2$  and  $\text{Au}_1/\text{FeO}_x$  are stable at  $800^\circ\text{C}$  and  $400^\circ\text{C}$  in oxidation conditions, respectively [4,5]. (c) Iron single atom embedded on a  $\text{SiO}_2$  surface exhibits high selectivity for conversion of methane to ethylene, aromatics [6]. (d) SACs are less expensive than supported nanoparticles and metal catalysts.

description and comparison of the two models by taking the reaction environment, particle size and morphology, support type and defects, and metal–reactant interaction into account [7,8]. We have proposed a complete theoretical model to predict the chemical potential of supported single metal atoms and supported nanoparticles, and taken the CO oxidation reaction as an example to guide the design of stable SACs. As a measure of the degree of change of free energy of a system by adding 1 mole of metal atoms to the system at a given temperature and pressure, the chemical potentials for SACs and metal particles were discussed in our recent work [8]. Both thermodynamic and kinetic criteria are considered to determine the stability of SACs. The thermodynamic part includes (i) the

energetics of supported metal particles, which is based on the Gibbs–Thomson (G–T) relation with considering the adsorbed reactants and (ii) the chemical potential of monomers (both the metal adatoms and metal–reactant complexes) on supports. And the kinetic part includes (i) the diffusion barrier of monomers on perfect surfaces and defects and (ii) the barrier of moving one metal atom from a supported metal nanoparticle to a substrate surface with corresponding sintering rate equations.

Here, we discuss the support effect on the stability of supported metal atoms first using selected examples [9]. We have found that the quantum primogenic effect plays a vital role in determining the valence states and charge distribution of single-atom gold and the adsorption

mode of CO on various supports, as shown in Fig. 2d, which is consistent with results from others [10]. Remarkably,  $\text{Au}_1$  atoms are positively charged on reductive supports (e.g.  $\text{CeO}_2$ ,  $\text{TiO}_2$ ) by charge transfer from metal adatoms to support cations, which leads to strong interaction between CO's  $5\sigma$  orbital and  $6s$  orbital of  $\text{Au}^+$ , whereas  $\text{Au}_1$  keeps a zero oxidation state on the irreducible metal dioxides (e.g.  $\text{ZrO}_2$ ,  $\text{HfO}_2$  and  $\text{ThO}_2$ ) and has a weak interaction with CO via a bent  $\text{Au}-\text{CO}$  coordination with partial electron donation to the  $\text{CO } \pi^*$  anti-bonding orbital. For the same substrate, exposing different surfaces also affects the relative stability of single atoms. For example, the stability sequence of doped Pt single atoms on different surfaces of  $\text{CeO}_2$  follows  $(110) > (100) > (111)$  [11]. The high stability of Pt single atoms on (110) surface benefits from the spontaneous formation of an  $\text{O}_2^{2-}$  species from two surface oxygen atoms that reduces  $\text{Pt}^{\text{IV}}$  to  $\text{Pt}^{\text{II}}$ . A different anchoring site for a single atom in a given surface is another significant factor of stability. It has been found that the presence of special defects such as vacancies or steps can improve the stability of an Au single atom on a  $\text{CeO}_2(111)$  surface and the stability sequence is calculated as cation vacancy  $>$  steps  $>$  oxygen vacancy  $>$  perfect (defect-free) surface [8].

Besides the support effect, reactant species also change the stability of SACs. It is now well recognized that sintering is often accelerated by the presence of reducing gases that convert high- and medium-valent metal ions into zerovalent atoms, whereas nanoparticles can also re-disperse to single atoms in some cases. Jones *et al.* reported that Pt nanoparticles can disperse onto ceria surfaces under an oxygen atmosphere and  $800^\circ\text{C}$  [4]. Li and colleagues recently observed noble metal nanoparticles transforming to thermally stable single atoms [12]. Parkinson *et al.* observed CO-induced coalescence of Pd adatoms supported on the  $\text{Fe}_3\text{O}_4(001)$  surface at room temperature [13]. Those phenomena can also be attributed to the chemical potential of single atoms affected by reactants. As shown in Fig. 2c, reducing

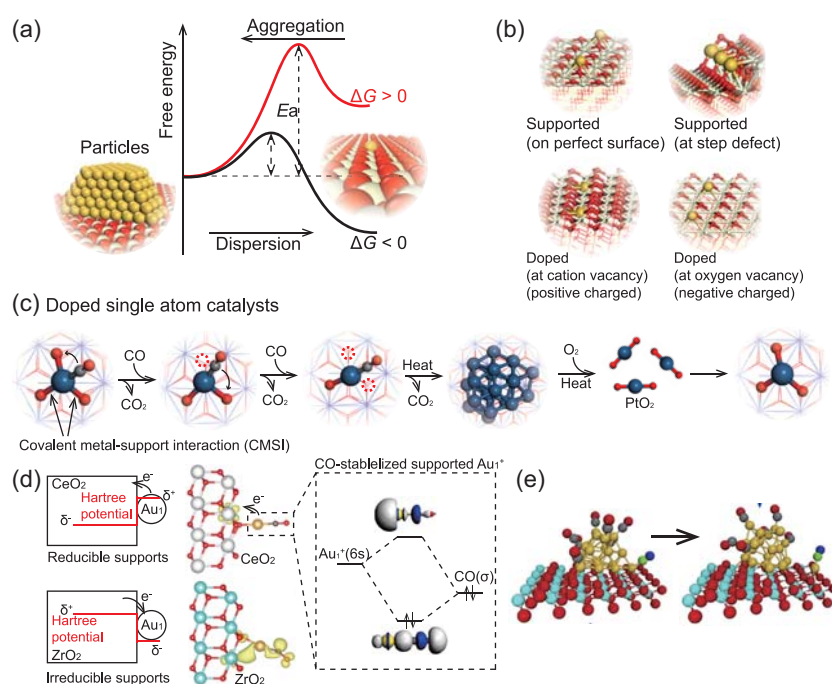


**Figure 2.** (a) Schematic illustration of free-energy diagram of sintering and dispersion processes between Au NPs and SAs. (b) Four types of single atom on oxide support. (c) Aggregation and redispersion processes of Pt<sub>1</sub>/FeO<sub>x</sub> under CO and O<sub>2</sub> atmosphere. (d) Schematic representation of the relationship between Hartree potential and charge transfer on reducible and irreducible substrates, and the molecular orbital of Au<sup>+</sup>CO species on CeO<sub>2</sub> support [9]. (e) Dynamic formation of single-atom catalytic active sites on ceria-supported gold nanoparticles (adapted from [15]).

gases such as CO and H<sub>2</sub> can react with the lattice oxygen after adsorption onto single metal atoms, which breaks the covalent bond between metal and oxygen, especially for doped atoms at cation vacancy. When all the relevant metal-support covalent bonds are broken by CO, the charge state of Pt changes from positive to neutral. And, simultaneously, the chemical potential of single Pt atoms increases to be higher than Pt nanoparticles. Such Pt<sup>0</sup> species become highly mobile with CO adsorption and thus aggregated to particles rapidly by overcoming the diffusion barrier. On the contrary, when Pt nanoparticles are exposed to oxygen atmospheres at high temperature, the chemical potential of separated PtO<sub>2</sub> species can become lower than that on nanoparticles. Should there be enough suitable surface sites (such as cation vacancies or steps on ceria) to trap PtO<sub>2</sub>, Pt nanoparticles will transfer to single atoms on support.

It is worth noting that single metal atoms may also be dynamically generated

during the catalytic processes. Based on large-scale *ab initio* molecular dynamic (AIMD) simulations, we have found that, on reducible oxide-supported gold nanocatalysts [14,15], the gold cation can migrate from the gold nanoparticle to support to catalyze CO oxidation and reintegrate back to the nanoparticle after completing the reaction. This dynamic phenomenon of SACs is named as dynamic single-atom catalysis [15]. Especially, by a combination of *ab initio* electronic structure and molecular dynamics simulations, as well as a microkinetic simulation, we have shown that, on TiO<sub>2</sub>-supported Au nanocatalysts, formation of dynamic SACs is the dominant reaction pathway for CO oxidation under oxidizing conditions and  $T < 400$  K [14]. The dynamic formation of single gold atoms under realistic conditions is ultimately attributed to the reducibility of the oxide support that strongly couples with the charge state of gold and makes the single gold atom active during the catalytic processes, which is attributed to dynamic sta-

bility. In recent work, we found that dynamic single atoms under reaction conditions account for the notorious size effect in gold nanocatalysts [16].

In summary, intrinsic thermodynamic stability, kinetic stability and dynamic stability are the key factors in determining the reactivity of SACs. Although experimental results present a complicated picture from system to system, it all complies with the rules of chemical potential, which can be quantitatively evaluated from thermodynamic and dynamic aspects. Single-atom catalysis pushes the traditional catalytic theory from a band-structure-based interpretation to a more local chemical-bonding interpretation, where the local chemical coordination and local molecular orbitals dominate the physical and chemical properties, especially the stability and activity. Exploring these intriguing factors on stability of SACs based on theoretical models [7,8] may lead to better and deeper understanding of single-atom catalysis and provide guidance for the rational design of exactly controllable catalytic reactions.

Jin-Cheng Liu<sup>1</sup>, Yan Tang<sup>1</sup>, Yang-Gang Wang<sup>1,2</sup>, Tao Zhang<sup>3</sup> and Jun Li<sup>1,\*</sup>

<sup>1</sup>Department of Chemistry and Key Laboratory of Organic Optoelectronics & Molecular Engineering of Ministry of Education, Tsinghua University, China

<sup>2</sup>Department of Chemistry, Southern University of Science and Technology, China

<sup>3</sup>Dalian Institute of Chemical Physics, Chinese Academy of Sciences, China

\*Corresponding author.

E-mail: junli@tsinghua.edu.cn

## REFERENCES

1. Qiao B, Wang A and Yang X *et al. Nat Chem* 2011; **3**: 634–41.
2. Yang X-F, Wang A and Qiao B *et al. Acc Chem Res* 2013; **46**: 1740–8.
3. Liu P, Zhao Y and Qin R *et al. Science* 2016; **352**: 797–800.
4. Jones J, Xiong H and DeLaRiva AT *et al. Science* 2016; **353**: 150–4.
5. Qiao B, Liang J-X and Wang A *et al. Nano Res* 2015; **8**: 2913–24.
6. Guo X, Fang G and Li G *et al. Science* 2014; **344**: 616–9.

7. Ouyang R, Liu JX and Li WX. *J Am Chem Soc* 2013; **135**: 1760–71.
8. Liu JC, Wang YG and Li J. *J Am Chem Soc* 2017; **139**: 6190–9.
9. Tang Y, Zhao S and Long B *et al.* *J Phys Chem C* 2016; **120**: 17514–26.
10. Bruix A, Lykhach Y and Matolinova I *et al.* *Angew Chem Int Ed* 2014; **53**: 10525–30.
11. Tang Y, Wang YG and Li J. *J Phys Chem C* 2017; **121**: 11281–9.
12. Wei S, Li A and Liu J-C *et al.* *Nat Nanotech* 2018; doi: 10.1038/s41565-018-0197-9.
13. Parkinson GS, Novotny Z and Argentero G *et al.* *Nat Mater* 2013; **12**: 724–8.
14. Wang Y-G, Cantu DC and Lee M-S *et al.* *J Am Chem Soc* 2016; **138**: 10467–76.
15. Wang YG, Mei D and Glezakou VA *et al.* *Nat Commun* 2015; **6**: 6511.
16. He Y, Liu J-C and Luo L *et al.* *Proc Natl Acad Sci USA* 2018; doi: 10.1073/pnas.1800262115.

National Science Review  
5: 638–641, 2018

doi: 10.1093/nsr/nwy094

Advance access publication 5 September 2018

## CHEMISTRY

Special Topic: Single-Atom Catalysts

# Single-atom heterogeneous catalysts based on distinct carbon nitride scaffolds

Zupeng Chen<sup>1</sup>, Evgeniya Vorobyeva<sup>1</sup>, Sharon Mitchell<sup>1,\*</sup>, Edwin Fako<sup>2</sup>, Núria López<sup>2</sup>, Sean M. Collins<sup>3</sup>, Rowan K. Leary<sup>3</sup>, Paul A. Midgley<sup>3</sup>, Roland Hauert<sup>4</sup> and Javier Pérez-Ramírez<sup>1,\*</sup>**ABSTRACT**

Carbon nitrides integrating macroheterocycles offer unique potential as hosts for stabilizing metal atoms due to their rich electronic structure. To date, only graphitic heptazine-based polymers have been studied. Here, we demonstrate that palladium atoms can be effectively isolated on other carbon nitride scaffolds including linear melem oligomers and poly(triazine/heptazine imides). Increased metal uptake was linked to the larger cavity size and the presence of chloride ions in the polyimide structures. Changing the host structure leads to significant variation in the average oxidation state of the metal, which can be tuned by exchange of the ionic species as evidenced by X-ray photoelectron spectroscopy and supported by density functional theory. Evaluation in the semi-hydrogenation of 2-methyl-3-butyn-2-ol reveals an inverse correlation between the activity and the degree of oxidation of palladium, with oligomers exhibiting the highest activity. These findings provide new mechanistic insights into the influence of the carbon nitride structure on metal stabilization.

**Keywords:** single-atom heterogeneous catalysts, carbon nitride scaffolds, alkyne semi-hydrogenation, density functional theory, metal–host interaction

**INTRODUCTION**

The exploration of single-atom heterogeneous catalysts (SACs) based on noble metals has been stimulated by the prospect of improving metal utilization and selectivity simultaneously in sustainable catalytic processes [1–6]. Unfortunately, atomically dispersed metals on common hosts (e.g. metals, metal oxides and carbons) are often thermodynamically unstable and aggregate into clusters or nanoparticles, especially at elevated temperature [7]. In this regard, graphitic carbon nitride (herein denoted as GCN) emerges as a unique host for preparing SACs due to the presence of nitrogen-rich macroheterocycles in the lattice, which can anchor metal atoms firmly [8,9]. The density of the adsorption pockets also helps to maintain dispersion by configurational entropy considerations. In comparison to SACs supported

on other nitrogen-doped carbons, which typically exhibit significant structural heterogeneity, the higher content and uniform type and arrangement of nitrogen species within GCN materials offer abundant and more precisely defined coordination sites.

Graphitic carbon nitride is regarded as the most stable polymorph upon polymerization of common nitrogen-rich precursors (e.g. cyanamide, dicyanamide and melamine) under ambient conditions, and is widely used as a photocatalyst [10–14]. In agreement with density functional theory (DFT) predictions of the higher thermodynamic stability, most experimental studies report the formation of heptazine- rather than triazine-based molecular structures [8,9,15–19]. Since the preparation of GCN is a stepwise polymerization process, various intermediate phases including melam, melem and linear melem oligomers (LMO) can be obtained by

<sup>1</sup>Institute for Chemical and Bioengineering, Department of Chemistry and Applied Biosciences, ETH Zurich, 8093 Zurich, Switzerland; <sup>2</sup>Institute of Chemical Research of Catalonia (ICIQ), The Barcelona Institute of Science and Technology, 43007 Tarragona, Spain; <sup>3</sup>Department of Materials Science and Metallurgy, University of Cambridge, Cambridge, CB3 0FS, UK and <sup>4</sup>Empa, Swiss Federal Laboratories for Materials Science and Technology, 8600 Dübendorf, Switzerland

\*Corresponding authors. E-mails: sharon.mitchell@chem.ethz.ch; jpr@chem.ethz.ch

Received 5 February 2018; Revised 10 April 2018; Accepted 13 April 2018

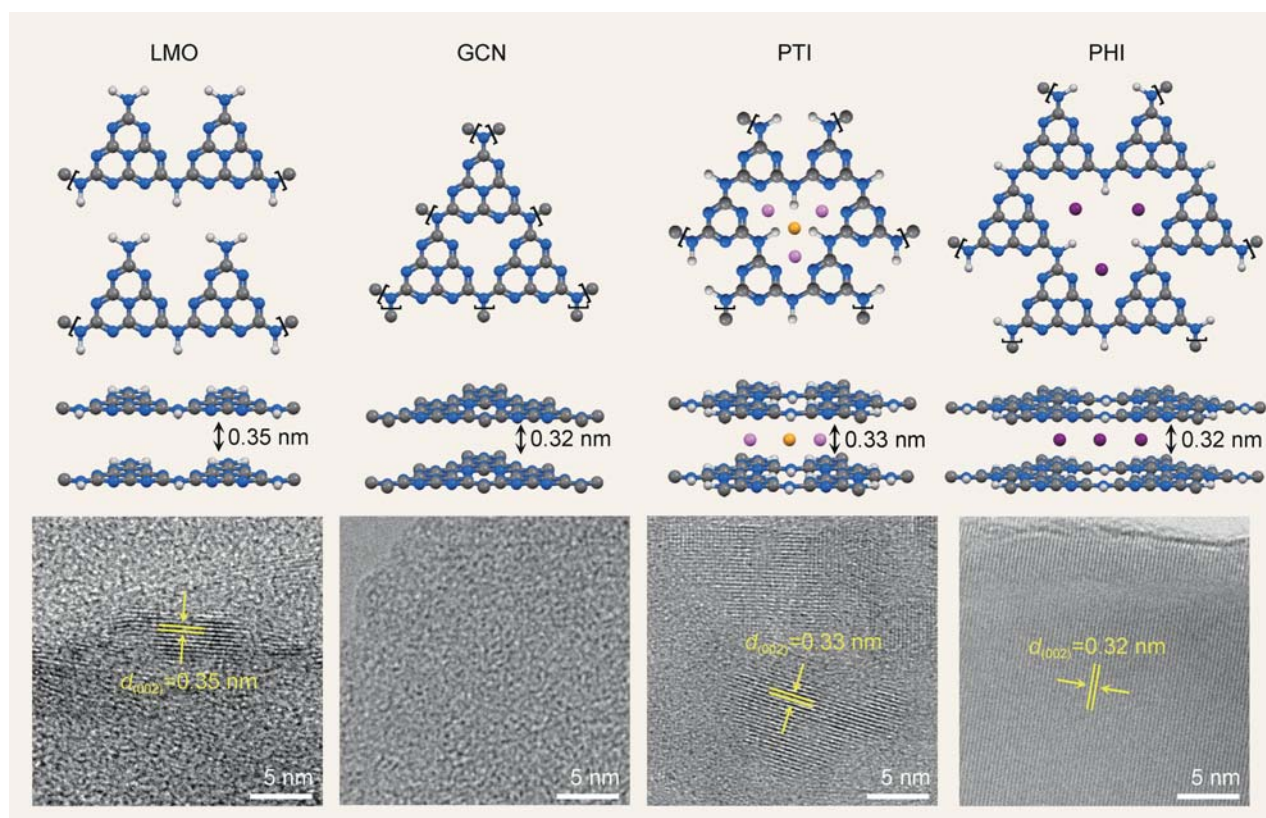


**Figure 1.** Idealized structure motifs and high-resolution TEM images of LMO, GCN, PTI and PHI. Sites that further polymerize in the extended structure are indicated with parentheses. Color codes: gray, C; blue, N; white, H; pink, Li; purple, K; orange, Cl. The relaxed structures are shown in Supplementary Fig. 16.

varying the synthesis conditions (temperature, pressure or atmosphere) [20,21]. On the other hand, highly crystalline carbon nitrides comprising ordered poly(triazine imide) (PTI) or poly(heptazine imide) (PHI) can be assessed either by increasing the temperature or pressure [22,23] or by ionothermal synthesis employing eutectic salt mixtures of  $\text{LiX/KX}$  ( $X = \text{Cl}$  or  $\text{Br}$ ) [23–26] or simply single alkaline metal chlorides [27,28] as the solvent.

Various metals (Pd, Ag, Pt or Ir) have been stabilized as single atoms on GCN by using both direct (e.g. copolymerization, *in-situ* doping) and post-synthetic (e.g. wet deposition optionally assisted by microwave irradiation and/or combined with chemical reduction) approaches [29–36]. The method of metal introduction is known to impact the distribution of metal centers within the host, the post-synthetic deposition resulting in higher surface metal densities and consequently increased turnover frequencies in the three-phase semi-hydrogenation of alkynes. Furthermore, both the accessibility and electronic properties of adsorbed metal species could also be altered by varying the morphology and porosity of GCN [33]. By doping carbon into the lattice of GCN, we

recently reported the controlled variation of the C/N ratio, pointing out the potentially critical role of the strength of the metal–host interaction [35]. However, to date, the preparation of SACs based on other carbon nitrides including LMO and crystalline PTI and PHI phases has not been attempted.

To guide the design of improved SACs and gain insight into the effect of the host structure on metal stabilization, a series of carbon nitride materials (LMO, GCN, PTI and PHI) have been prepared (the idealized structure motifs are illustrated in Fig. 1). The comparative properties of the distinct scaffolds are studied in depth before and after the introduction of palladium via microwave-assisted deposition. The single-atom dispersion is confirmed in all cases by aberration-corrected scanning transmission electron microscopy, while analysis by X-ray photoelectron spectroscopy reveals significant variation in the formal oxidation state of the metal. DFT calculations are conducted to shed further light on the interaction of the metal with the different scaffolds, which is fundamental to understand the performance that in our case was interrogated through the semi-hydrogenation of 2-methyl-3-butyn-2-ol. The possibility to tune the electronic properties of

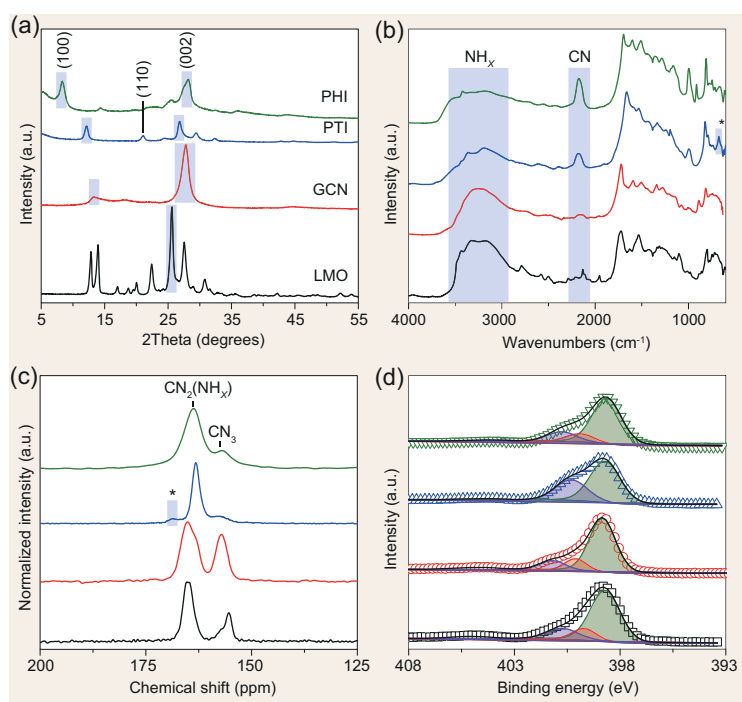


**Figure 2.** (a) XRD patterns, (b) DRIFTS spectra, (c)  $^{13}\text{C}$  CP/MAS NMR spectra and (d) N 1s XPS spectra of the investigated carbon nitride scaffolds. The sample color codes in (a) apply to all panels. The transparent blue boxes indicate the reflections and stretching assignments, where the asterisks indicate bands characteristic of the PTI structure. In (d), the black lines show the fitted result of the raw data (open symbols), whereas the green, red and purple peaks corresponding to the deconvoluted C-N=C,  $\text{NC}_3$  and  $-\text{NH}_x$  components.

the metal via the exchange of intercalated ions in the polyimides is also demonstrated.

## RESULTS AND DISCUSSION

### Host properties

The distinct carbon nitride scaffolds were prepared adapting previously reported protocols [22–25,37]. In particular, LMO and GCN were obtained by direct polymerization of melamine at different temperatures, while PTI and PHI were synthesized by a similar approach exploiting eutectic salt mixtures of LiCl/KCl as the solvent. Analysis by X-ray diffraction (XRD) confirms the characteristic crystalline structures of the resulting materials (Fig. 2a). In particular, GCN exhibits an intense reflection at  $27.3^\circ$   $2\theta$  (002) associated with the graphite-like interlayer stacking and a weak in-plane reflection stemming from heptazine repeating units at  $13.1^\circ$   $2\theta$  (100). PTI features a number of well-resolved reflections, which are consistent with the expected hexagonal structure and  $P6_3cm$  space group [23]. The strongest reflection at  $26.8^\circ$   $2\theta$  indexed as the (002) plane corresponds to an interlayer distance of 0.33 nm,

whereas the (002) reflection of PHI was found to be at  $26.2^\circ$   $2\theta$  (0.32 nm). Note that the reflection at  $12.2^\circ$   $2\theta$  of PTI corresponding to the (100) in-plane periodicity shifts to a lower angle ( $8.3^\circ$   $2\theta$ ) in PHI. In the case of LMO, the XRD pattern agrees well with previously reported observations, where the (002) reflection at  $25.5^\circ$   $2\theta$  features an interlayer distance of 0.35 nm [37]. The high crystalline order of the carbon nitride hosts was further evidenced by high-resolution transmission electron microscopy (TEM) imaging (Fig. 1). Although not observed in GCN due to the in-plane structural disorder and beam sensitivity, LMO, PTI and PHI exhibited lattice fringes with spacings of 0.35, 0.33 and 0.32 nm, respectively, corresponding to the (002) planes in these stacked aromatic structures. Additional lattice fringes with distances of 0.44 and 0.74 nm were also observed in the case of PTI (Supplementary Fig. 1), which can be assigned to the (110) and (100) planes, respectively.

The distinct structures were further corroborated by diffuse reflectance infrared Fourier transform spectroscopy (DRIFTS),  $^{13}\text{C}$  solid-state cross-polarization/magic angle spinning nuclear magnetic resonance (CP/MAS NMR) spectroscopy and X-ray photoelectron spectroscopy (XPS). The DRIFTS spectra (Fig. 2b) evidence the existence of the aromatic heterocycles in all hosts, showing the stretching at  $1100\text{--}1650\text{ cm}^{-1}$ , while the broad bands at  $3000\text{--}3300\text{ cm}^{-1}$  are assigned to the bending of  $-\text{NH}_x$  terminations [38]. Though bearing the same building units of heptazine, LMO shows more intense  $-\text{NH}_x$  breathing modes than GCN, indicative of more peripheral  $-\text{NH}_x$  terminations in LMO. The cumulated double bonds ( $-\text{N}=\text{C}=\text{N}-$ ) at  $2184\text{ cm}^{-1}$  are obvious in PTI and PHI, evidencing the presence of  $-\text{NH}-$  bridges as in ketene imines [39]. In addition to the deformation vibrations of the triazine or heptazine rings at  $814\text{ cm}^{-1}$ , a unique band at  $670\text{ cm}^{-1}$  in PTI suggests that triazine rings are the building units [23,40], instead of the heptazine in the other cases. LMO and GCN show similar  $^{13}\text{C}$  NMR spectra (Fig. 2c) with two main peaks at 164 and 155–157 ppm, attributed to  $\text{CN}_2(\text{NH}_x)$  and  $\text{CN}_3$  moieties, respectively. These signals are also present in PTI and PHI, but the ratio between the intensity at 164 and 157 ppm is much higher, demonstrating more carbon species close to periphery  $-\text{NH}_x$ . On the other hand, an additional peak at 168 ppm indicates the presence of triazine rings in PTI, which can be ascribed to the carbons with few protons in its proximity [41]. Furthermore, the main contribution at 288.3 eV in the C 1s XPS spectra (Supplementary Fig. 2) originates from the carbon species in the triazine or heptazine rings. Comparatively, deconvolution of N 1s spectra (Fig. 2d)

**Table 1.** Characterization data of the carbon nitride scaffolds and associated SACs.

Host <sup>a</sup>	Formula <sup>b</sup>	S <sub>BET</sub> <sup>c</sup> (m <sup>2</sup> g <sup>-1</sup> )	Pd <sup>b</sup> (wt.%)	Loading efficiency <sup>d</sup> (%)	Pd surface density <sup>e</sup> (μmol <sub>Pd</sub> m <sup>-2</sup> )
LMO	C <sub>3</sub> N <sub>4.86</sub> H <sub>2.69</sub> O <sub>0.11</sub>	3 (29)	0.66	33	8.6
GCN	C <sub>3</sub> N <sub>4.64</sub> H <sub>1.59</sub> O <sub>0.10</sub>	8 (11)	0.58	29	63.8
PTI	C <sub>3</sub> N <sub>4.52</sub> H <sub>2.89</sub> O <sub>0.82</sub> Li <sub>0.16</sub> K <sub>0.05</sub> Cl <sub>0.12</sub>	68 (76)	0.56	100	1.7
PHI	C <sub>3</sub> N <sub>4.27</sub> H <sub>3.11</sub> O <sub>1.43</sub> Li <sub>0.04</sub> K <sub>0.27</sub> Cl <sub>0.01</sub>	31 (30)	0.47	95	4.7
PTI-Mg	C <sub>3</sub> N <sub>4.55</sub> H <sub>2.96</sub> O <sub>0.84</sub> Li <sub>0.15</sub> K <sub>0.01</sub> Cl <sub>0.08</sub> Mg <sub>0.02</sub>	80 (110)	0.50	100	1.6
PHI-Mg	C <sub>3</sub> N <sub>4.36</sub> H <sub>3.38</sub> O <sub>1.49</sub> Li <sub>0.00</sub> K <sub>0.09</sub> Cl <sub>0.01</sub> Mg <sub>0.10</sub>	31 (40)	0.48	96	4.2

<sup>a</sup>LMO, linear melem oligomer; GCN, graphitic carbon nitride; PTI, poly(triazine imide); PHI, poly(heptazine imides); PTI-Mg and PHI-Mg, magnesium ion-exchanged PTI and PHI.

<sup>b</sup>Determined by elemental analysis (non-metals) or ICP-OES (metals).

<sup>c</sup>BET method (in parentheses, the surface area of the SACs).

<sup>d</sup>Determined by  $100 \times (\text{actual metal content}/\text{targeted metal content})$ .

<sup>e</sup>Determined from the surface Pd concentration (from XPS) and area (from gas sorption) of the SACs.

of LMO, GCN and PHI evidence three main peaks at 398.8, 399.9 and 401.0 eV, which can be ascribed to the ring nitrogen (C-N=C), tertiary nitrogen (NC<sub>3</sub>) and terminal -NH<sub>x</sub> groups. The ratio of C-N=C/NC<sub>3</sub> was calculated to be around 6, confirming the presence of heptazine as the building unit [25]. Taking account of the relative nitrogen content from elemental analysis (Table 1), the surface NH<sub>x</sub> concentration for LMO was calculated to be 6.8 mmol g<sup>-1</sup>, which is 1.3-fold more than that of GCN (5.3 mmol g<sup>-1</sup>). On the other hand, the absence of the tertiary nitrogen (NC<sub>3</sub>) and the C-N=C/NC<sub>3</sub> ratio of around 2, accompanied by some shift in the terminal -NH<sub>x</sub>, suggest again that the obtained PTI is built of triazine instead of heptazine units.

The chemical composition of the hosts was determined by elemental analysis and inductively coupled plasma-optical emission spectrometry (ICP-OES) (Table 1). The C/N molar ratio of LMO is 0.62, which is lower than its GCN counterpart (0.65), likely due to the abundant -NH<sub>x</sub> terminations in LMO. Meanwhile, the C/N ratios of PTI and PHI are 0.66 and 0.70, respectively, which are very close to the theoretical values (0.67 for PTI and 0.71 for PHI). The Li, K, Cl molar contents (in mol.%) in PTI and PHI (PTI/PHI) were calculated to be 2.3/0.3, 0.5/2.2 and 1.0/0.1, respectively. Therefore, it can be concluded that PTI is intercalated by Li<sup>+</sup> and Cl<sup>-</sup> simultaneously, while PHI is preferentially intercalated with K<sup>+</sup>. The presence of exchangeable ions in PTI and PHI offers a further possibility to tune the electronic properties of the hosts. Magnesium was chosen as the exchanged species, since Mg<sup>2+</sup> is known to interact well with the N species in porphyrins and it has a comparable or smaller ionic radius ( $r_{\text{ion}} = 86$  pm) than that of the Li<sup>+</sup> (90 pm) and K<sup>+</sup> (152 pm) ions initially present in the structures. As shown in

Table 1, only 0.41 wt.% Mg was exchanged into the framework of PTI, while the Mg content can be introduced into PHI up to 1.94 wt.%, indicating that K<sup>+</sup> in PHI can be efficiently exchanged with Mg<sup>2+</sup>. The structure of PTI and PHI remains unchanged upon Mg<sup>2+</sup> exchange, as suggested by the similarity of the XRD patterns (Supplementary Fig. 3).

The distinct morphology of the applied hosts was visualized by TEM and scanning electron microscopy (SEM) (Supplementary Fig. 4). In contrast to the irregularly shaped LMO and GCN, PTI displays fiber-like morphology constituted by cubic and hexagonal nanocrystals, while PHI presents a mixture of rod-like structures and plates. As evidenced by argon sorption (Supplementary Fig. 2), PTI and PHI exhibit higher surface areas (68 and 31 m<sup>2</sup> g<sup>-1</sup>, respectively) than non-porous LMO and GCN (3 and 8 m<sup>2</sup> g<sup>-1</sup>, respectively), which is linked to the nanostructured characteristics of the polyimide structures.

## Metal stabilization

To study the capacity of the distinct carbon nitride scaffolds as hosts for single atoms, palladium was introduced via a microwave-assisted deposition targeting a loading of 2 wt.%. Increased metal deposition was observed for the polyimide structures, taking up 66% (PTI) and 68% (PHI) of the available metal leading to palladium contents of 1.32 and 1.35 wt.%, respectively. Comparatively, lower uptakes 33% (LMO) and 29% (GCN) were observed for the other carbon nitrides (incorporating 0.66 and 0.58 wt.%, respectively). This is tentatively attributed to the specific binding of palladium by the former carriers (*vide infra*) although the higher surface area of these materials could also enhance the capacity as a metal host. For an improved catalytic evaluation, two additional SACs based on PTI



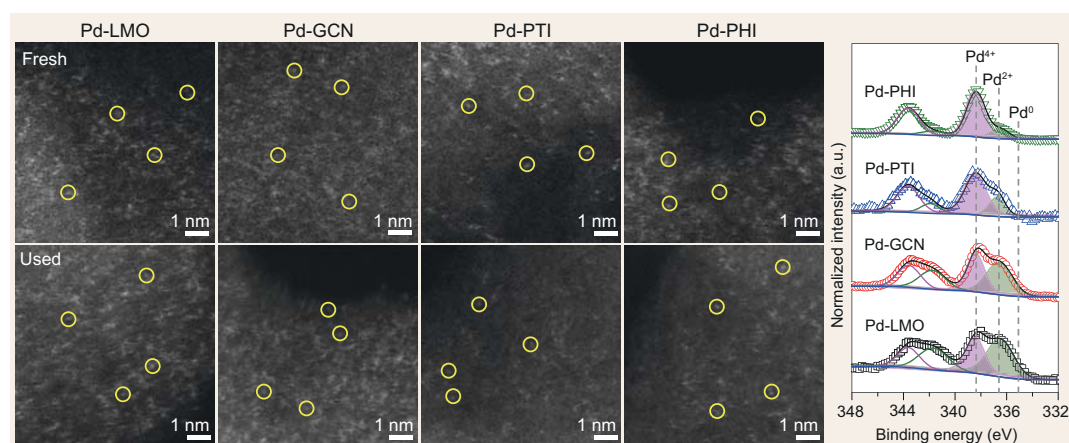


**Figure 3.** AC-HAADF-STEM images of the fresh and used Pd-SACs based on different carbon nitride scaffolds and Pd 3d core-level XPS spectra of the fresh catalysts. Some isolated Pd atoms are identified by yellow circles. Additional low-magnification HAADF-STEM images of the fresh samples are shown in Supplementary Fig. 17. In the XPS spectra, the black lines show the fitted result of the raw data (open symbols), whereas the magenta and green peaks correspond to the deconvoluted components. The dashed lines indicate the positions formally assigned to Pd<sup>4+</sup>, Pd<sup>2+</sup> and Pd<sup>0</sup> species.

and PHI were prepared with metal contents close to 0.5 wt.% (Table 1).

The examination by aberration-corrected high-angle annular dark-field scanning transmission electron microscopy (AC-HAADF-STEM) verified the single-atom dispersion of palladium, where the higher-atomic-number metal atoms are visible as the sub-nanometer bright spots on a smoothly varying gray background signal from the lower-atomic-number hosts (Fig. 3 and Supplementary Fig. 5). To assess the macroscopic metal distribution, thin cross-sections of the embedded materials were mapped by energy-dispersive X-ray (EDX) spectroscopy, indicating a relatively uniform presence of palladium throughout LMO, PTI and PHI (Supplementary Fig. 6). In contrast, a surface enrichment in the concentration of palladium was observed for GCN, suggesting that the metal is unable to penetrate deeply into the material.

The influence of the host structure on the electronic properties of palladium was studied by XPS. The presence of two different oxidation states was clearly distinguishable from the Pd 3d core-level spectra (Fig. 3), at around 338.3 and 336.5 eV, respectively. Based on formal assignments, these peaks can be attributed to Pd<sup>4+</sup> (338.3 eV) and Pd<sup>2+</sup> (336.5 eV). Notably, no signal corresponding to the metallic Pd fingerprint (appearing at 334.9 eV) was detected in any of the catalysts. These observations are consistent with the expected strong interaction between the isolated atoms and hosts and the absence of nanoparticles evidenced by microscopy. Notice that the direct assignment of formal charges is debatable, and the values above are only used for reference purposes indicating the existence of palla-

dium species with differing degrees of oxidation or coordination to atoms with different electronegativity. Significant variation of the ratio of Pd<sup>2+</sup>/Pd<sup>4+</sup> was observed, ranging from 0.19 (Pd-PHI) and 0.31 (Pd-PTI) to 1.04 (Pd-GCN) and 1.32 (Pd-LMO), indicating that the strength of the metal–host interaction can be manipulated depending on the framework structure of carbon nitriles. The relatively high contribution of Pd<sup>4+</sup> in PTI and PHI is rationalized by the possible interaction of palladium with intercalated ionic species in these materials (*vide infra*). To assess the chemical state of sub-surface palladium atoms in the SACs, a depth-profiling analysis by XPS coupled with Ar<sup>+</sup> beam etching was conducted to remove the surface layer (Supplementary Fig. 7). In all cases, the Pd 3d core-level spectra are slightly shifted to higher binding energies, showing an evolution towards Pd<sup>4+</sup>. The charge assignment is done by comparison with standards and thus they might differ from the charges obtained in the DFT calculations.

To gain insight into the relative thermal stability, the distinct Pd-SACs were treated both in air at 673 K and in a flowing 5%H<sub>2</sub>/He mixture at 433 K, the latter conditions representative of those typically employed in gas-phase hydrogenation reactions [32,42]. The Pd atoms over LMO, PTI and PHI exhibit high resistance to sintering with no sign of nanoparticle formation (Supplementary Fig. 8), while abundant Pd clusters become visible at the surface of GCN. The lower stability of single atoms over GCN can be due to several reasons. Comparatively, Pd atoms bind weakly to GCN, as evidenced by the lowest average oxidation state of the metal observed by XPS and supported by DFT calculations (*vide infra*). In addition, the surface density of metal

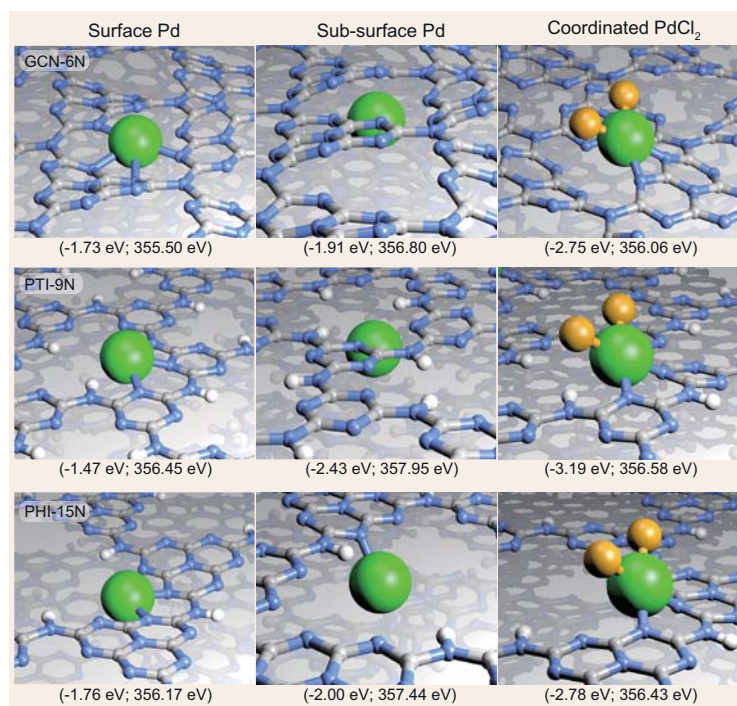


**Figure 4.** Optimized Pd coordination sites within different carbon nitride scaffolds with 6 N, 9 N and 15 N pockets. Values in parentheses beneath each image indicate the corresponding formation energies (left), calculated versus an isolated Pd atom or PdCl<sub>2</sub> coordination and the relaxed scaffold (the chlorinated system contains Mg<sup>2+</sup> counter cations between planes) and the calculated Pd 3d XPS assignments (right), respectively. The top view representations are shown in Supplementary Fig. 18. Coordinated PdCl<sub>2</sub> within GCN was calculated for reference purposes despite the absence of Cl<sup>-</sup> in GCN. Color codes: gray, C; blue, N; white, H; green, Pd; orange, Cl.

atoms in the case of GCN is significantly higher compared to the other hosts (Table 1), which could also contribute to their lower stability under thermal treatment. No reflections associated with Pd phases are observed in the XRD patterns (Supplementary Fig. 9) after calcination, in agreement with the preserved high dispersion in all cases. Note that, in the case of LMO, the appearance of a reflection at  $6.3^\circ 2\theta$  and the merging of the reflections at around  $12.6$  and  $27.4^\circ 2\theta$  after calcination indicate the likely formation of a new layered complex, which could have a similar structure to previously reported complexes between melamine and cyanuric acid [43]. On the other hand, the disappearance of the in-plane reflection peak at  $8.3^\circ$  suggests a lower stability in the case of PHI.

### DFT calculations

DFT has been employed to gain insight into the stabilization of palladium in the distinct carbon nitride scaffolds and their speciation in terms of Bader charge and XPS shift (Fig. 4, Supplementary Table 2 and Supplementary Discussion). The optimized lat-

tices present cavities with different numbers of nitrogen atoms (denoted as 6 N, 9 N and 15 N pockets for GCN, PTI and PHI, respectively). The small 6 N cavity in GCN can efficiently stabilize Pd in the center of the pocket (Pd-6 N) or alternatively by coordinating with four N atoms (Pd-4 N) between two neighboring planes. In the case of the larger cavities (9 N and 15 N), Pd is found to adsorb close to two N centers. A consistent range of Pd 3d shift was noticed during the simulation of the XPS profiles. In general, the Pd atoms preferentially reside at the subsurface layer of carbon nitrides, particularly for PTI. For all scaffolds, the surface Pd appears to be the least oxidized (Pd<sup>2+</sup>) and they are suggested to be more active than their more oxidized counterparts (Pd<sup>4+</sup>) that are buried more deeply in the material (especially in the case of PTI and PHI) and therefore less accessible, which is consistent with the XPS depth-profiling analysis. In the presence of chlorine, palladium can coordinate in the form of PdN<sub>2</sub>Cl<sub>2</sub> that is also more oxidized than their surface counterparts. The PdCl<sub>2</sub> are less likely in the smallest cavities, as they imply a larger perturbation in the scaffold. The presence of Cl<sup>-</sup> negatively affects the activity, since it lowers the *d*-band position of the Pd levels (Supplementary Table 2) and it would be necessary to cleave Pd-Cl bonds (energetically more favorable than cleavage of Pd-N bonds) to adsorb reactants. Furthermore, the incorporation of Mg<sup>2+</sup> in the subsurface vacancy of PTI and PHI steadily propels the Pd species to the surface, which would be expected to positively influence the activity. *Ab-initio* molecular dynamics (MD) simulations were conducted on Pd-GCN, highlighting the high stability of this system. Upon increasing the temperature, the Pd atoms are observed to fluctuate between the surface (less oxidized) and subsurface (more oxidized) configurations (Supplementary Fig. 10). The stability of the Pd-SACs was further assessed in the presence of O<sub>2</sub> or H<sub>2</sub>, sampling the potential energy surface with relevant intermediates (Supplementary Fig. 11). In all cases, the adsorption of oxygen is found to have a stabilizing effect. Two distinct scenarios are observed for the activation of hydrogen, which is found to occur homolytically, resulting in improved stability of the single atoms on PTI and PHI, but occurs heterolytically, slightly weakening the coordination of Pd (by 0.24 eV), on GCN with smaller cavity. The adsorption energy of 2-methyl-3-butyn-2-ol was probed, confirming the preferred interaction with surface sites (Supplementary Table 3).

### Alkyne semi-hydrogenation performance

The catalytic performance was evaluated in the semi-hydrogenation of 2-methyl-3-butyn-2-ol,

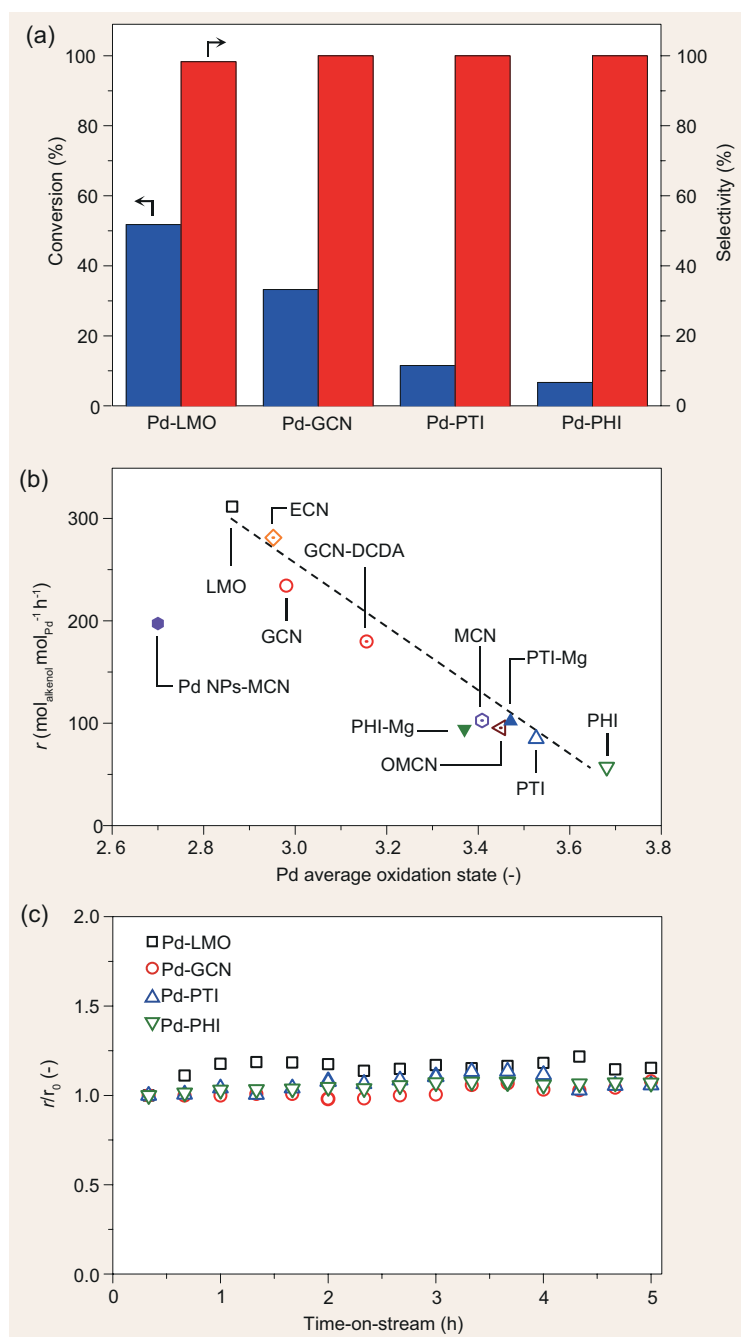


**Figure 5.** (a) Conversion and selectivity to 2-methyl-3-buten-2-ol in the hydrogenation of 2-methyl-3-buten-2-ol of Pd-SACs based on carbon nitride scaffolds of different lattice structure. (b) Correlation of the rate of 2-methyl-3-buten-2-ol formation with the palladium average oxidation state. This trend was generalized by considering additional Pd-SACs based on carbon nitrides with different morphology and ion-exchanged form, and the nanoparticle-based catalyst on a mesoporous carbon nitride host. The metal loading was  $\sim 0.5$  wt.% in all cases. Characterization data of the additional samples is shown in Supplementary Table 1. (c) The relative rate ( $r/r_0$ ) as a function of time-on-stream over Pd-SACs based on different carbon nitride scaffolds.

which is an important reaction in fine-chemical manufacturing [44]. Despite comparable metal contents of the examined SACs, Pd-LMO exhibits a significantly higher conversion (52%) than other catalysts (Pd-GCN, 33%; Pd-PTI, 11%; Pd-PHI, 7%) (Fig. 5a). Under the conditions investigated, the selectivity towards 2-methyl-3-buten-2-ol approaches 100% over all samples, evidencing the high chemoselectivity of isolated single atoms. As presented in Fig. 5b, the rate of alkenol (2-methyl-3-buten-2-ol) formation is well correlated with the average oxidation state of palladium ( $\text{Pd}_{\text{avg}}$ ). For instance, the rate over Pd-LMO with the lowest  $\text{Pd}_{\text{avg}}$  of 2.86 reaches  $311 \text{ mol}_{\text{alkenol}} \text{mol}_{\text{Pd}}^{-1} \text{h}^{-1}$ , which is more than five times higher than that observed over Pd-PHI ( $57 \text{ mol}_{\text{alkenol}} \text{mol}_{\text{Pd}}^{-1} \text{h}^{-1}$ ) with a  $\text{Pd}_{\text{avg}}$  of 3.68. These findings suggest the critical role of tuning the electronic properties of the host structure in tailoring the strength of metal–host interaction. The stability of the SACs was further evaluated in continuous mode in order to exclude the effects of deactivation due to Pd leaching or aggregation. Importantly, all Pd-SACs display a constant rate towards 2-methyl-3-buten-2-ol formation for 5 h on stream with no variation in conversion or selectivity (Fig. 5c). As additional references, four SACs based on GCN were specifically prepared from different precursor (dicyandiamide (DCDA) and different morphology (exfoliated, mesoporous and ordered mesoporous carbon nitride (denoted as ECN, MCN and OMCN)) (Supplementary Table 1). Impressively, the rates towards 2-methyl-3-buten-2-ol also fall in the same correlation, despite presenting distinct morphology and single-atom distribution. Although it cannot be assessed by standard techniques, the abundant  $-\text{NH}_x$  terminations over the oligomer were suggested to improve the accessibility of the active Pd centers. Analysis of the used catalysts confirms the virtually identical atomic dispersion (Fig. 3), electronic properties (Supplementary Fig. 12 and Supplementary Table 4) and crystalline structure (Supplementary Fig. 13) compared to the fresh materials, verifying the stability of the SACs. For reference, the traditional catalyst for the liquid-phase selective hydrogenation of alkynes based on supported lead-modified palladium nanoparticles (Lindlar catalyst, 5 wt.% Pd-3 wt.% Pb/ $\text{CaCO}_3$ ) was evaluated as a benchmark. While this catalyst yields a slightly higher rate towards 2-methyl-3-buten-2-ol ( $517 \text{ mol}_{\text{alkenol}} \text{mol}_{\text{Pd}}^{-1} \text{h}^{-1}$ ), it exhibits significantly reduced selectivity (78% to 2-methyl-3-buten-2-ol) due to over-hydrogenation (22% selectivity to 2-methyl-3-buten-2-ol). This further highlights the superior performance of the

SACs (>95% selectivity to 2-methyl-3-buten-2-ol). To address the impact of magnesium incorporation on the catalytic performance, ~0.5 wt.% Pd was introduced into PTI-Mg and PHI-Mg (Table 1, Supplementary Fig. 3 and Supplementary Fig. 14). The alkenol formation rates over Pd-PTI-Mg and Pd-PHI-Mg are 102 and 94 mol<sub>alkenol</sub> mol<sub>Pd</sub><sup>-1</sup> h<sup>-1</sup>, respectively, which is 1.2 and 1.6 times better compared to those without Mg<sup>2+</sup> incorporation, while the selectivity towards 2-methyl-3-buten-2-ol is 100% all samples. Again, the reaction rates also correlate with the palladium average oxidation state (Fig. 5b), which further demonstrates the impact of tuning metal–host interaction by tailoring the electronic properties of carbon nitride scaffolds. For comparative purposes, a nanoparticle-containing catalyst based on a mesoporous carbon nitride host (Pd NPs-MCN, with average Pd oxidation state of 2.7; see STEM image in Supplementary Fig. 15) was prepared. Evaluation of this material evidenced a lower rate towards 2-methyl-3-buten-2-ol than the expected trend (Fig. 5), which is consistent with the different metal speciation in this catalyst.

## CONCLUSIONS

This study demonstrated the obtainment of SACs on three previously unreported carbon nitride scaffolds, namely linear melem oligomers poly(triazine imides) and poly(heptazine imides). The larger cavity size and presence of chloride ions in the polyimide structures facilitate the accommodation of palladium and enhance the metal–host interaction and thus higher resistance to sintering. An inverse correlation is observed between the activity for semi-hydrogenation of 2-methyl-3-buten-2-ol and the degree of oxidation of palladium, where the oligomers exhibit the highest activity. This was further generalized over additional previously reported materials, highlighting the critical importance of controlling the oxidation state of isolated metal atoms. The intercalated alkaline metals within the network of PTI and PHI were demonstrated to be able to exchange with other ions such as magnesium, presenting another opportunity to tune the catalytic performance in hydrogenation. The least oxidized surface Pd<sup>2+</sup> species are suggested to be more active than the Pd<sup>4+</sup> species that reside deeper in the material; however, this high positive charge can also appear if some ligand remains as PdN<sub>2</sub>Cl<sub>2</sub> coordination appears. The findings provide an opportunity to systemically design effective SACs to boost the atom efficiency at an atomic level by constructing the host lattice structure.

## METHODS

### Carbon nitride synthesis

LMO and polymeric GCN were prepared by calcining melamine (8 g) at the desired temperature (723 K for LMO and 823 K for GCN with a ramp rate of 2.3 K min<sup>-1</sup>) in a crucible for 4 h under a nitrogen flow (15 cm<sup>3</sup> min<sup>-1</sup>). PTI and PHI were prepared by ball milling eutectic salt mixtures of LiCl (4.52 g)/KCl (5.48 g) together with a corresponding precursor (melamine (1 g) for PTI and 3-amino-1,2,4-triazole-5-thiol (2 g) for PHI) for 10 min, in a Retsch PM 100 bioMETA planetary ball mill (500 rpm). Afterwards, the mixtures were transferred into a crucible and calcined at 823 K for 4 h (ramp rate, 2.3 K min<sup>-1</sup>) under a nitrogen flow (15 cm<sup>3</sup> min<sup>-1</sup>). The resulting products were washed with hot water for 48 h to remove any excess salts. Finally, the carbon nitride products were collected by filtration, washed thoroughly with distilled water and ethanol, and dried at 338 K overnight.

### Metal introduction by microwave-assisted deposition

Different carbon nitride hosts (0.5 g) was first dispersed in H<sub>2</sub>O (20 cm<sup>3</sup>) under sonication for 1 h. Then, an aqueous solution of Pd(NH<sub>3</sub>)<sub>4</sub>(NO<sub>3</sub>)<sub>2</sub> containing 5 wt.% Pd (0.05 cm<sup>3</sup>, targeting 0.5 wt.%; 0.2 cm<sup>3</sup>, targeting 2 wt.%) was added and stirred overnight for complete adsorption. The resulting solution was placed in a microwave reactor (CEM Discover SP), applying a cyclic program (20 repetitions) of irradiation (15 s) and cooling (3 min) using a power of 100 W. The resulting powder was collected by filtration, washed with distilled water and ethanol, and dried at 333 K overnight.

### Ion exchange

In a typical synthesis, PTI or PHI (0.7 g) was dispersed in an aqueous solution of MgCl<sub>2</sub>·6H<sub>2</sub>O (3.4 g, 20 cm<sup>3</sup>) and then stirred at room temperature for 24 h, after which the solids were collected by centrifugation. These steps were repeated three times and the products were thoroughly washed with water and ethanol, and subsequently dried at 338 K overnight. The samples are denoted as PTI-Mg and PHI-Mg.

### Characterization

XRD was performed in a PANalytical X'Pert PRO-MPD diffractometer operated in Bragg-Brentano geometry using Ni-filtered Cu K $\alpha$  ( $\lambda = 0.1541$  nm)

radiation. Data were recorded in the range of  $5\text{--}60^\circ$   $2\theta$  with an angular step size of  $0.05^\circ$  and a counting time of 2 s per step. DRIFTS was performed using a Bruker Optics Vertex 70 spectrometer equipped with a high-temperature DRIFT cell (Harrick) and an MCT detector. The samples were pretreated at 423 K for 1 h under Ar before analysis. Spectra were recorded in the range of  $4000\text{--}400\text{ cm}^{-1}$  under Ar flow ( $20\text{ cm}^3\text{ min}^{-1}$ ) and at room temperature by co-addition of 64 scans with a nominal resolution of  $4\text{ cm}^{-1}$ . The  $^{13}\text{C}$  solid-state cross-polarization/magic angle spinning nuclear magnetic resonance (CP/MAS NMR) spectra were recorded on a Bruker AVANCE III HD NMR spectrometer at a magnetic field of 16.4 T corresponding to a  $^1\text{H}$  Larmor frequency of 700.13 MHz. A 4-mm double resonance probe head at a spinning speed of 10 kHz was used for all experiments. The  $^{13}\text{C}$  spectra were acquired using a cross-polarization experiment with a contact time of 2 ms and a recycle delay of 1 s. A total of  $64 \times 10^3$  scans were added for each sample. Between  $39 \times 10^3$  and  $96 \times 10^3$  scans were acquired, depending on the sample. The  $^{13}\text{C}$  experiments used high-power  $^1\text{H}$  decoupling during acquisition using a SPINAL-64 sequence. X-ray photoelectron spectroscopy (XPS) was performed in a Physical Electronics Instruments Quantum 2000 spectrometer using monochromatic Al  $K\alpha$  radiation generated from an electron beam operated at 15 kV and 32.3 W. The spectra were collected under ultra-high vacuum conditions (residual pressure =  $5 \times 10^{-8}$  Pa) at a pass energy of 46.95 eV. All spectra were referenced to the C 1s peak of ternary carbon at 288.3 eV. Prior to peak deconvolution, X-ray satellites and inelastic background (Shirley type) were subtracted for all the spectra. The Pd average oxidation state was calculated based on the relative content determined by the peak area of different palladium species from Pd 3d core-level XPS spectra. Elemental analysis was determined by infrared spectroscopy using a LECO CHN-900 combustion furnace. Inductively coupled plasma-optical emission spectrometry (ICP-OES) was conducted using a Horiba Ultra 2 instrument equipped with photomultiplier tube detection. The samples were dissolved in a piranha solution and left under sonication until the absence of visible solids in the solution. SEM images were acquired using a Zeiss ULTRA 55 operated at 5 kV. Argon sorption was measured at 77 K in a Micrometrics 3Flex instrument, after evacuation of the samples at 423 K for 10 h. The specific surface area was determined via the Brunauer-Emmett-Teller (BET) method. Samples for TEM studies were prepared by dusting respective powders onto lacey-carbon-coated copper or nickel grids. High-resolution

TEM, conventional STEM, and energy-dispersive X-ray spectroscopy (EDX) measurements were performed on a Talos F200X instrument operated at 200 kV and equipped with an FEI SuperX detector. Thin cross-sections were prepared by embedding the powder in a suitable resin (Polysciences Inc., Hard Grade) followed by cutting the sections (100 nm) with a diamond knife. The sections were mounted on carbon-coated copper grids. AC-HAADF-STEM was performed using an FEI Titan<sup>3</sup> 80–300 (Thermo Fisher Scientific) microscope equipped with a high-brightness extreme field emission gun and a CEOS (Corrected Electron Optical Systems GmbH) aberration corrector for the probe-forming lenses, operated at 300 kV. The AC-STEM images were acquired with an illumination semi-angle of 18 mrad and a detector inner semi-angle greater than 35 mrad, chosen to minimize any possible Bragg diffraction contrast and maximize overall image signal and especially atomic number ( $Z$ ) contrast between Pd atoms/clusters and the underlying support. Images were obtained in suitably thin regions of the specimen for minimal background from the support and for reduced overlap of Pd atoms. Per-pixel dwell times of 5–10  $\mu\text{s}$  and probe currents of 40–60 pA were selected to achieve sufficient signal-to-noise for single Pd atom visibility whilst minimizing beam-induced changes, providing images representative of the Pd atom species and their distribution on the LMO, GCN, PTI and PHI hosts.

### Hydrogenation of 2-methyl-3-butyn-2-ol

The hydrogenation was carried out in a microwave reactor (CEM Discover SP) with a pressure-controlled vessel under continuous stirring. In a typical reaction, the feed solution containing 0.4 M substrate in toluene ( $1.5\text{ cm}^3$ ) was microwaved in the presence of the catalyst (15 mg) for 1 h at 323 K. The initial hydrogen pressure was 3 bar in all experiments. The resulting reaction mixture was filtered (pore size,  $0.45\text{ }\mu\text{m}$ ) and the products were collected. The continuous tests were carried out in a flooded-bed micro-reactor (ThalesNano H-Cube Pro<sup>TM</sup>), in which the liquid-feed-containing 0.4-M substrate in toluene and gaseous hydrogen (generated *in situ* by Millipore water electrolysis) flowed concurrently upward through a cylindrical cartridge (3.5-mm internal diameter) containing a fixed bed of catalyst (0.1 g) and silicon carbide (0.2 g) particles, both with a size of 0.2–0.4 mm. The reactions were conducted at  $T = 323\text{ K}$ ,  $P = 3\text{ bar}$ , liquid ( $1\text{ cm}^3\text{ min}^{-1}$ ) and  $\text{H}_2$  ( $36\text{ cm}^3\text{ min}^{-1}$ ) flow rates. The products were collected every 20 min after reaching steady state. All collected samples

were analyzed offline using a gas chromatograph (HP-6890) equipped with a HP-5 capillary column and a flame ionization detector. The conversion ( $X$ ) of the substrate was determined as the amount of reacted substrate divided by the amount of substrate at the reactor inlet. The selectivity ( $S$ ) to each product was quantified as the amount of the particular product divided by the amount of reacted substrate. The reaction rate ( $r$ ) was expressed as the number of moles of product formed per mole of Pd and unit of time.

### DFT simulations

Slab models representing different carbon nitride scaffolds have been described through the DFT as implemented in the Vienna Ab initio Simulation Package (VASP) code [45], using the Perdew-Burke-Ernzerhof (PBE) functional together with D3 dispersion terms [46,47]. Core electrons were replaced by projector augmented wave (PAW) method [48] and the valence electrons were expanded in plane waves with a kinetic cut-off energy of 450 eV. The bulk structures were derived from our previous carbon nitride system by expanding the building motifs. The  $k$ -point densities were  $5 \times 5 \times 5$  for GCN and PTI system and  $3 \times 3 \times 5$  for PHI. Slab models were cut along the van der Waals planes; the slabs contain four layers and are interleaved by at least 12 Å of vacuum. The optimized crystal lattices are presented in the Supplementary Material. The  $k$ -point sampling in these cases was  $3 \times 3 \times 1$  (GCN and PTI) and  $1 \times 1 \times 1$  (PHI). The PdCl<sub>2</sub> precursor and Pd atoms were anchored at different positions in the cavities and within the two uppermost layers, which are preferential sites for the simplest carbon nitrides as observed in first-principles MD. The Heyd-Scuseria-Ernzerhof (HSE03) [49] functional was used to generate the partial density of states (PDOS) of the relaxed structures, including 25% of exact Hartree-Fock exchange. *Ab-initio* MD simulations were conducted on the Perdew-Burke-Ernzerhof (PBE) level, and comprised heating/equilibration cycles in which the system was heated to 500 K with a cycle step of 100 K for a total duration of 10 ps. The structures can be retrieved from the ioChem-BD database [50] at the following dataset: DOI:10.19061/iochem-bd-1-75.

### SUPPLEMENTARY DATA

Supplementary data are available at NSR online.

### ACKNOWLEDGEMENTS

ScopeM at ETH Zurich for access to its facilities. The service of Microelemental Analysis at ETH Zurich for CHN analysis. BSC-RES for providing generous computational resources. Dr R. Verel for NMR measurements. Dr A.J. Martin for SEM measurements.

### FUNDING

This work was supported by ETH Zurich, the Swiss National Science Foundation (200021-169679), the Spanish Ministerio de Economía y Competitividad (CTQ2015-68770-R) and the European Research Council under the European Union's Seventh Framework Program (291522-3DIMAGE). E.F. thanks the Spanish Ministerio de Economía y Competitividad (MINECO) La Caixa-Severo Ochoa for a pre-doctoral grant through Severo Ochoa Excellence Accreditation 2014-2018 (SEV-2013-0319). S.M.C. acknowledges support from the Henslow Research Fellowship at Girton College, Cambridge.

*Conflict of interest statement.* None declared.

### REFERENCES

1. Qiao B, Wang A and Yang X *et al.* Single-atom catalysis of CO oxidation using Pt<sub>1</sub>/FeO<sub>x</sub>. *Nat Chem* 2011; **3**: 634-41.
2. Kamiya K, Kamai R and Hashimoto K *et al.* Platinum-modified covalent triazine frameworks hybridized with carbon nanoparticles as methanol-tolerant oxygen reduction electrocatalysts. *Nat Commun* 2014; **5**: 5040.
3. Lucci FR, Liu J and Marcinkowski MD *et al.* Selective hydrogenation of 1,3-butadiene on platinum-copper alloys at the single-atom limit. *Nat Commun* 2015; **6**: 8550.
4. Wei H, Liu X and Wang A *et al.* FeO<sub>x</sub>-supported platinum single-atom and pseudo-single-atom catalysts for chemoselective hydrogenation of functionalized nitroarenes. *Nat Commun* 2014; **5**: 5634.
5. Kyriakou G, Boucher MB and Jewell AD *et al.* Isolated metal atom geometries as a strategy for selective heterogeneous hydrogenations. *Science* 2012; **335**: 1209-12.
6. Sun S, Zhang G and Gauquelin N *et al.* Single-atom catalysis using Pt/graphene achieved through atomic layer deposition. *Sci Rep* 2013; **3**: 1775.
7. Taylor HS. A theory of the catalytic surface. *Proc R Soc London Ser A* 1925; **108**: 105-11.
8. Wang Y, Wang X and Antonietti M. Polymeric graphitic carbon nitride as a heterogeneous organocatalyst: from photochemistry to multipurpose catalysis to sustainable chemistry. *Angew Chem Int Ed* 2012; **51**: 68-89.
9. Thomas A, Fischer A and Goettmann F *et al.* Graphitic carbon nitride materials: variation of structure and morphology and their use as metal-free catalysts. *J Mater Chem* 2008; **18**: 4893-908.
10. Liu AY and Cohen ML. Prediction of new low compressibility solids. *Science* 1989; **245**: 841-2.
11. Molina B and Sansores LE. Electronic structure of six phases of C<sub>3</sub>N<sub>4</sub>: a theoretical approach. *Mod Phys Lett B* 1999; **13**: 193-201.

12. Lin Z and Wang X. Nanostructure engineering and doping of conjugated carbon nitride semiconductors for hydrogen photosynthesis. *Angew Chem Int Ed* 2013; **52**: 1735–8.
13. Wang X, Chen X and Thomas A *et al.* Metal-containing carbon nitride compounds: a new functional organic–metal hybrid material. *Adv Mater* 2009; **21**: 1609–12.
14. Chen X, Zhang J and Fu X *et al.* Fe-g-C<sub>3</sub>N<sub>4</sub>-catalyzed oxidation of benzene to phenol using hydrogen peroxide and visible light. *J Am Chem Soc* 2009; **131**: 11658–9.
15. Kroke E, Schwarz M and Horath-Bordon E *et al.* Tri-s-triazine derivatives. Part I. From trichloro-tri-s-triazine to graphitic C<sub>3</sub>N<sub>4</sub> structures. *New J Chem* 2002; **26**: 508–12.
16. Liu J, Wang H and Antonietti M. Graphitic carbon nitride ‘reloaded’: emerging applications beyond (photo)catalysis. *Chem Soc Rev* 2016; **45**: 2308–26.
17. Chen ZP, Antonietti M and Dontsova D. Enhancement of the photocatalytic activity of carbon nitrides by complex templating. *Chem Eur J* 2015; **21**: 10805–11.
18. Fina F, Callear SK and Carins GM *et al.* Structural investigation of graphitic carbon nitride via XRD and neutron diffraction. *Chem Mater* 2015; **27**: 2612–8.
19. Wang X, Maeda K and Thomas A *et al.* A metal-free polymeric photocatalyst for hydrogen production from water under visible light. *Nat Mater* 2009; **8**: 76–80.
20. Sattler A, Pagano S and Zeuner M *et al.* Melamine-melam adduct phases: investigating the thermal condensation of melamine. *Chem Eur J* 2009; **15**: 13161–70.
21. Kessler FK, Zheng Y and Schwarz D *et al.* Functional carbon nitride materials-design strategies for electrochemical devices. *Nat Rev Mater* 2017; **2**: 17030.
22. Doblinger M, Lotsch BV and Wack J *et al.* Structure elucidation of polyheptazine imide by electron diffraction—a templated 2D carbon nitride network. *Chem Commun* 2009; 1541–3.
23. Wirmhier E, Doblinger M and Gunzelmann D *et al.* Poly(triazine imide) with intercalation of lithium and chloride ions [(C<sub>3</sub>N<sub>3</sub>)<sub>2</sub>(NH<sub>x</sub>Li<sub>1-x</sub>)<sub>3</sub>•LiCl]: a crystalline 2d carbon nitride network. *Chem Eur J* 2011; **17**: 3213–21.
24. Bojdys MJ, Müller J-O and Antonietti M *et al.* Ionothermal synthesis of crystalline, condensed, graphitic carbon nitride. *Chem Eur J* 2008; **14**: 8177–82.
25. Dontsova D, Pronkin S and Wehle M *et al.* Triazoles: a new class of precursors for the synthesis of negatively charged carbon nitride derivatives. *Chem Mater* 2015; **27**: 5170–9.
26. Savateev A, Dontsova D and Kurpil B *et al.* Highly crystalline poly(heptazine imides) by mechanochemical synthesis for photooxidation of various organic substrates using an intriguing electron acceptor-elemental sulfur. *J Catal* 2017; **350**: 203–11.
27. Liang Q, Huang Z-H and Kang F *et al.* Facile synthesis of crystalline polymeric carbon nitrides with an enhanced photocatalytic performance under visible light. *ChemCatChem* 2015; **7**: 2897–902.
28. Chen Z, Savateev A and Pronkin S *et al.* ‘The easier the better’ preparation of efficient photocatalysts—metastable poly(heptazine imide) salts. *Adv Mater* 2017; **29**: 1700555.
29. Vilé G, Albani D and Nachtegaal M *et al.* A stable single-site palladium catalyst for hydrogenations. *Angew Chem Int Ed* 2015; **54**: 11265–9.
30. Chen Z, Pronkin S and Fellinger T-P *et al.* Merging single-atom-dispersed silver and carbon nitride to a joint electronic system via copolymerization with silver tricyanomethanide. *ACS Nano* 2016; **10**: 3166–75.
31. Li X, Bi W and Zhang L *et al.* Single-atom Pt as co-catalyst for enhanced photocatalytic H<sub>2</sub> evolution. *Adv Mater* 2016; **28**: 2427–31.
32. Huang X, Xia Y and Cao Y *et al.* Enhancing both selectivity and coking-resistance of a single-atom Pd<sub>1</sub>/C<sub>3</sub>N<sub>4</sub> catalyst for acetylene hydrogenation. *Nano Res* 2017; **10**: 1302–12.
33. Chen Z, Mitchell S and Vorobyeva E *et al.* Stabilization of single metal atoms on graphitic carbon nitride. *Adv Funct Mater* 2017; **27**: 1605785.
34. Liu W, Cao L and Cheng W *et al.* Single-site active cobalt-based photocatalyst with a long carrier lifetime for spontaneous overall water splitting. *Angew Chem Int Ed* 2017; **56**: 9312–7.
35. Vorobyeva E, Chen Z and Mitchell S *et al.* Tailoring the framework composition of carbon nitride to improve the catalytic efficiency of the stabilised palladium atoms. *J Mater Chem A* 2017; **5**: 16393–403.
36. Zheng Y, Jiao Y and Zhu Y *et al.* Molecule-level g-C<sub>3</sub>N<sub>4</sub> coordinated transition metals as a new class of electrocatalysts for oxygen electrode reactions. *J Am Chem Soc* 2017; **139**: 3336–9.
37. Lau VW-h, Mesch MB and Duppel V *et al.* Low-molecular-weight carbon nitrides for solar hydrogen evolution. *J Am Chem Soc* 2015; **137**: 1064–72.
38. Lotsch BV, Doblinger M and Sehnert J *et al.* Unmasking melon by a complementary approach employing electron diffraction, solid-state NMR spectroscopy, and theoretical calculations—structural characterization of a carbon nitride polymer. *Chem Eur J* 2007; **13**: 4969–80.
39. Zimmerman JL, Williams R and Khabashesku VN *et al.* Synthesis of spherical carbon nitride nanostructures. *Nano Lett* 2001; **1**: 731–4.
40. Komatsu T. Attempted chemical synthesis of graphite-like carbon nitride. *J Mater Chem* 2001; **11**: 799–801.
41. Chong SY, Jones JTA and Khimyak YZ *et al.* Tuning of gallery heights in a crystalline 2D carbon nitride network. *J Mater Chem A* 2013; **1**: 1102–7.
42. Yan H, Cheng H and Yi H *et al.* Single-atom Pd<sub>1</sub>/graphene catalyst achieved by atomic layer deposition: remarkable performance in selective hydrogenation of 1,3-butadiene. *J Am Chem Soc* 2015; **137**: 10484–7.
43. Jun Y-S, Lee EZ and Wang X *et al.* From melamine-cyanuric acid supramolecular aggregates to carbon nitride hollow spheres. *Adv Funct Mater* 2013; **23**: 3661–7.
44. Vernuccio S, von Rohr PR and Medlock J. General kinetic modeling of the selective hydrogenation of 2-methyl-3-butyn-2-ol over a commercial palladium-based catalyst. *Ind Eng Chem Res* 2015; **54**: 11543–51.
45. Kresse G and Furthmüller J. Efficient iterative schemes for ab initio total-energy calculations using a plane-wave basis set. *Phys Rev B* 1996; **54**: 11169–86.
46. Perdew JP, Chevary JA and Vosko SH *et al.* Atoms, molecules, solids, and surfaces: applications of the generalized gradient approximation for exchange and correlation. *Phys Rev B* 1992; **46**: 6671–87.
47. Grimme S, Antony J and Ehrlich S *et al.* A consistent and accurate ab initio parametrization of density functional dispersion correction (DFT-D) for the 94 elements H–Pu. *J Chem Phys* 2010; **132**: 154104.
48. Kresse G and Joubert D. From ultrasoft pseudopotentials to the projector augmented-wave method. *Phys Rev B* 1999; **59**: 1758–75.
49. Heyd J, Scuseria GE and Ernzerhof M. Hybrid functionals based on a screened coulomb potential. *J Chem Phys* 2003; **118**: 8207–15.
50. Álvarez-Moreno M, de Graaf C and López N *et al.* Managing the computational chemistry big data problem: the ioChem-BD platform. *J Chem Inf Model* 2015; **55**: 95–103.

## CHEMISTRY

Special Topic: Single-Atom Catalysts

**Single-atom catalyst: a rising star for green synthesis of fine chemicals**Leilei Zhang<sup>1,†</sup>, Yujing Ren<sup>1,2,†</sup>, Wengang Liu<sup>1,2,†</sup>, Aiqin Wang<sup>1,\*</sup> and Tao Zhang<sup>1,\*</sup>**ABSTRACT**

The green synthesis of fine chemicals calls for a new generation of efficient and robust catalysts. Single-atom catalysts (SACs), in which all metal species are atomically dispersed on a solid support, and which often consist of well-defined mononuclear active sites, are expected to bridge homogeneous and heterogeneous catalysts for liquid-phase organic transformations. This review summarizes major advances in the SAC-catalysed green synthesis of fine chemicals in the past several years, with a focus on the catalytic activity, selectivity and reusability of SACs in various organic reactions. The relationship between catalytic performance and the active site structure is discussed in terms of the valence state, coordination environment and anchoring chemistry of single atoms to the support, in an effort to guide the rational design of SACs in this special area, which has traditionally been dominated by homogeneous catalysis. Finally, the challenges remaining in this research area are discussed and possible future research directions are proposed.

**Keywords:** single-atom catalysts, fine chemicals, green synthesis, structure–reactivity relationship, heterogeneous catalysis

**INTRODUCTION**

Fine chemicals (<1000 tons/year) are important and valuable (>\$10/kg) ingredients and intermediates for the manufacture of pharmaceuticals, agrochemicals and other specialty chemicals such as adhesives, sealants, dyestuffs, pigments, flavors, fragrances, food additives, biocides and corrosion inhibitors [1]. Due to their high purity, specialized nature, technology intensiveness and high added value, the manufacture of fine chemicals is always among the most active and strategic areas of the chemical industries [2].

Traditional synthetic routes for fine chemicals generally involve stoichiometric chemical reactions or use hazardous catalysts and thus produce serious environmental pollution and waste; the quantity of unwanted by-products may even exceed the amount of the desired products produced. Typical examples include the coupling of aromatic compounds with diazonium salts derived from stoichiometric amounts of nitrite salts to synthesize

aromatic azo compounds [3] and the stoichiometric reduction of nitroarenes by iron metal to produce functional anilines [4]. With the increasing concern for the environment and safety, there is an urgent demand for the development of new, mild, efficient and straightforward methodologies and catalysts to achieve the green and sustainable synthesis of fine chemicals [5]. Such green strategies are characterized by several principles: atom-efficient catalytic processes, environmentally benign reagents and solvents, and one-pot tandem synthetic routes. On these grounds, a great number of efficient organometallic compounds and accompanying straightforward synthetic processes have been developed, which led to the flourishing of the fine chemical industry in the twentieth century, such as homogeneous Rh catalysts for hydroformylation reactions of olefins [6,7]. However, although these transition metal complexes exhibit high catalytic activity and selectivity, they are usually sensitive to moisture and/or air and are difficult to separate from

<sup>1</sup>State Key Laboratory of Catalysis, Dalian Institute of Chemical Physics, Chinese Academy of Sciences, Dalian 116023, China and <sup>2</sup>University of Chinese Academy of Sciences, Beijing 100049, China

\*Corresponding authors. E-mails: aqwang@dicp.ac.cn; taozhang@dicp.ac.cn  
†Equally contributed to this work.

Received 20 April 2018; Revised 24 June 2018; Accepted 31 July 2018



the products, which sometimes leads to the contamination of the products. With the rapid growth of nanoscience, heterogeneous catalysts, mainly supported transition metal nanoparticles, have been exploited to tackle these problems; however, their overall catalytic efficiencies are usually inferior to their homogeneous analogs. Therefore, the development of a new class of catalysts that integrates the merits of homogeneous and heterogeneous catalysts for the green synthesis of fine chemicals is highly desirable.

Single-atom catalysts (SACs) are defined as catalysts in which all of the active metal species exist as isolated single atoms stabilized by the support of or by alloying with another metal [8,9]. Since the seminal work of Zhang, Li, Liu and coworkers, who reported in 2011 that the  $\text{Pt}_1/\text{FeO}_x$  SAC was three times more active than its nano-Pt counterpart for CO oxidation [8], single-atom catalysis has become a new frontier in heterogeneous catalysis. SACs are distinguished from nanoparticle (NP) catalysts in that they do not contain metal–metal bonds and that the single metal atoms are usually positively charged. These unique geometric and electronic properties bring about significant alterations in the interactions with reactants/intermediates/products, leading to enhanced activity and/or selectivity, which are particularly desired for fine-chemicals production. Therefore, SACs are expected to combine the advantages of high catalytic activity, selectivity, stability and reusability for the green synthesis of fine chemicals. The past seven years have confirmed this expectation; a variety of SACs have been developed and have demonstrated excellent catalytic performance for various organic transformations, including selective hydrogenation, oxidation, hydroformylation and C–C coupling reactions. For example,  $\text{FeO}_x$ -supported Pt single-atom and pseudo-single-atom catalysts exhibited the best catalytic activity (at least 20-fold more active than any previously reported catalyst) and selectivity ( $\sim 99\%$ ) for the rather challenging selective hydrogenation of 3-nitrostyrene [10]; single-atom  $\text{Rh}_1/\text{ZnO}$  catalysts showed comparable activity to the benchmark homogeneous catalyst  $\text{RhCl}(\text{PPh}_3)_3$  in the hydroformylation reaction of olefins [11]; and non-precious-metal  $\text{Co}(\text{Fe})\text{-N-C}$  catalysts demonstrated ‘platinum-like’ performance for selective hydrogenation or oxidation reactions [12–18].

This review summarizes recent advances in SAC-catalysed organic reactions for the green synthesis of fine chemicals under liquid-phase reaction conditions—an area in which SACs are expected to find wide application and bridge homogeneous and heterogeneous catalysis. It should be mentioned that many of the examples discussed in this review are

only simple model reactions, rather than real fine chemical substrates or intermediates. As preparation methods and characterization techniques for SACs have been described in detail in several recent excellent reviews [19–24], they are not emphasized in this review. The focus of this review is the catalytic performance of SACs in organic transformations as well as the coordination structure and oxidation state of the central single metal atoms. The stabilization mechanisms of the single atoms against leaching or aggregation in the liquid phase are also discussed. The aim of this review is to provide illustrative accounts of the recent progress in this research field and to extract fundamental principles to guide the rational design of SACs for green chemical synthesis.

## SYNTHESIS OF FINE CHEMICALS PROMOTED BY SACs

SACs, with their well-defined mononuclear structures, have been expected to bridge homogeneous and heterogeneous catalysis since the term ‘SAC’ was first introduced in 2011 [8,9]. Over the past years, various supported SACs have been tested for a plethora of organic transformations, including selective hydrogenation of nitroarenes, ketones, alkynes and alkenes; selective oxidation of alcohols to aldehydes and ketones, of benzene to phenol and of silanes to silanols; hydroformylation of olefins; C–C coupling reactions; and biomass-related hydrodeoxygenation reactions. Compared with their NP counterparts, SACs afford enhanced activity by a factor of several to hundreds per metal atom and unparalleled selectivity in some reactions. The excellent stability of SACs provides additional advantages over their homogeneous analogs. While the active site structures of SACs may be less uniform than those of homogeneous catalysts due to their heterogeneous support surface, the well-defined structures arising from the coordination between single atoms and the support provide SACs with promising properties to mimic homogeneous catalysis in organic transformations.

### Catalytic hydrogenation

Catalytic hydrogenations of unsaturated organic compounds represent one of the most important classes of chemical transformations and are widely applied in both the chemical industry and laboratory organic synthesis [25]. The majority of hydrogenation reactions involve the direct use of  $\text{H}_2$  as the hydrogen source and are catalysed by VIII–X group metals such as Ni, Pd, Ru and Pt.

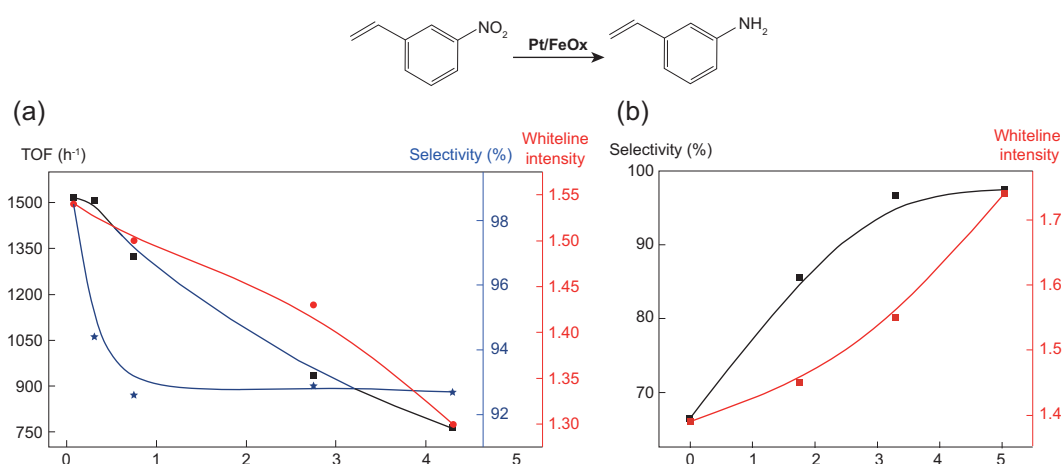


**Figure 1.** The dependence of activity/selectivity on the Pt content of the Pt/FeO<sub>x</sub> catalysts (a) and on the Na content of the Na-2.16%Pt/FeO<sub>x</sub> catalysts (b) for the chemoselective hydrogenation of 3-nitrostyrene, as well as the correlation between activity/selectivity and the oxidation state (white-line intensity) of Pt in the two systems.

The manufacture of functional anilines is of great significance in the chemical industry due to their versatility in biologically active natural products, agrochemicals, pharmaceuticals, dyes and ligands of organometallic complexes [4,26,27]. Compared with traditional synthetic methodologies (e.g. reduction by the transition metals iron and tin), catalytic hydrogenation is more efficient and environmentally benign. However, when one or more reducible organic groups (e.g. C = C) are present on the aryl ring containing the nitro group, the chemoselective hydrogenation of the nitro group is very challenging. Modification of the transition metal catalysts with proper additives achieved enhanced selectivity [28]; however, the catalytic activity was severely compromised. The hydrogenation of the nitro group is generally considered to be size-insensitive, whereas the reduction of the C = C group is highly sensitive to the size of the transition metal, with the reaction rate increasing with particle size [29]. Consequently, downsizing the active metal to its ultimate dispersion, namely single-atom dispersion, is expected to accomplish excellent chemoselectivity by suppressing the C = C double bond hydrogenation. Zhang, Wang and coworkers designed a FeO<sub>x</sub>-supported Pt single/pseudo-single-atom catalyst. The term ‘pseudo-single-atom catalyst’ indicates a special structure composed of a few to tens of atoms that are loosely and randomly associated with each other, but do not form strong metallic bonds, and thus show structure and function similar to that of isolated single atoms. The catalyst was able to hydrogenate a broad scope of nitroarenes with different functional groups to the corresponding functionalized anilines with a turnover frequency (TOF) as high as 1514 h<sup>-1</sup> and a chemoselectivity above 95% [10]. The loading of Pt on the

FeO<sub>x</sub> support had a significant effect on both the activity and chemoselectivity. As shown in Fig. 1a, both the activity per metal atom (TOF) and the chemoselectivity increased with decreasing Pt content until atomic dispersion was reached at 0.08 wt% Pt, at which the catalyst contained exclusively single atoms of Pt, and therefore achieved the highest activity and chemoselectivity (98.6% at a conversion of 96.5%). Interestingly, the white-line intensity of Pt in XANES (X-ray Adsorption Near-Edge Structure spectroscopy), which reflects the oxidation state of Pt, followed the same trend as the catalytic activity and chemoselectivity—that is, the higher the oxidation state, the higher the activity and chemoselectivity. This result indicated that the isolated, positively charged Pt on the FeO<sub>x</sub> support acted as the main active site for the chemoselective hydrogenation of functionalized nitroarenes. Keeping this point in mind, and considering that the alkali metals could yield positively charged metal centers and also promote the dispersion of metal species [30,31], the same authors further tuned the electronic properties of the Pt center by introducing alkali metals to the high-Pt-loading catalyst (2.16 wt% Pt/FeO<sub>x</sub>) [32]. By increasing the amount of Na to 5.03 wt%, the chemoselectivity increased remarkably from 66.4 to 97.4% (Fig. 1b); concurrently, the oxidation state of Pt increased as well. Moreover, detailed EXAFS (extended X-ray absorption fine structure) data analysis reveals that the structure of the central Pt sites changes with varying the amount of sodium; the Pt–Pt contribution decreases while the Pt–O contribution increases. Consistently with this trend, HAADF-STEM (high angle annular dark field scanning transmission electron microscopy) images clearly show that the Pt particles in the Na-containing samples all featured

abundant dark regions, which are probably due to lighter elements such as Na and Fe. In combination with the  $^{57}\text{Fe}$  Mössbauer spectroscopy result that the  $\text{NaFeO}_2$  species forms in the Na-containing sample, the authors proposed that the active sites were likely Pt–O–Na–O–Fe species. This scenario is reminiscent of that of a homogeneous catalyst, if the Na–O–Fe surrounding the single-atom Pt center is viewed as a robust ligand bridged by oxygen. Due to the higher contribution from Pt–O bonding than Pt–Pt bonding, the performance of this Na-modified Pt/ $\text{FeO}_x$  catalyst is quite similar to that of the SAC in terms of activity and selectivity. Nevertheless, in comparison to the SACs with relatively low metal loading, (e.g. 0.08% Pt/ $\text{FeO}_x$ ), the high-metal-loading Na-modified Pt/ $\text{FeO}_x$  catalysts afforded a more than 20-fold increase in the productivity (activity per catalyst mass, rather than per Pt), which is of high importance in practical applications. In order to make the process more environmentally benign, the authors further studied the reaction in a  $\text{CO}_2$ -expanded toluene/THF system. The results showed that both the conversion and chemoselectivity could reach above 95% over Pt/ $\text{FeO}_x$  SAC, while the amount of the solvent toluene could be reduced by 90% in the  $\text{CO}_2$ -expanded toluene system [33].

It is noted that, even with the same single-atom dispersion and the same support, the activity and chemoselectivity of an SAC may vary depending on the intrinsic properties of the metal used. For example, while both Pt<sub>1</sub>/ $\text{FeO}_x$  and Ir<sub>1</sub>/ $\text{FeO}_x$  SACs are highly chemoselective towards the hydrogenation of 3-nitrostyrene to 3-aminostyrene, the Pd/ $\text{FeO}_x$  SAC is poorly selective (selectivity lower than 20%) for this reaction due to the intrinsically high activity of Pd towards the hydrogenation of C = C bonds [10]. Similarly, Zhang *et al.* found that sub-nanometric Pd clusters supported on  $\text{CeO}_2$  nanorods were highly active (TOF as high as  $44\,059\text{ h}^{-1}$ ) for hydrogenation of 4-nitrophenol and chemoselective for a broad scope of nitroarenes containing –OH, –X, –C = O and –CN groups, but poorly selective for substrates possessing a –C = C group [34]. It would be highly interesting to engineer the metal–support interaction to develop a new Pd SAC that is both highly active and chemoselective for the hydrogenation of nitro-styrenes.

The reaction mechanism of the chemoselective hydrogenation of nitroarenes over SACs has yet to be clarified. The results of control experiments involving the competitive adsorption of nitrobenzene and styrene revealed that the unique selectivity of SACs is not due to their intrinsically low activity for styrene hydrogenation, but instead due to the favorable adsorption of the nitro group in the presence of –C = C group [10], which is similar to

the case behavior of the nanogold catalyst as well as the  $\text{TiO}_2$ -decorated nano-Pt catalyst [29,35]. Based on Fourier transform infrared spectroscopy (FT-IR) and density functional theory (DFT) theoretical studies [36], the nitro group is preferentially adsorbed on the support; the oxygen vacancies on the support surface (e.g. reducible supports like  $\text{FeO}_x$  and  $\text{CeO}_2$ ) or the basicity of the support (e.g. the addition of Na increases the basicity of the support in the above-mentioned work) facilitate the preferential adsorption of the nitro group. This interaction can be understood in terms of Lewis acid–base interactions. The oxygen atoms in the nitro group are Lewis bases, while the oxygen vacancies of the reducible support act as Lewis acids; this ensures the strong and preferential adsorption of the nitro groups on the support surface, even in the presence of other reducible groups. Additionally, hydrogen can be easily dissociated at the isolated Pt (or other noble metal) single atoms, and the hydrogenation reaction probably occurs at the interface between the single metal atoms and the support, as illustrated in Fig. 2a. Nevertheless, this mechanism cannot completely justify the key role of single atoms in governing the high chemoselectivity. Alternatively, the nitro group could be adsorbed at the interface of the single metal atom and the support via the interaction of its two oxygen atoms with both the single metal atom and a nearby support cation, as illustrated in Fig. 2b. In either of the plausible scenarios above, the key point to be underscored is that the isolated and positively charged metal centers can successfully suppress the adsorption of C = C bonds, which would occur easily on their nanoparticle counterparts. Therefore, the single-atom dispersion is of paramount importance to achieve the chemoselective hydrogenation of nitroarenes to anilines, although cooperation between the single metal atoms and the specific support is required. Achieving an atomic-scale understanding of the reaction mechanism will require combined spectroscopic and theoretical studies.

There are two reaction pathways for the nitroarene reduction: a direct pathway involving nitro-nitroso-hydroxylamine-aniline steps and a condensation pathway involving nitro-nitroso-hydroxylamine-azoxy-azo-hydrazo-aniline steps [37]. In the above SAC systems, steric hindrance should prevent the reaction from proceeding via the condensation pathway, which requires the adsorption of two nitroarene molecules. However, in some cases, the azo is the desired product rather than the aniline, because aromatic azo compounds, with their great diversity of structures, represent the most widely used class of synthetic organic colorants by far [3]. For this purpose, Wang, Zhang and

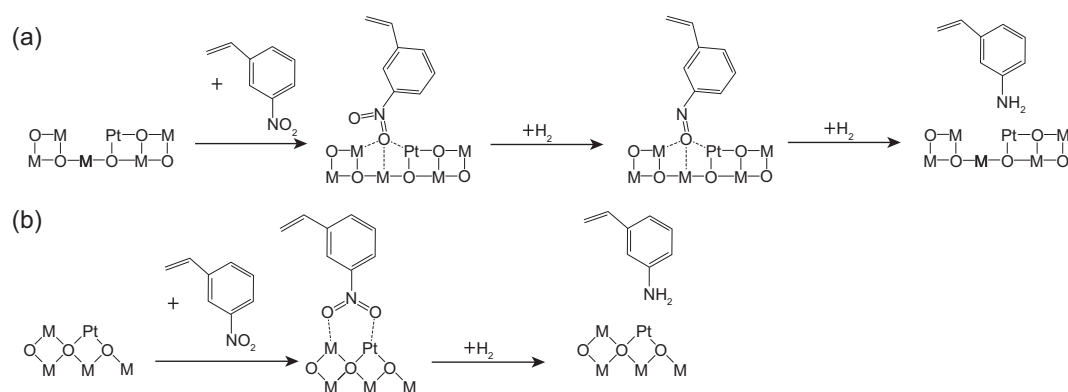


**Figure 2.** Two possible scenarios for the hydrogenation mechanism of nitroarenes on Pt-SACs with a reducible support.

coworkers explored atomically dispersed Co–N–C catalysts for the direct synthesis of azo compounds from nitroarenes [12]. The synthesis of this type of SACs involved the impregnation of a Co, N, C-containing precursor (e.g. a  $\text{Co}^{2+}$  phenanthroline complex) on a basic support (e.g.  $\text{Mg}(\text{OH})_2$ ) followed by pyrolysis at 600–800°C and etching with acid to remove the basic support as well as any particles of  $\text{Co}^0$  or  $\text{CoO}_x$ . Extensive characterization with aberration-corrected HAADF-STEM, XAS (X-ray absorption spectroscopy) and XPS (X-ray photoelectron spectroscopy) in combination with DFT calculations revealed that the resulting material was a truly atomically dispersed catalyst in which cobalt existed exclusively as single atoms and was bonded strongly to four pyridinic N atoms within a deformed graphitic layer and weakly to two oxygen molecules in the axial direction, as shown in Fig. 3a and b. Differently from the rigid plane structure generally proposed in the literature [38], the deformed  $\text{CoN}_4\text{C}_8-2\text{O}_2$  configuration might impart structural flexibility to the SACs similar to that of metal–ligand complexes and thus their catalytic activities may be comparable or even superior to that of their homogeneous analogs. In the hydrogenation of nitroarenes under mild conditions and in the presence of additional base (80°C, 3 MPa  $\text{H}_2$ , 1.5 h, *tert*-butyl alcohol as the solvent, catalyst loading of 0.7 mol% Co, 0.2 equivalents of NaOH), the Co–N–C SACs afforded good activity (TOF 35.9  $\text{h}^{-1}$ ) and excellent selectivity to azo compounds (Fig. 3c). Various functional groups including  $-\text{CH}_3$ ,  $-\text{C}=\text{C}$ ,  $-\text{CF}_3$ ,  $-\text{Cl}$ ,  $-\text{Br}$  and  $-\text{I}$  were tolerated in the reaction, and the catalyst could be reused without decay in the selectivity. The basic additive is the key to the condensation between nitrosobenzene and hydroxylamine to produce the target azo product; otherwise, anilines would be produced as the final product, as shown by the pioneering work of Beller and coworkers [39].

While the molecular-scale understanding of the reaction mechanism of these atomically dispersed

Co–N–C catalysts has yet to be clarified, the M–N<sub>x</sub> motif (where M refers to transition metals such as Co, Fe, Ni, Cu, etc.) is probably the active site, even in the earlier reported  $\text{Co}_x\text{O}_y/\text{N-C}$  or  $\text{Fe}_x\text{O}_y/\text{N-C}$  systems [39,40]. To determine the real active species, Zhang *et al.* prepared a catalyst composed of metallic Co,  $\text{Co}_x\text{O}_y$ ,  $\text{Co}_x\text{C}_y$  and  $\text{CoN}_x$  species using carbon as the support [41]. After acid etching, 78% of the Co-containing species had leached out and the residual Co species were encapsulated in thick graphitic nanoshells and thus inaccessible to any molecules, except for Co–N<sub>x</sub>, which is stable against acid etching. Interestingly, the performance of the catalyst in the oxidative cross-coupling of primary and secondary alcohols remained the same, strongly suggesting that the atomically dispersed M–N<sub>x</sub> is the active site. This work also indicates that some complicated heterogeneous systems may need to be revisited to identify the real active sites by means of state-of-the-art characterization techniques.

For the hydrogenation reactions occurring on the SACs, one key question is how hydrogen molecules are activated on the single atoms. Recently, an increasing number of studies have suggested that  $\text{H}_2$  is activated on SACs via a heterolytic pathway [42–45], which is quite different from the case of NP systems in which the homolytic dissociation of  $\text{H}_2$  is favorable. For example, Zheng and coworkers reported a high-loading  $\text{Pd}_1/\text{TiO}_2$  SAC that was obtained via a photochemical route on an ethylene glycolate (EG)-protected  $\text{TiO}_2$  nanosheet material [42]. In their method, the EG radicals that were generated by ultraviolet (UV) radiation played a key role in producing and stabilizing the Pd single atoms at a relatively high loading (1.5 wt%). The coordination of the single Pd atoms with oxygen atoms from the EG molecule allowed the dissociation of  $\text{H}_2$  in a heterolytic mode to produce  $\text{O-H}^{\delta+}$  and  $\text{Pd-H}^{\delta-}$  (Fig. 4), as proven by both kinetic isotope effect (KIE) and DFT calculations. The  $\text{Pd}_1/\text{TiO}_2$  SAC exhibited high activity and stability for  $\text{C}=\text{C}$  and  $\text{C}=\text{O}$  hydrogenations; the TOF was enhanced

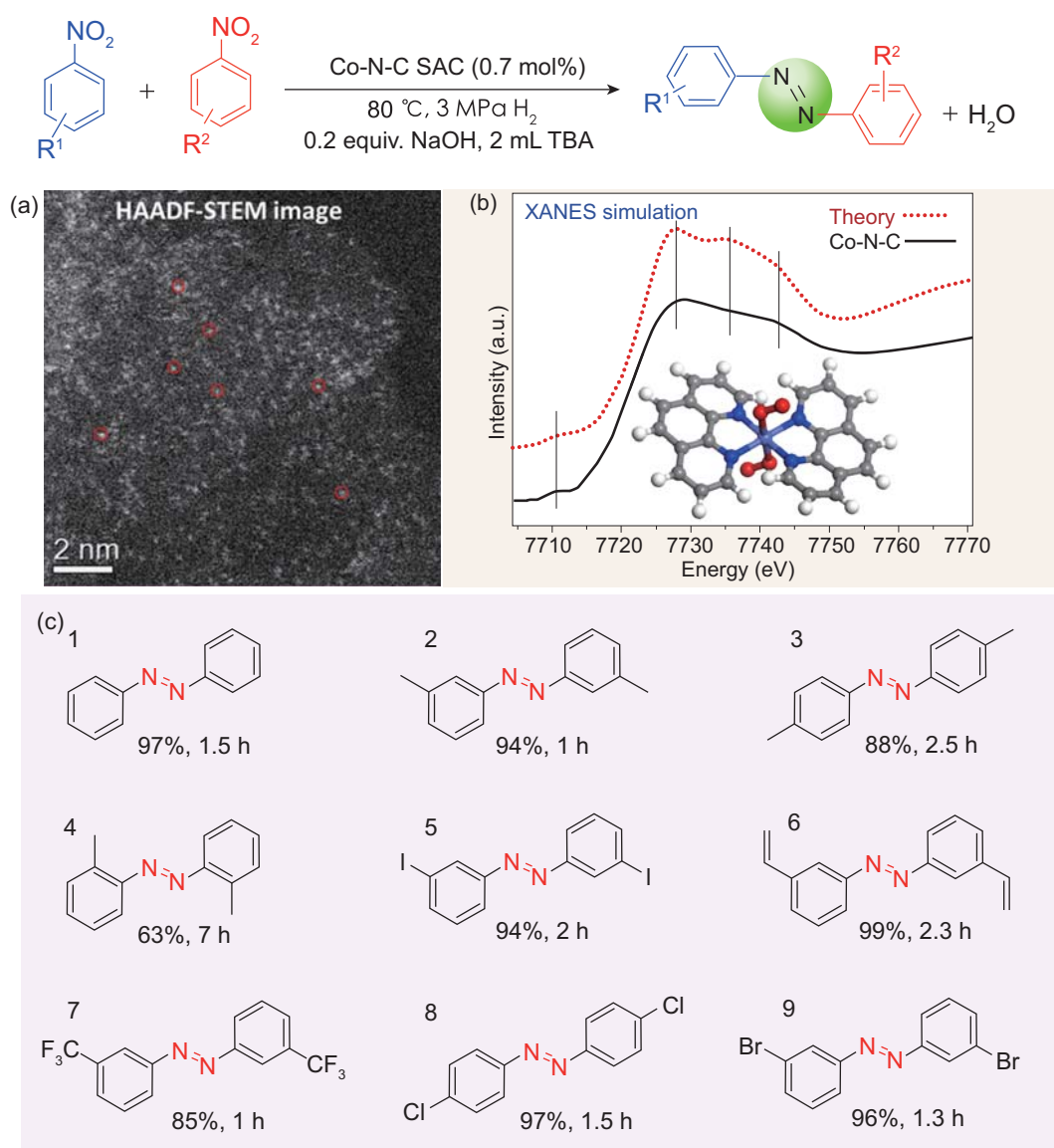


**Figure 3.** (a) HAADF-STEM image of the Co-N-C catalyst; (b) X-ray absorption spectroscopy (XAS) fitting and density functional theory (DFT) calculations of the Co-N-C catalyst; (c) substrate scope of the hydrogenation reaction on the Co-N-C catalyst. Adapted with permission from [12].

by a factor of 9 for styrene hydrogenation and a factor of 55 for aldehyde hydrogenation compared to the commercial Pd/C catalyst. The higher activity of the Pd<sub>1</sub>/TiO<sub>2</sub> for the hydrogenation of polar unsaturated bonds probably originated from the heterolytic dissociation of H<sub>2</sub> at the Pd<sub>1</sub>-O interface. Similarly, Yan and coworkers reported that single Pt<sub>1</sub> atoms anchored on active-carbon-supported phosphomolybdic acid (PMA) were more active for the hydrogenation of polar -C=O groups than of non-polar -C=C groups, implying the heterolytic dissociation of hydrogen on the Pt<sub>1</sub>-O<sub>4</sub> active sites [43]. In our recent work on the single/pseudo-single-atom catalyst Pt/WO<sub>x</sub>, hydrogen was also found to dissociate in a heterolytic fashion at the interface of

Pt and WO<sub>x</sub>. The H<sup>+</sup> formed on WO<sub>x</sub> and the H<sup>-</sup> on the single Pt atom provided Brønsted acid sites and hydrogenation sites, respectively, for the concerted dehydration-hydrogenation reaction of glycerol to produce 1,3-propanediol [44], as shown in Fig. 5. Moreover, the introduction of single gold atoms to this Pt/WO<sub>x</sub> system further promoted the heterolytic dissociation of H<sub>2</sub>, possibly by modulating the interaction between Pt and WO<sub>x</sub>, leading to remarkably enhanced activity and chemoselectivity towards 1,3-propanediol [45].

The heterolytic dissociation of H<sub>2</sub> favored on SACs is reminiscent of that of frustrated Lewis pairs (FLPs) in homogeneous catalysts, where H<sub>2</sub> is heterolytically dissociated at the sterically

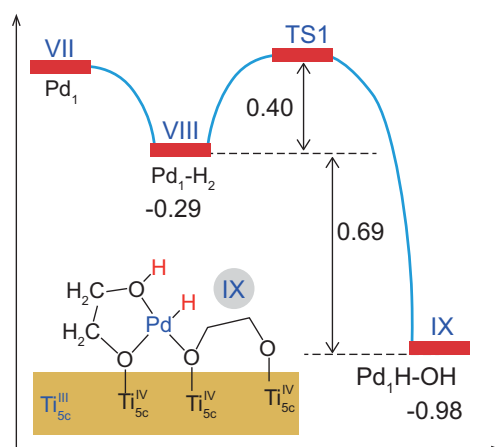


**Figure 4.** Energies and a model of the intermediates and transition states in the heterolytic  $\text{H}_2$  activation process of  $\text{Pd}_1/\text{TiO}_2$ . Adapted with permission from [42].

encumbered Lewis acids and bases [46]. In supported SACs, the single metal atoms are usually positively charged and therefore act as a Lewis acid, while the nearby oxygen or nitrogen atoms from the support can act as a Lewis base; the combination of the two facilitates the dissociation of hydrogen via a heterolytic pathway.

SACs not only show higher activity than their NPs counterparts in catalysing the hydrogenation of polar unsaturated groups, but also catalyse the hydrogenation of alkynes with high selectivity towards alkenes. This kind of reaction was initially investigated on single-atom alloy (SAA) catalysts. The term SAA was first introduced by Sykes and coworkers [47]. SAA catalysts are special SACs in which the active metal atom (e.g. Pd) is isolated completely by the surrounding less active metal atoms (e.g. Cu). This configuration allows for the easy dissociation of hydrogen on the active single metal atoms and simultaneously weakens the binding of intermediates by spillover to the less active metal metals, thus accomplishing both high activity and high selectivity in the hydrogenation of alkynes to alkenes. Various combinations of SAA catalysts have been explored, such as Au–Pd [48], Ag–Pd [49], Cu–Pd [50], Zn–Pd [51], In–Pd [52] and Pt–Cu [53]. In addition to these SAAs, single Pd atoms on other supports have also been demonstrated to be effective [54–56]. For example, Perez-Ramirez and coworkers reported a Pt SAC supported on mesoporous polymeric graphitic carbon nitride (mpg- $\text{C}_3\text{N}_4$ ) that was 3 orders of magnitude more active than traditional NP catalysts (e.g. Au, Ag and  $\text{CeO}_2$ ) in the hydrogenation of 1-hexyne, with 100% 1-hexene selectivity [56]. When the reaction was performed at  $70^\circ\text{C}$  and 5 bar  $\text{H}_2$ ,  $[\text{Pd}]/\text{mpg-}\text{C}_3\text{N}_4$  was more active than

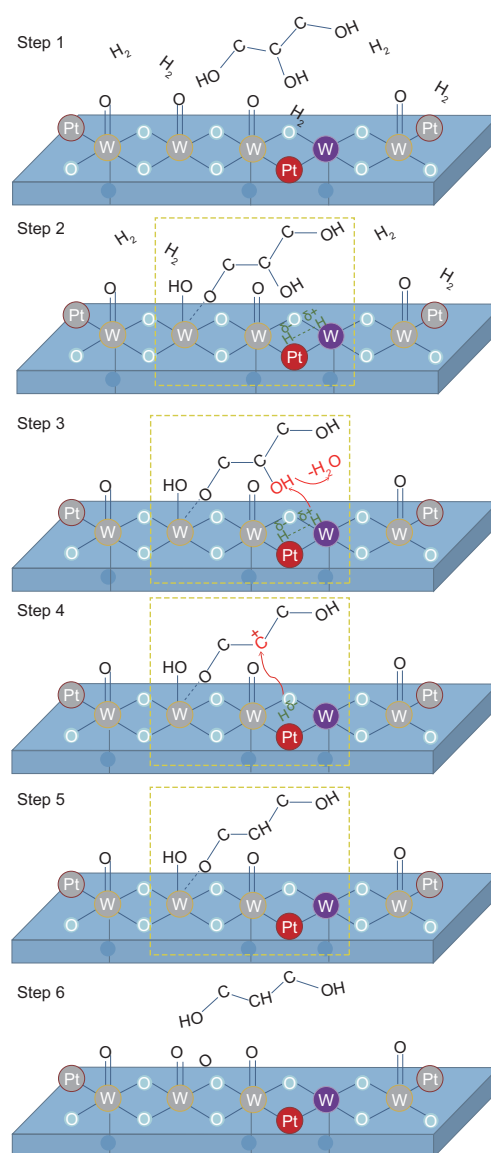


**Figure 5.** Proposed reaction scheme for the hydrogenolysis of glycerol to 1,3-PD over single-atom and pseudo-single-atom Pt/ $\text{WO}_x$  catalysts. Adapted with permission from [44].

$\text{Pd-Pb}/\text{CaCO}_3$  by a factor of 4, more selective than  $\text{Pd}/\text{Al}_2\text{O}_3$  (90 vs 69%) and was as active as the  $\text{Pd}/\text{TiS}$  modified by ligands. Furthermore, no decrease in activity or selectivity was observed during 20 h of time-on-stream. Other substrates, such as 2-methyl-3-butyn-2-ol and 3-hexyne, could also be smoothly converted with excellent chemo- and stereo-selectivity (*cis/trans* ratio >20). DFT calculations revealed that hydrogen underwent heterolytic dissociation assisted by the support, leaving one H atom bonded to a N atom in the support and the second one to a Pd atom. When alkyne molecules were adsorbed, the semi-hydrogenation reaction proceeded smoothly and the alkene product was easily desorbed without over-hydrogenation or

oligomerization. The proposed reaction mechanism is quite similar to that of the gas-phase selective hydrogenation of acetylene to ethylene over Au(Ag, Cu) alloyed Pd SACs and Pd-Zn intermetallic compounds reported by Zhang and coworkers [48–51], in which ethylene was demonstrated to interact with the single Pd atoms via a weak  $\pi$ -bonding pattern, and could be readily desorbed without saturation.

### Oxidation reaction

Selective oxidation is an important strategy for producing oxygenates, such as aldehydes, ketones or acid products, to be employed as building blocks in chemical processes that range from kilogram-scale applications in pharmaceuticals to 1000-ton-scale in chemicals. Traditional catalytic routes generally use expensive homogeneous complexes and are performed under harsh operating conditions, which bring about serious environmental issues and inevitable over-oxidation side reactions.

With the successful synthesis of SACs, a number of SACs have been explored in selective oxidation reactions and have shown promising catalytic performances. Pioneering work in this area was reported in 2007 by Lee and coworkers, in which a single-site Pd/Al<sub>2</sub>O<sub>3</sub> catalyst showed 30 times greater catalytic activity (TOF: 4096–7080 h<sup>-1</sup>) and selectivity (>91%) than its NP counterpart in the aerobic oxidation of allylic alcohols including cinnamyl alcohol, crotyl alcohol and benzyl alcohol [57]. This single-site Pd/Al<sub>2</sub>O<sub>3</sub> catalyst was obtained by using mesoporous alumina as the support and an extremely low loading of Pd (0.03 wt%), both of which ensured the atomic dispersion of the Pd species. The isolated Pd<sup>II</sup> surface species, which was identified using atomic-resolution HAADF-STEM, EXAFS and XANES, were proposed to be the active sites for the reaction. This catalyst also demonstrated impressive stability; the catalytic performance remained unchanged during the course of reaction over periods of days. This exceptional durability could be attributed to the high stability of the isolated Pd<sup>II</sup> species, as well as that of the mesoporous structure of the support. Very recently, Li *et al.* reported an Au<sub>1</sub>/CeO<sub>2</sub> SAC system that also showed excellent activity, selectivity and durability for the selective oxidation of alcohols to the corresponding aldehydes [58]. Based on isotopic exchange experiments, they proposed that the lattice oxygen from the CeO<sub>2</sub> support participated in the oxidation reaction, leading to the high selectivity towards aldehyde. The SAC system facilitated the removal and replenishment of the lattice oxygen by maximizing the interfacial sites between the single gold atoms and the CeO<sub>2</sub> support.

In contrast, the gas-phase oxygen activation on the surface of gold NPs was less selective towards the aldehyde. Another important factor determining the selectivity is the adsorption of the aldehyde, which was found to be much weaker on the single atoms than on the NPs.

Toshima and coworkers constructed a ‘crown-jewel’-structured Pd-alloyed Au SAC via replacing the Pd atoms at the top position of Pd<sub>147</sub> particles with an Au atom [59]. The as-prepared catalysts showed excellent catalytic activity in the oxidation of glucose. The specific activity of the Au SAC was 20–30-fold higher than that of the Pd and Au mother clusters and 8–10 times those of the Pd/Au alloys with different Au/Pd ratios, although all had similar average particle sizes. The higher catalytic activity of the Pd-alloyed Au SAC than the Pd–Au alloys indicated position-dependent catalysis beyond the synergistic effects of Au and Pd, as the top atoms are assumed to be more active than the edge and face atoms owing to the more unsaturated coordination. To confirm this proposal, the authors prepared three Pd-alloyed Au SACs with different amounts of Au using the same method, in which Au would preferentially replace the top Pd atoms, then edge and lastly face Pd atoms. As the Au concentration was increased, the specific activity normalized to the Au mass decreased, which unambiguously demonstrated the lower activity of the edge and face Au atoms compared to that of top Au atoms. The Au 4f XPS spectra of the Pd-alloyed Au SACs showed a negative shift in binding energy compared with that of monometallic Au, indicating electron transfer from Pd to Au; thus, Au was negatively charged. The Au<sup>δ-</sup> species could effectively donate electrons to O<sub>2</sub> to generate hydroperoxo-like species, which were considered to play an important role in the oxidation of glucose. Additionally, Tsukuda and coworkers reported a Pd<sub>1</sub>Au<sub>24</sub> SAC supported on a carbon nanotube (CNT) and investigated its catalytic performance in the aerobic oxidation of benzyl alcohol [60]. Compared with the monometallic Au<sub>25</sub>/CNT, the single-Pd-atom-doped Pd<sub>1</sub>Au<sub>24</sub>/CNT exhibited significantly enhanced conversion of benzyl alcohol (from 22 to 74%). The synergistic effect between Au and Pd was attributed to electron transfer from Pd to Au, which promoted the activation of O<sub>2</sub>. However, the selectivity of the catalyst was unsatisfactory and aldehyde, acid and ester products were produced with similar yields.

It should be noted that the oxidation mechanism on the single Pd atoms might be quite different from that on the single gold atoms or NPs. In the former case, the active oxygen mostly likely arises from the isolated PdO species and the Pd reduced during the reaction can be quickly re-oxidized by oxygen gas,

thus completing the redox cycle [57], while, in the latter case, oxygen is first activated on the electron-rich gold atoms to form  $O^{2-}$ , which then oxidizes the alcohol substrate [59].

In addition to noble metal SACs, atomically dispersed M–N–C catalysts have also been explored for aerobic oxidation reactions. In 2016, Davis's group reported a series of M–N–C SACs with non-noble metals, including Cr, Fe, Co, Ni and Cu, confined in a nitrogen-containing carbon matrix for the aerobic oxidation of alcohols in aqueous media [14]. Among these catalysts, Cu–N–C showed the highest catalytic activity for benzyl alcohol oxidation ( $TOF = 3.4 \times 10^{-2} s^{-1}$ ), followed by Co–N–C and Cr–N–C. The activity of Fe–N–C was lower than that of Cu–N–C by a factor of 50, although Fe–N–C is usually more active than Cu–N–C in the oxygen reduction reaction (ORR). KIE experiments were conducted to investigate the difference in catalytic activity between them. A large KIE effect (4.6) was observed on Fe–N–C, indicating that the elimination of  $\beta$ -H in benzyl alcohol was the rate-determining step, whereas a weaker KIE effect (2.2) was observed for Cu–N–C, suggesting Cu–N–C could abstract the  $\beta$ -H more easily. However, it should be noted that the as-prepared catalysts also contained nanoparticles encapsulated by carbon shells, whose role in the catalysis was not clearly determined.

Guan and coworkers also developed atomically dispersed Co SACs supported on nitrogen-doped graphene and investigated their catalytic behavior in the selective oxidation of alcohols [15]. The Co SAC exhibited excellent catalytic activity for a broad scope of substrates including aromatic and aliphatic alcohols, and moderate to excellent yields (54–92.4%) of the corresponding aldehydes were obtained. The base-free conditions and the use of air/oxygen as an oxidant seem attractive for practical application, although the organic solvent *N,N*-dimethylformamide (DMF) was used. Furthermore, some critical points, such as the doping effect of N in graphene, structure of the Co–N moiety and effect of calcination temperature, have yet to be clarified.

The selective oxidation of C–H bonds is a more demanding class of reactions than alcohol oxidation due to the high dissociation energy of C–H bonds and the over-oxidation side reactions [61]. Very recently, Liu *et al.* studied the selective oxidation of C–H bonds in aromatic and aliphatic hydrocarbons by using an atomically dispersed Fe–N–C catalyst [16]. By employing *tert*-butyl hydroperoxide (TBHP) as the oxidant, Fe–N–C SAC afforded excellent activity and selectivity even at room temperature, and a broad spectrum of substrates

could be smoothly converted into the corresponding ketones. The performance was highly dependent on the pyrolysis temperature at which the SAC was derived from the  $Fe(phen)_x$  ( $phen = 1,10$ -phenanthroline) precursor. Although the Fe–N–C catalysts obtained at different pyrolysis temperatures (ranging from 700 to 900°C) included almost exclusively or even exclusively atomically dispersed Fe species, their exact structures were rather complicated and in fact consisted of a mixture of  $FeN_x$  species ( $x = 4-6$ ). The employment of the powerful  $^{57}Fe$  Mössbauer spectroscopy technique allowed the identification and quantification of the different Fe centers. As shown in Fig. 6a, the relative concentration of each species differed with the pyrolysis temperature, and the most active species was the medium-spin  $FeN_5$  site (D4 in Fig. 6a), which afforded a TOF of  $6455 h^{-1}$  for the oxidation of ethylbenzene to acetophenone. This TOF was more than 1 order of magnitude higher than that of the high-spin  $FeN_6$  species (D2) and low-spin  $FeN_6$  species (D3), and even several times more active than the  $Fe(II)N_4$  species (D1). The high activity of the  $FeN_5$  structure was attributed to the unsaturated coordination of the Fe single atoms (actually  $Fe^{3+}$  cations), which provided adsorption sites for TBHP (H–O–O–, Fig. 6b). This behavior resembles the oxygen activation of the hemoglobin molecule [62]. In this aspect, the Fe–N–C SACs are expected to mimic the metalloenzymes in more important but complicated organic transformations. However, in the current Fe–N–C SACs, the most active species are unfortunately the least abundant (28% or less based on Fig. 6a). Evidently, there is plenty of room for future research in the design and synthesis of atomically dispersed single-site catalysts.

The direct catalytic conversion of benzene to phenol is a demanding and practically important reaction in the field of C–H activation. Bao and coworkers prepared a highly dispersed  $FeN_4/GN$  catalyst via the high-energy ball milling of iron phthalocyanine ( $FePc$ ) and graphene nanosheets under controllable conditions [17]. The graphene-matrix-confined coordinatively unsaturated iron sites demonstrated excellent catalytic activity in the oxidation of benzene with  $H_2O_2$  as the oxidant at room temperature. For example, the TOF value reached  $84.7 h^{-1}$  and a phenol yield of 18.7% was obtained at a conversion of 23.4%. Notably, the reaction even proceeded efficiently at 0°C, reaching a phenol yield of 8.3% after 24 h of reaction. Furthermore, the catalyst could be reused six times without a decrease in its catalytic activity. *In situ* XAS and Mössbauer measurements were performed to investigate the catalytic mechanism. For the fresh catalyst, both the Fe K-edge XANES spectra and



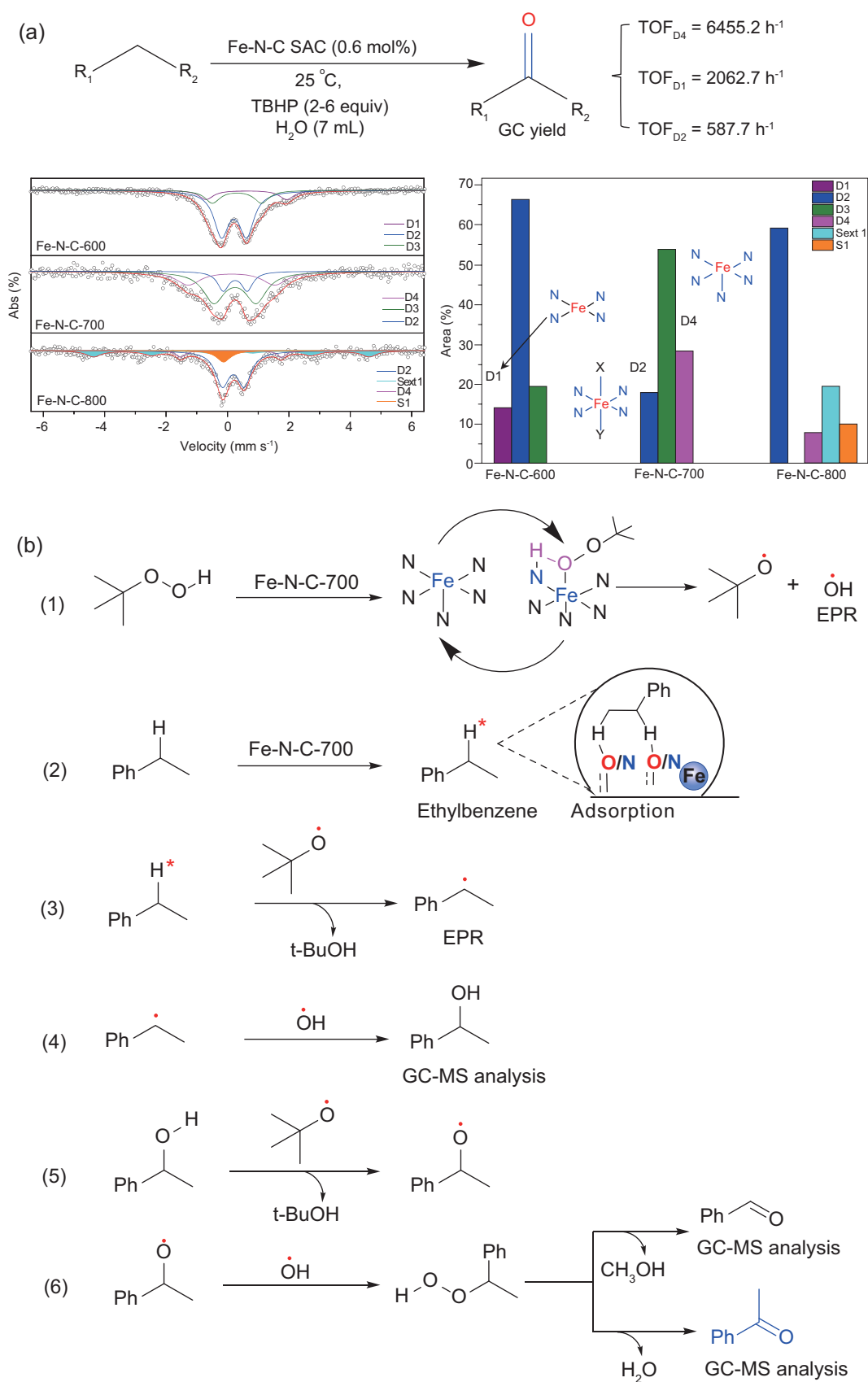


**Figure 6.** (a)  $^{57}\text{Fe}$  Mössbauer spectra of the Fe–N–C-600/700/800 catalysts and the relative concentration of each species; (b) proposed reaction mechanism of ethylbenzene oxidation on the  $\text{FeN}_5$  site. Adapted with permission from [16].

Fourier transformed EXAFS spectra in *r*-space were quite similar to that of FePc, indicating that the Fe in FeN<sub>4</sub>/GN adopted the same FeN<sub>4</sub> structure, with Fe coordinated to four N atoms within a planar sheet, as that of FePc. Upon treatment with H<sub>2</sub>O<sub>2</sub>, the pre-edge peak in the Fe K-edge XANES spectra broadened and increased in intensity due to the formation of Fe = O. The intensity of the first strong peak in the FT-EXAFS spectra in *r*-space was also enhanced, suggesting that a sharp increase in the coordination of Fe resulted from the formation of Fe = O/O = Fe = O. <sup>57</sup>Fe Moössbauer measurements also revealed that the amount of Fe = O increased after H<sub>2</sub>O<sub>2</sub> treatment and then decreased upon contact with benzene. These results, together with DFT calculations, showed that the single Fe atom was oxidized by H<sub>2</sub>O<sub>2</sub> to form an O = Fe = O intermediate, which then oxidized benzene to form phenol.

Li *et al.* also constructed Fe–N–C SACs by the pyrolysis of metal hydroxides or oxides coated with polymers of dopamine, followed by acid leaching [18]. The obtained Fe–N–C SAC exhibited high catalytic activity for the hydroxylation of benzene to phenol (45% benzene conversion with 94% selectivity). Based on electron paramagnetic resonance (EPR) analysis and DFT calculations, they proposed a similar reaction mechanism to that of Bao, in which the H<sub>2</sub>O<sub>2</sub> oxidant was activated on the single Fe atom, and the resulting Fe<sup>IV</sup> = O species was considered to be the active intermediate in the reaction. Notably, although Fe–N<sub>4</sub> moieties were proposed as the active species in both works, the selectivity towards phenol (94%) in Li's report was higher than that of Bao's (~80%), indicating that there might be some subtle discrepancy in the exact structure of the two active sites. Further efforts are expected to identify the active species using XAS and Moössbauer characterization and/or poisoning experiments. In addition, the use of a large excess of H<sub>2</sub>O<sub>2</sub> as oxidant decreased the catalytic efficiency to some extent in both cases.

Silanols are important building blocks in polymer chemistry. The selective oxidation of silanes with water to synthesize silanols has attracted increasing attention for its safety (nonexplosive, nonflammable and nontoxic) and atomic economy (hydrogen gas as the only by-product) [63]. Chen and coworkers prepared Au SACs supported by mesoporous carbon graphitic carbon nitride (mpg–C<sub>3</sub>N<sub>4</sub>), which showed excellent catalytic performance in the oxidation of silanes by water [64]. Nevertheless, in comparison with the gold NPs supported on silica previously reported for the same reaction [65], the Au<sub>1</sub>/C<sub>3</sub>N<sub>4</sub> showed only comparable activity. One advantage of the Au<sub>1</sub>/C<sub>3</sub>N<sub>4</sub> SAC is its excellent stability; it could be recovered and reused at least

10 times with its activity and selectivity being maintained well. The characteristic coordination cavity surrounded by N atoms in the mpg–C<sub>3</sub>N<sub>4</sub> could anchor and stabilize the Au single atoms; this effect was believed to contribute to the high durability of the catalyst.

## Hydroformylation of olefins

The hydroformylation of olefins involves the addition of syngas (a mixture of CO and H<sub>2</sub>) to olefins for the production of aldehydes and represents a typical example of an efficient and clean chemical process with 100% atom economy. The aldehydes are valuable final products and important intermediates for the synthesis of bulk chemicals such as alcohols, esters and amines; more than 10 million tons of aldehydes are manufactured per year globally [66]. Cobalt-based catalysts were the first generation of catalysts for these transformations; however, they required harsh reaction conditions and had low productivity. In 1968, a Rh-based catalyst [RhCl(PPh<sub>3</sub>)<sub>3</sub>] was reported by Wilkinson *et al.* [67], and was much more active and selective than the Co-based catalysts under mild reaction conditions, thus opening a new era of rhodium–alkylphosphine/phosphite complexes for the hydroformylation reaction [66]. The alkyl–phosphorous ligands, with their unique steric bulk and electron-donating effects, contribute greatly to the high activity and selectivity. However, these homogeneous complexes are difficult to recover. Thus, great efforts have been devoted to the heterogenization of Rh-based hydroformylation catalysts, including immobilization of the homogeneous complexes on a solid support by ion exchange, adsorption or covalent grafting [68]. However, the interaction between the post-heterogenization Rh metallorganics and the support is relatively weak. Degradation of the ligands and/or the Rh complexes tends to occur during the course of the reaction, which necessitates the periodic supplementation of the active components. Furthermore, only a low concentration of phosphorous ligands can be grafted onto the surface of the support using these methods, which usually results in poor catalytic activity, selectivity and stability because of the low P/Rh ratio [69,70].

Recently, the groups of Ding and Xiao groups have made great progress in the heterogenization of homogeneous Rh catalysts by designing porous organic ligands (POLs) to support Rh [71–73]. They chose the well-known electron-donating ligand triphenylphosphine (PPh<sub>3</sub>) as the backbone of the monomer and grafted a vinyl group to the three benzene rings in PPh<sub>3</sub> to construct vinyl-functionalized PPh<sub>3</sub> (3V–PPh<sub>3</sub>), which then

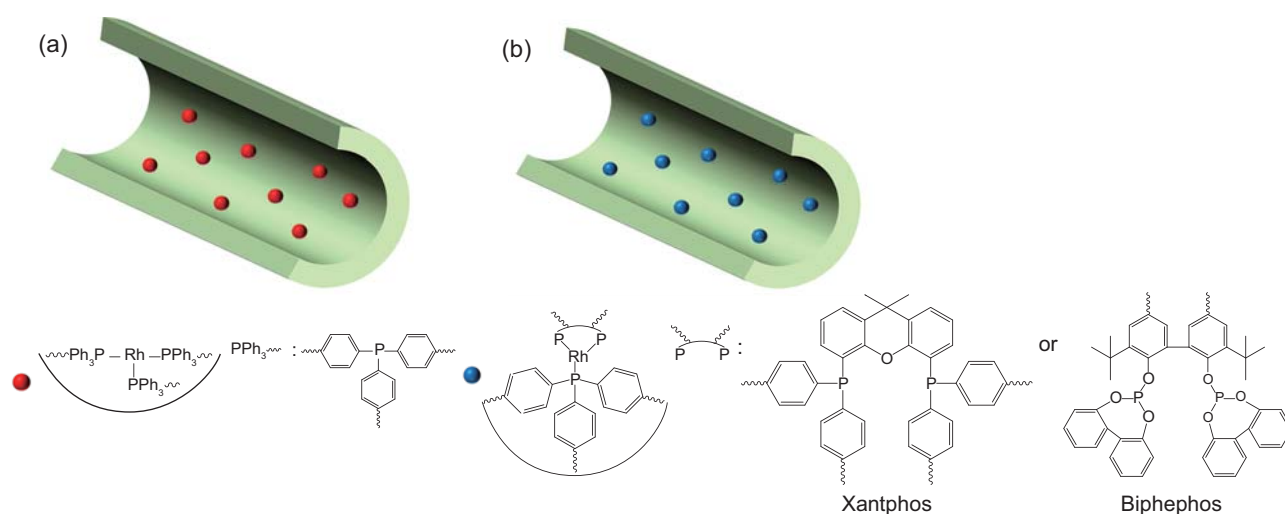


**Figure 7.** The proposed structures of the (a) Rh/POL-PPh<sub>3</sub> and (b) bidentate-ligand-doped Rh/POPs-PPh<sub>3</sub> catalysts.

underwent polymerization under solvothermal conditions to yield a porous organic polymer (POP) with high surface area and rich porosity (Fig. 7a). One of the most significant advantages of this method is that the PPh<sub>3</sub> moieties can be anchored with a high loading and are homogeneously distributed throughout the support via covalent bonding (C–C). This not only stabilizes the active Rh species exclusively as single atoms, but also ensures the high P/Rh ratio that is required for high catalytic activity and selectivity. In the hydroformylation of 1-dodecene, the conversion reached 86.4% with a high linear/branched aldehyde ratio ( $l/b = 6.6$ ). The high selectivity towards linear aldehydes was thought to arise from the confinement effect of the micropores (0.7–1.5 nm) in the support. More impressively, in contrast to the vulnerability of most previously reported heterogenized molecular catalysts [68,74], the Rh SAC was quite stable for more than 500 h time-on-stream in continuous flow reaction, demonstrating its great potential for practical applications. However, the substrate tolerance of the catalyst was unsatisfactory and, for the hydroformylation of the shorter-chain substrate 1-octene, the linear/branched ratio was poor (45/55), and a large amount of isomerized alkene was produced. To improve the regio-selectivity, the authors doped bidentate ligands such as Xantphos, which was reported by Van Leuween [75], and biphephos, which was developed by the Union Carbide Corp. [76,77], onto the POP-PPh<sub>3</sub> (Fig. 7b). These bidentate ligands usually exhibit large natural bite angles ( $\sim 120^\circ$ ) and, when coordinated with an Rh cation, the formed complex preferentially adopted a diequatorial rather than an equatorial-apical configuration, which led to an increase in the steric congestion around the Rh center and resulted in more selective formation of the sterically less demanding linear

alkyl rhodium species and subsequently of the linear aldehydes [75]. Using a similar method, Ding and coworkers functionalized the Xantphos and biphephos ligands with vinyl groups, which then underwent co-polymerization with the 3V-PPh<sub>3</sub> to yield the support [78]. The Rh species in these catalysts still existed as single atoms. Compared with Rh/POP-3V-PPh<sub>3</sub>, the Xantphos- and biphephos-doped catalysts afforded greatly enhanced regio-selectivity, although the catalytic activity was decreased to some extent, most likely due to the limited mass transfer. For example, the  $l/b$  ratio in the hydroformylation of 1-octene over Xantphos-doped Rh/POPs-PPh<sub>3</sub> increased from 45/50 to 90/10 and, in the hydroformylation of propene on biphephos-doped catalysts, the  $l/b$  ratio reached as high as 24.2. Impressively, the biphephos-doped catalyst was also effective for the isomerization–hydroformylation of internal olefins and the regio-selectivity for linear aldehyde reached up to 92%. The authors proposed that the PPh<sub>3</sub> ligands contributed mainly to the overall catalytic activity and stability owing to their strong electron-donating capacity and multiple binding with Rh cations, whereas the bidentate ligands were mainly responsible for the high regio-selectivity due to their steric hindrance. The POLs strategy developed by Ding and Xiao opened a new approach for the heterogenization of metallorganic molecular catalysts that could maintain their high activity and regio-selectivity while creating robustness. Nevertheless, the tedious procedures required to prepare the polymers and the use of expensive ligands and Grignard reagents represent barriers to their future industrial application. Further efforts must be devoted to developing facile and inexpensive synthetic routes and exploring other P-containing materials (e.g. MOFs, COFs) for such transformations.

Given the high cost and vulnerability of the phosphorous ligands, supported Rh NPs catalysts without P-ligands were developed for the hydroformylation of olefins; however, their catalytic performances were inferior to those of their homogeneous analogs [79]. SACs, in which the single metal atoms are coordinated to heteroatoms on the support, are regarded as a mimic of supported homogeneous catalysts and thus are expected to perform well in the hydroformylation of olefins. Indeed, the Rh SACs met some of the criteria for the hydroformylation of olefins. First, in most Rh homogeneous catalysts, Rh(I) species are considered to be the active sites; fortunately, Rh single atoms are generally positively charged. Second, Rh single atoms are reported to effectively activate both H<sub>2</sub> and CO, and the isolated Rh centers are believed to interact with olefins weakly without hydrogenation. Third, the confinement in some SACs is expected to have steric effects similar to those of bulky P-ligands. Recently, several exciting examples have demonstrated the feasibility of Rh SACs for the hydroformylation of olefins. Lang *et al.* fabricated a Rh<sub>1</sub>/ZnO catalyst for the hydroformylation reaction [11]. They chose ZnO nanowires (ZnO-nw) as a support and a Rh SAC with a loading of 0.006 wt% was prepared. For comparison, ZnO-nw-supported Rh NPs were also synthesized. In the hydroformylation of styrene, when the Rh loading was decreased from 0.3 to 0.006 wt%, the turn over number (TON) increased from  $7 \times 10^3$  to  $4 \times 10^4$ . Notably, the TONs of Rh<sub>1</sub>/ZnO-nw were even higher than those of homogeneous RhCl<sub>3</sub> and Wilkinson's catalyst RhCl(PPh<sub>3</sub>)<sub>3</sub> (TON = 3324 and  $1.9 \times 10^4$ , respectively). Moreover, the chemoselectivity of the Rh<sub>1</sub>/ZnO-nw catalyst reached 99%, which was much higher than those of its homogeneous counterparts (83–92%). Almost no hydrogenation of olefins occurred on the catalyst, indicating that the single Rh atoms interacted with the olefins through a  $\pi$ -mode interaction, which was in good agreement with the behavior of other SACs for hydrogenation reactions [10,42,56]. Unfortunately, the Rh<sub>1</sub>/ZnO-nw SAC did not exhibit regio-selectivity towards the linear aldehydes; the linear/branched ratio was about 1. Generally, high regio-selectivity can only be obtained when the Rh centers have significant steric hindrance during the insertion of CO. The unsatisfactory regio-selectivity of the Rh<sub>1</sub>/ZnO-nw SAC may imply that the Rh center had low steric congestion. XPS and *in situ* XANES characterization results indicated that the single Rh atoms were in a nearly metallic state, which implied that the single Rh atoms might have been located atop a Zn atom. This position would leave the Rh single atoms open to CO insertion from every direction and thus lead to poor regio-selectivity.

However, high regio-selectivity and high activity over Rh SACs was achieved by fine-tuning the valence state and location of the single Rh atoms on the support, as demonstrated by Zeng and coworkers [80]. They constructed a Rh<sub>1</sub>/CoO SAC by confining the single Rh atoms in the CoO layers via galvanic replacement between Rh(III) and CoO. Inductively coupled plasma atomic emission spectroscopy (ICP-AES) examination and HAADF-STEM images suggested that the single Rh atoms occupied the Co positions. In the liquid-phase hydroformylation of propene, the 0.2% Rh/CoO SAC achieved a TOF value of 2065 h<sup>-1</sup>, which was even higher than that of Rh/POPs-PPh<sub>3</sub>. Furthermore, the catalyst showed impressive chemoselectivity (>99%) and regio-selectivity for 1-butaldehyde (94.4%), higher than those of its nano-counterparts (68.7 and 53.9% for 1.0% Rh/CoO and 4.8% Rh/CoO). This high chemo- and regio-selectivity may arise from two features. First, XPS measurements demonstrated that the single Rh atoms were positively charged even under the reaction conditions, allowing the single Rh atoms to stably fill the Co(II) vacancies; that is, the Rh single atoms were coordinated to four oxygen atoms within the CoO layer in the equatorial direction of an octahedral configuration. Second, the single Rh atoms were confined within the CoO sheets, although according to DFT calculations, Rh moved 1.3 Å out of the plane during the reaction. This confinement limited the possible CO insertion pathways, which in turn preferentially yielded the linear aldehyde due to steric hindrance. Furthermore, the CoO support might have assisted in the activation of H<sub>2</sub> and CO, as in the case of Au/Co<sub>3</sub>O<sub>4</sub> [81], which would increase the catalytic activity. This work subverted the traditional opinion that high regio-selectivity can only be obtained with the assistance of expensive phosphorous ligands, and demonstrated that the heteroatoms (e.g. O) in the support can fulfill the role of the bulky P-ligands in a carefully designed SAC.

### C–C coupling reaction

The construction of C–C bonds, which is a vital method for the formation of complex molecules from simple substrates, is one of the central themes in modern synthetic chemistry. Typical powerful approaches include the Suzuki cross-coupling reaction [82], Heck reaction [83] and  $\alpha$ -alkylation of enolates [84], which are generally catalysed by Pd, Ir or Pt complexes. When aryl halides are used as substrates, the chlorides are cheaper and more readily available than the bromides and iodides, but are more difficult to activate because of the higher

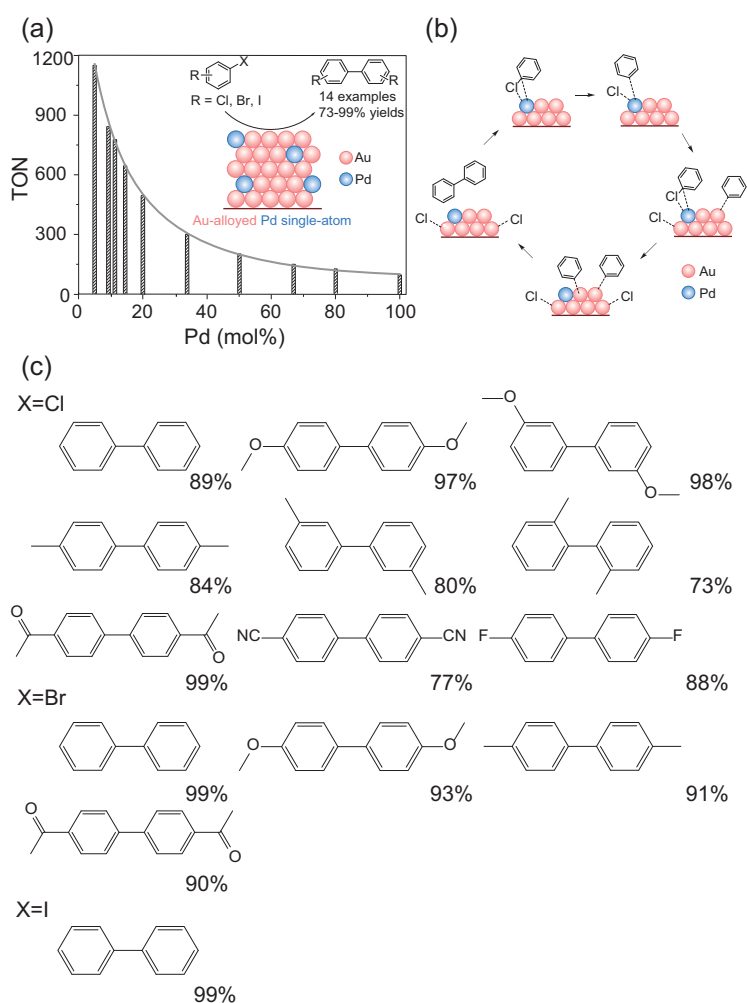


**Figure 8.** (a) Relationship between activity (turnover number, TON) and Pd concentration in the Au-Pd/resin catalysts for the Ullmann reaction of chlorobenzene; (b) proposed reaction mechanism; (c) substrate tolerance (the percentages in C indicate the product yield). Adapted with permission from [85].

dissociation energy of the C-Cl bond. Zhang *et al.* prepared an ion-exchange-resin-supported Au-Pd SAA catalyst that exhibited high catalytic activity and selectivity in the Ullmann reaction of aryl chlorides [85]. Both CO-DRIFTS (diffuse reflectance infrared Fourier transform spectroscopy) and EXAFS characterization confirmed the formation of an SAA structure at Au/Pd  $\geq 6$ , with the Pd atoms isolated by the surrounding Au atoms. In the Ullmann reaction of chlorobenzene, an exponential increase of the TON (normalized by Pd mass) was observed with decreasing Pd concentration (Fig. 8a). This interesting trend can be rationalized by the assumption that, with an increase in the Au/Pd ratio, the Pd single atoms are mainly located at the edges and corner positions of the Au nanoparticles (Fig. 8b), which should be more active than those on facets because of the more unsaturated coordination environment, as in the case of the aforementioned 'crown-

jewel'-structured Au SACs [59]. Furthermore, the catalyst exhibited promising substrate tolerance and durability for Ullmann reactions of aryl chlorides, bromides and iodides (Fig. 8c) and could be reused eight times without decay in their activity. Hot filtration experiments demonstrated a heterogeneous reaction mechanism. It was proposed that the Au in the catalysts not only played a role in separating Pd to form single atoms, but also promoted the dissociation of the C-Cl bond and the coupling of two aryl groups, thus opening a new method of fabricating efficient alloyed SACs for other reactions. Future work can be devoted to exploring other inexpensive transition metals to isolate Pd, in light of the high price of Au.

In addition to the SAA, a TiO<sub>2</sub>-supported Pd SAC was also explored for the Sonogashira coupling reactions of aryl bromides and iodides with phenylacetylene [86]. The catalyst afforded complete conversion of phenylacetylene after reaction at 60°C for 3 h in the Sonogashira coupling reaction of phenylacetylene and iodobenzene, with the product selectivity reaching over 90%. The coupling reaction also proceeded readily for substituted phenylacetylenes with different functional groups and aryl bromides and iodides, and the corresponding products were obtained in high yields. However, for the more challenging aryl chloride substrates, the catalyst showed rather low activity. XAS and XPS characterization, in combination with DFT calculations, revealed a Pd<sub>1</sub>O<sub>4</sub> structure in which the positively charged and isolated Pd<sup>δ+</sup> species interact strongly with four surface lattice O atoms of the TiO<sub>2</sub> support. Such a structure provides multifunctional Pd, O<sub>ad</sub> and Ti<sub>5c</sub> atoms for the activation of the reactants, and therefore a lower apparent activation energy of 28.9 kJ/mol is required in comparison with that of the homogeneous catalyst Pd(PPh<sub>3</sub>)<sub>2</sub>Cl<sub>2</sub> (51.7 kJ/mol), demonstrating the concerted catalysis by the TiO<sub>2</sub> support and single Pd atoms.

Kim *et al.* reported a thiolated multiwalled nanotube (MWNT) supported Pt SAC that acted as a good catalyst for the Suzuki cross-coupling reaction of 4-iodoanisole and 4-methylbenzene boronic acid [87]. The Pt-S-MWNT SAC afforded a high product yield of 99.5%, which was much higher than that on Pd-S-MWNTs, Pd/C or H<sub>2</sub>PtCl<sub>6</sub>. However, for bromide and chloride, much lower yields of 10.4 and 4.8% were obtained, respectively. The catalyst could be recovered by filtration and could be reused 12 times without significant decrease in the yield. XANES spectra showed a white-line intensity slightly higher than that of Pt foil, but much lower than that of H<sub>2</sub>PtCl<sub>6</sub>, suggesting that the single Pt single atoms were positively charged. The positively charged single Pt atoms could easily dissociate the

C–I bond and were believed to be responsible for the high activity. It was also noted that, in the Pt-S-MWNT SACs, the single Pt atoms were coordinated to the thiol groups, which not only resulted in a positive charge on the single Pt atoms, but also helped to stabilize them against aggregation and leaching.

Recently, Wang *et al.* constructed a Pd<sup>II</sup>@PDMS single-atom catalyst for the oxidative coupling of benzene to synthesize biphenyl compounds using O<sub>2</sub> as the terminal oxidant with only H<sub>2</sub>O as a by-product [88]. In this catalyst, the porous organic copolymer PDMS (a copolymer of divinylbenzene, maleic anhydride and p-styrene sulfonate) containing abundant carboxylic acid and sulfonate groups was used as the support for anchoring single Pd atoms. In the oxidative coupling reaction of benzene, a 26.1% yield of biphenyl with a high selectivity of 98.3% was obtained after 4 h at 120°C, affording a TON value of 363. Under the optimized reaction conditions, an even higher TON of 487 was obtained, which surpassed those achieved on Pd(OAc)<sub>2</sub> and other reported heterogeneous catalysts. Benzene, toluene, o-xylene, m-xylene and p-xylene were also good substrates, and the corresponding products were obtained with high selectivity (90.8–97.6%) and yields (10.3–30.8%). Hot filtration experiment results revealed that the reaction did not proceed after the catalyst was removed, thus ruling out the possible contribution of leached Pd to the catalysis. The bidentate –COOH in the Pd<sup>II</sup>@PDMS catalyst contributed greatly to the stabilization of Pd(II) against reduction as well as the subsequent catalytic activity; in contrast, for catalysts with both –SO<sub>3</sub>H and mono-carboxylic groups, or those possessing solely –COOH or –SO<sub>3</sub>H groups, much lower yields (0.2–14.2%) were obtained because of their weaker ability to stabilize Pd(II). Evidently, the isolated Pd(II) species was the active site for this reaction.

## STABILITY OF SACs

One of the greatest concerns regarding the use of SACs for liquid-phase reactions is their stability. Generally, leaching (the detachment of the single atoms from the support) and aggregation (the formation of clusters and NPs from the single atoms through migration) are the two major factors that severely deteriorate the stability, and the stability of the SACs is strongly dependent on the interaction between the single atoms and the support.

Free single atoms are known to have an extremely high surface energy and therefore cannot be stable. In contrast, upon being fixed on a support, whether on the surface, in the cation position

(lattice substitution), confined in a cavity or alloyed with another metal, the single atoms tend to interact strongly with the support via chemical bonding with the donor atoms of the support, such as oxygen or nitrogen atoms or a second metal atom in the case of SAA; these atoms are analogous to the ligands of organometallic complexes. This bonding lowers the surface energy and sometimes even has covalent characteristics [9]. The strong ionic or covalent bonding of the single atoms with the support significantly improves their stability against leaching and/or aggregation. Here, we provide several examples that demonstrate the superior stability of SACs in biomass conversions.

The transformation of biomass into fuels and value-added chemicals is an important and active research area. Biomass-related hydrogenation/hydrodeoxygenation reactions often require harsh reaction conditions, such as elevated hydrogen pressure, moderate to high reaction temperatures and hot water or even acidic reaction media. For example, in the hydrogenation of levulinic acid (LA) to  $\gamma$ -valerolactone (GVL), commercially available Ru/C has proven to be highly active and selective. However, it suffers from severe deactivation under hydrothermal and/or acidic reaction conditions due to Ru leaching [89]. Wang, Zhang and coworkers reported a single-atom Ru/ZrO<sub>2</sub>@C (0.85 wt%) catalyst that was highly active and ultra-stable for the hydrogenation reaction of LA [90]. When the reaction was performed in water, the conversion of LA dropped from 69.2% in the first run to 40% in the third cycle on Ru/C, whereas the conversion remained unchanged even after six runs over Ru/ZrO<sub>2</sub>@C. The stability of Ru/ZrO<sub>2</sub>@C was further demonstrated under harsher conditions (pH = 1); the LA conversion decreased from 77.7 to 25% on Ru/C after three runs, whereas no apparent drop of activity was observed over Ru/ZrO<sub>2</sub>@C. ICP-AES results indicated that 14.8 and 7.4% of the Ru leached into acid media and H<sub>2</sub>O for Ru/C, respectively, which caused the severe deactivation of the catalyst. In contrast, no leaching of Ru was detected for Ru/ZrO<sub>2</sub>@C, which was attributed to the strong interaction between Ru and ZrO<sub>2</sub>. Similar results were also reported by other groups [91], although the unambiguous identification of single atoms of Ru on ZrO<sub>2</sub> remains a challenge due to the similar atomic numbers of the two elements.

Another class of ultra-stable SACs are the M–N–C catalysts, in which M is exclusively dispersed as single atoms and bonds with the nearby N atoms to form M–N<sub>x</sub> active sites. The M–N<sub>x</sub> structure is expected to be highly resistant against high-temperature aggregation and acid leaching based on the strong bonding between the M cation and N

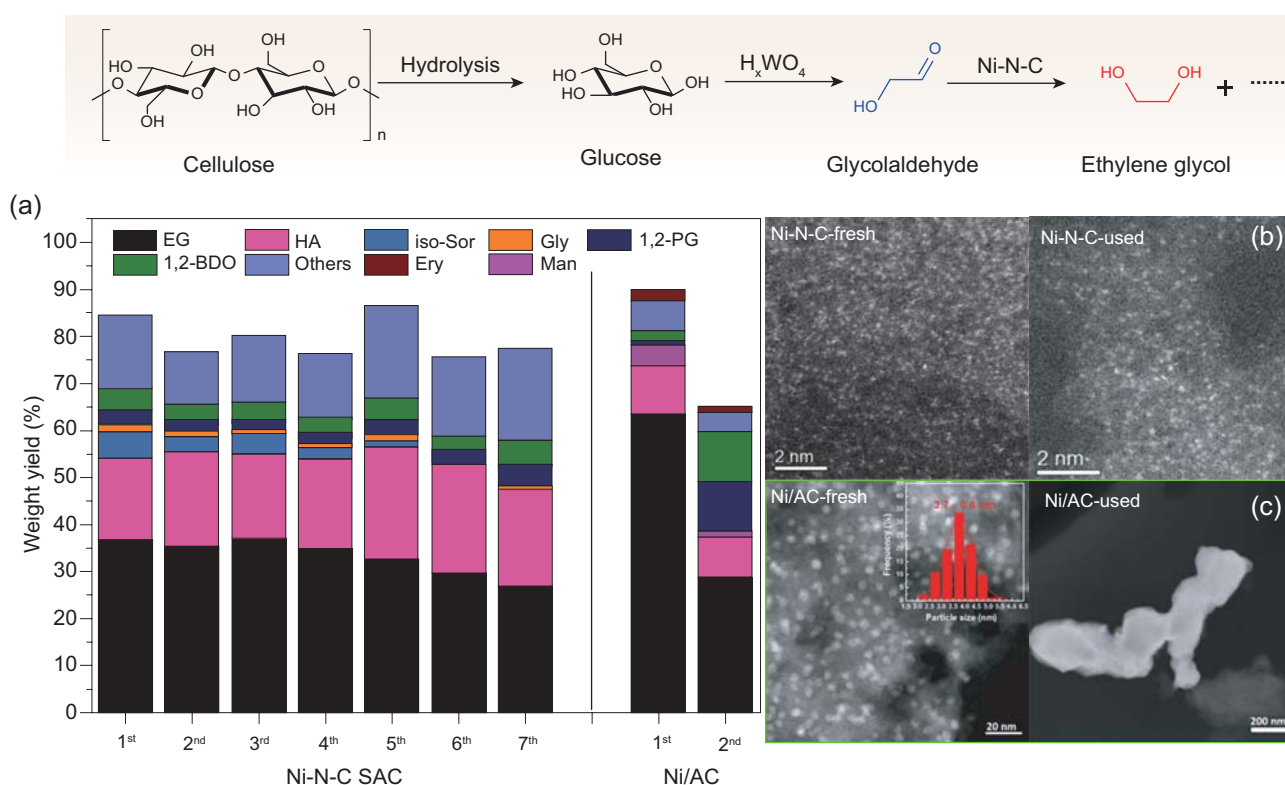


**Figure 9.** (a) Stability tests of the Ni-N-C catalyst and Ni/AC catalyst, and HAADF-STEM images of fresh and used (b) Ni-N-C and (c) Ni/AC catalysts. Adapted with permission from [13].

atoms. As expected, Wang, Li and coworkers recently reported an ultra-stable Ni-N-C SAC with a Ni loading of 7.5 wt% that exhibited excellent performance in the one-pot conversion of cellulose to EG [13], which is an important reaction for the valorization of biomass to value-added chemicals [92–94]. The Ni-N-C SAC exhibited superior stability compared to its Ni/AC NP counterpart under relatively harsh reaction conditions (245 °C, 60 bar  $H_2$ , presence of tungstic acid in hot water); it could be recycled seven times without any deactivation, while the Ni/AC lost half of its initial activity during the second run (Fig. 9). Characterizations of the used catalysts showed severe agglomeration of the Ni nanoparticles whereas the Ni-N-C catalyst maintained atomic dispersion. In another biomass-valorization reaction, an  $MoS_2$  monolayer doped with single-atom Co was reported to show superior activity and stability for the hydrodeoxygenation of 4-methylphenol to toluene [95], which is a model reaction for lignin transformations [96]. The single Co atoms were believed to fill S-atom vacancies to be immobilized as a part of the basal plane. The durability was greatly improved—that is, the catalysts could be reused at least seven times for a total reaction time of 56 h without decay in their activity and selectivity; moreover, no sulfur detachment was detected by

ICP-AES. This work demonstrated that, when single atoms—100% dispersion of active metal—meet with single layer sheets—the ultimate exfoliation of 2D materials—powerful catalysts can be created.

The above examples, among others, clearly demonstrate that single atoms that are strongly chemically bonded with the donor atoms of the support can behave even more stably than NPs in certain reactions.

## CONCLUSION AND PERSPECTIVE

SACs are of great interest and importance for the development of a new generation of low-cost, efficient and robust catalysts. Especially in the field of the green synthesis of fine chemicals, various SACs have been fabricated, and their catalytic potentials have been exploited in a variety of organic transformations, including, but not limited to, selective hydrogenation, oxidation, hydrogenolysis, hydrodeoxygenation, hydroformylation and C–C coupling reactions. In particular, some reactions that represent very important industrial processes, such as the hydrogenolysis of glycerol to 1,3-propanediol and the hydroformylation of propene, would be

very profitable if efficient and robust SACs could be successfully exploited. Traditional homogeneous or heterogeneous NP catalysts involve compromises in terms of activity, selectivity or recyclability. SACs integrate the merits of both these types of catalysts—that is, the unsaturated coordination environment of the single atoms imparts superior catalytic activity per metal atom; the uniform structure of the SACs results in unparalleled selectivity for the desired products; and strong covalent or electronic interactions with the support or another metal provide excellent stability under liquid-phase operating conditions. Therefore, in the field of green chemical synthesis, one can expect further progress in the use of SACs to bridge homogeneous and heterogeneous catalysis.

In spite of its exciting and encouraging beginning, the SAC field is still in its infancy. The following issues must be addressed to obtain an in-depth understanding of single-atom catalysis and eventually achieve the rational design of SACs for specific organic transformations.

(1) The role of the support must be further clarified. In SACs, the single atoms of the active metal interact strongly with the support, and the support serves as the ligands of the active metal centers, just as in homogeneous organometallic molecules. Therefore, the properties of the support can greatly affect the chemical state and coordination structure of the single atoms, and thus their ultimate catalytic performance. By tuning the properties of the support, for example, by grafting functional groups onto the support surface or changing the concentration of defect sites via thermal treatment, the electronic and geometric properties of the central single metal atoms can be changed, providing an effective way to tune the catalytic performance of the SACs. The single atoms may be located in the cation vacancies, the anion vacancies or atop the cation sites of the oxide/sulfide support, which results in different local structures around the single central single atoms, and thus different catalytic performance. For example, in the  $\text{Co}_1/\text{MoS}_2$  catalyst developed by Tsang *et al.* [95], DFT calculations revealed that, when the Co single atom was located in the sulfur vacancies within the  $\text{MoS}_2$  monolayer, the catalyst exhibited the highest stability. In addition, the support may directly participate in the reaction in concert with the single atoms. In such cases, the choice and the modification of the support become key factors in the success of the targeted reaction. Therefore, the elucidation of the multifarious roles played by the support will definitely help to develop an understanding the mechanism of single-atom catalysis and to develop efficient and robust SACs for green chemical synthesis.

(2) Multifunctional SACs should be developed. The green synthesis of fine chemicals calls for the combination of multi-step syntheses into one-pot tandem (domino) reactions. Thus, great effort should be devoted to the development of SACs with multiple functions; for example, the development of a dehydration–hydrogenation bi-functional catalyst through the use of an acidic support might be explored [44,45].

(3) Construction of SACs with a high surface density of the active metal species must be achieved. In order to ensure atomic dispersion, most of the SACs reported to date have had rather low surface densities of the active species (e.g. <0.5 wt%), which leads to a low-volume productivity, although the atom utilization is maximized. For practical applications, SACs with a high surface density of the active metal species are required; this can be accessed by engineering the metal–support interaction. The fabrication of support materials with a high density of defect sites will be favorable considering that the single atoms are usually anchored to the defect sites of the support (vacancies, coordination-unsaturated sites, etc.). For example, in the  $\text{Pt}/\text{WO}_x$  system [44,45,97], the mesoporous  $\text{WO}_x$  prepared by the alcoholysis method is rich in oxygen vacancies, which allows the Pt species interact strongly with the support and thereby be dispersed as single/pseudo single atoms even at a high loading of ~2.6 wt%. Nano-engineering of the support is another useful strategy to create abundant surface defects. When the support material is downsized to the nanoscale, both the surface area and density of defect sites will increase greatly, which should be favorable to the incorporation of more single atoms of the active metal. Typical examples include graphene-supported-Fe [17],  $\text{MoS}_2$ -monolayer-confined Co [95], CoO-nanosheet-supported Rh [80] and  $\text{TiO}_2$ -nanosheet-anchored Pd [42], all of which feature a practically high density of single atoms. Furthermore, because these 2D materials have distinct physical and chemical properties from their bulk counterparts, they might provide unique catalytic performance when loaded with single atoms. In some cases, doping heteroatoms into the support has also been found to be effective to stabilize a high density of single atoms. For example, the sodium cations in the  $\text{Pt-Na}/\text{FeO}_x$  SACs were found to enhance the dispersion and stabilization of Pt single atoms with a high loading (2.16 wt%) [32]; doping N atoms into carbon sheets can be effective to achieve a high loading of single Co (3.6 wt%) [12], Fe (1.0 wt%) [16] and Ni (7.5 wt%) [13] atoms.

Lastly, more *in situ* characterization techniques should be developed to monitor the dynamic structure of single atoms under operating conditions, as



this would be helpful for the understanding of the catalytic mechanism of SACs and the development of more efficient and robust SACs for the green synthesis of fine chemicals. Operando characterization is particularly challenging for liquid-phase reactions due to the involvement of solvent molecules, but it is of vital importance to efforts to establish a bridge between homogeneous and heterogeneous catalysis by the use of SACs.

## FUNDING

This work was supported by the National Natural Science Foundation of China (21373206, 21690080, 21690084, 21503219 and 21673228), the Strategic Priority Research Program of the Chinese Academy of Sciences (XDB17020100) and the National Key Projects for Fundamental Research and Development of China (2016YFA0202801).

## REFERENCES

- Pollak P. *Fine Chemicals: the Industry and the Business*. Hoboken: John Wiley & Sons, 2011.
- Joshi SS and Ranade VV. *Industrial Catalytic Processes for Fine and Specialty Chemicals*. Amsterdam: Elsevier, 2016.
- Merino E. Synthesis of azobenzenes: the coloured pieces of molecular materials. *Chem Soc Rev* 2011; **40**: 3835–53.
- Blaser HU, Steiner H and Studer M. Selective catalytic hydrogenation of functionalized nitroarenes: an update. *Chem Cat Chem* 2009; **1**: 210–21.
- Polshettiwar V and Varma RS. Green chemistry by nanocatalysis. *Green Chem* 2010; **12**: 743–54.
- Trost BM. Atom economy—a challenge for organic synthesis: homogeneous catalysis leads the way. *Angew Chem Int Ed Engl* 1995; **34**: 259–81.
- Beller M, Cornils B and Frohning CD *et al.* Progress in hydroformylation and carbonylation. *J Mol Catal A* 1995; **104**: 17–85.
- Qiao B, Wang A and Yang X *et al.* Single-atom catalysis of CO oxidation using Pt<sub>1</sub>/FeO<sub>x</sub>. *Nat Chem* 2011; **3**: 634–41.
- Yang X, Wang A and Qiao B *et al.* Single-atom catalysts: a new frontier in heterogeneous catalysis. *Acc Chem Res* 2013; **46**: 1740–8.
- Wei H, Liu X and Wang A *et al.* FeO<sub>x</sub>-supported platinum single-atom and pseudo-single-atom catalysts for chemoselective hydrogenation of functionalized nitroarenes. *Nat Commun* 2014; **5**: 5634.
- Lang R, Li T and Matsumura D *et al.* Hydroformylation of olefins by a rhodium single-atom catalyst with activity comparable to RhCl(PPh<sub>3</sub>)<sub>3</sub>. *Angew Chem Int Ed* 2016; **55**: 16054–8.
- Liu W, Zhang L and Yan W *et al.* Single-atom dispersed Co–N–C catalyst: structure identification and performance for hydrogenative coupling of nitroarenes. *Chem Sci* 2016; **7**: 5758–64.
- Liu W, Chen Y and Qi H *et al.* Ultra-durable Ni–N–C single-atom catalyst for biomass conversion under harsh conditions. *Angew Chem Int Ed* 2018; **57**: 7071–5.
- Xie J, Yin K and Serov A *et al.* Selective aerobic oxidation of alcohols over atomically-dispersed non-precious metal catalysts. *Chem Sus Chem* 2017; **10**: 359–62.
- Li M, Wu S and Yang X *et al.* Highly efficient single atom cobalt catalyst for selective oxidation of alcohols. *Appl Catal A Gen* 2017; **543**: 61–6.
- Liu W, Zhang L and Liu X *et al.* Discriminating catalytically active Fe<sub>Nx</sub> species of atomically dispersed Fe–N–C catalyst for selective oxidation of the C–H bond. *J Am Chem Soc* 2017; **139**: 10790–8.
- Deng D, Chen X and Yu L *et al.* A single iron site confined in a graphene matrix for the catalytic oxidation of benzene at room temperature. *Sci Adv* 2015; **1**: e1500462.
- Zhang M, Wang YG and Chen W *et al.* Metal (hydr) oxides@polymer core-shell strategy to metal single-atom materials. *J Am Chem Soc* 2017; **139**: 10976–9.
- Wang A, Li J and Zhang T. Heterogeneous single-atom catalysis. *Nat Rev Chem* 2018; **2**: 65–81.
- Liu J. Catalysis by supported single metal atoms. *ACS Catal* 2017; **7**: 34–59.
- Qin R, Liu P and Fu G *et al.* Strategies for stabilizing atomically dispersed metal catalysts. *Small Methods* 2018; **2**: 1700286.
- Zhang H, Liu G and Shi L *et al.* Single-atom catalysts: emerging multifunctional materials in heterogeneous catalysis. *Adv Energy Mater* 2018; **8**: 1701343.
- Asokan C, DeRita L and Christopher P. Using probe molecule FTIR spectroscopy to identify and characterize Pt-group metal based single atom catalysts. *Chin J Catal* 2017; **38**: 1473–80.
- Han B, Lang R and Qiao B *et al.* Highlights of the major progress in single-atom catalysis in 2015 and 2016. *Chin J Catal* 2017; **38**: 1498–507.
- Nishimura S. *Handbook of Heterogeneous Catalytic Hydrogenation for Organic Synthesis*. New York: Wiley, 2001.
- Downing RS, Kunkeler PJ and van Bekkum H. Catalytic syntheses of aromatic amines. *Catal Today* 1997; **37**: 121–36.
- Ren Y, Wei H and Yin G *et al.* Oxygen surface groups of activated carbon steer the chemoselective hydrogenation of substituted nitroarenes over nickel nanoparticles. *Chem Commun* 2017; **53**: 1969–72.
- Siegrist U, Baumeister P and Blaser HU *et al.* *Chemical Industries*. New York: Marcel Dekker, 1998, 207–20.
- Corma A, Serna P and Concepción P *et al.* Transforming non-selective into chemoselective metal catalysts for the hydrogenation of substituted nitroaromatics. *J Am Chem Soc* 2008; **130**: 8748–53.
- Zhai Y, Pierre D and Si R *et al.* Alkali-stabilized Pt–OH<sub>x</sub> species catalyze low-temperature water-gas shift reactions. *Science* 2010; **329**: 1633–6.
- Yang M, Li S and Wang Y *et al.* Catalytically active Au–O(OH)<sub>x</sub> species stabilized by alkali ions on zeolites and mesoporous oxides. *Science* 2014; **346**: 1498–501.
- Wei H, Ren Y and Wang A *et al.* Remarkable effect of alkalis on the chemoselective hydrogenation of functionalized nitroarenes over high-loading Pt/FeO<sub>x</sub> catalysts. *Chem Sci* 2017; **8**: 5126–31.

33. Xu G, Wei H and Ren Y *et al.* Chemoselective hydrogenation of 3-nitrostyrene over a Pt/FeO<sub>x</sub> pseudo-single-atom-catalyst in CO<sub>2</sub>-expanded liquids. *Green Chem* 2016; **18**: 1332–8.
34. Zhang S, Chang CR and Huang ZQ *et al.* High catalytic activity and chemoselectivity of sub-nanometric Pd clusters on porous nanorods of CeO<sub>2</sub> for hydrogenation of nitroarenes. *J Am Chem Soc* 2016; **138**: 2629–37.
35. Corma A and Serna P. Chemoselective hydrogenation of nitro compounds with supported gold catalysts. *Science* 2006; **313**: 332–4.
36. Wang L, Guan E and Zhang J *et al.* Single-site catalyst promoters accelerate metal-catalyzed nitroarene hydrogenation. *Nat Commun* 2018; **9**: 1362.
37. Makosch M, Sá J and Kartusch C *et al.* Hydrogenation of nitrobenzene over Au/MeO<sub>x</sub> catalysts—a matter of the support. *Chem Cat Chem* 2012; **4**: 59–63.
38. Zitolo A, Goellner V and Armel V *et al.* Identification of catalytic sites for oxygen reduction in iron- and nitrogen-doped graphene materials. *Nat Mater* 2015; **14**: 937–42.
39. Westerhaus FA, Jagadeesh RV and Wienhöfer G *et al.* Heterogenized cobalt oxide catalysts for nitroarene reduction by pyrolysis of molecularly defined complexes. *Nat Chem* 2013; **5**: 537–43.
40. Jagadeesh RV, Surkus AE and Junge H *et al.* Nanoscale Fe<sub>2</sub>O<sub>3</sub>-based catalysts for selective hydrogenation of nitroarenes to anilines. *Science* 2013; **342**: 1073–6.
41. Zhang L, Wang A and Wang W *et al.* Co-N-C catalyst for C-C coupling reactions: on the catalytic performance and active sites. *ACS Catal* 2015; **5**: 6563–72.
42. Liu P, Zhao Y and Qin R *et al.* Photochemical route for synthesizing atomically dispersed palladium catalysts. *Science* 2016; **352**: 797–800.
43. Zhang B, Asakura H and Zhang J *et al.* Stabilizing a platinum<sub>1</sub> single-atom catalyst on supported phosphomolybdic acid without compromising hydrogenation activity. *Angew Chem Int Ed* 2016; **55**: 8319–23.
44. Wang J, Zhao X and Lei N *et al.* Hydrogenolysis of glycerol to 1,3-propanediol under low hydrogen pressure over WO<sub>x</sub>-supported single/pseudo-single atom Pt catalyst. *Chem Sus Chem* 2016; **9**: 784–90.
45. Zhao X, Wang J and Yang M *et al.* Selective hydrogenolysis of glycerol to 1,3-propanediol: manipulating the frustrated lewis pairs by introducing gold to Pt/WO<sub>x</sub>. *Chem Sus Chem* 2017; **10**: 819–24.
46. Stephan DW. Frustrated Lewis pairs: from concept to catalysis. *Acc Chem Res* 2015; **48**: 306–16.
47. Kyriakou G, Boucher MB and Jewell AD *et al.* Isolated metal atom geometries as a strategy for selective heterogeneous hydrogenations. *Science* 2012; **335**: 1209–12.
48. Pei GX, Liu XY and Wang A *et al.* Promotional effect of Pd single atoms on Au nanoparticles supported on silica for the selective hydrogenation of acetylene in excess ethylene. *New J Chem* 2014; **38**: 2043–51.
49. Pei GX, Liu XY and Wang A *et al.* Ag alloyed Pd single-atom catalysts for efficient selective hydrogenation of acetylene to ethylene in excess ethylene. *ACS Catal* 2015; **5**: 3717–25.
50. Pei GX, Liu XY and Yang X *et al.* Performance of Cu-alloyed Pd single-atom catalyst for semihydrogenation of acetylene under simulated front-end conditions. *ACS Catal* 2017; **7**: 1491–500.
51. Zhou H, Yang X and Li L *et al.* PdZn intermetallic nanostructure with Pd-Zn-Pd ensembles for highly active and chemoselective semi-hydrogenation of acetylene. *ACS Catal* 2016; **6**: 1054–61.
52. Feng Q, Zhao S and Wang Y *et al.* Isolated single-atom Pd sites in intermetallic nanostructures: high catalytic selectivity for semihydrogenation of alkynes. *J Am Chem Soc* 2017; **139**: 7294–301.
53. Lucci FR, Liu J and Marcinkowski MD *et al.* Selective hydrogenation of 1,3-butadiene on platinum–copper alloys at the single-atom limit. *Nat Commun* 2015; **6**: 8550.
54. Yan H, Cheng H and Yi H *et al.* Single-atom Pd<sub>1</sub>/graphene catalyst achieved by atomic layer deposition: remarkable performance in selective hydrogenation of 1,3-butadiene. *J Am Chem Soc* 2015; **137**: 10484–7.
55. Huang X, Xia Y and Cao Y *et al.* Enhancing both selectivity and coking-resistance of a single-atom Pd<sub>1</sub>/C<sub>3</sub>N<sub>4</sub> catalyst for acetylene hydrogenation. *Nano Res* 2017; **10**: 1302–12.
56. Vilé G, Albani D and Nachtegaal M *et al.* A stable single-site palladium catalyst for hydrogenations. *Angew Chem Int Ed* 2015; **54**: 11265–9.
57. Hackett SFJ, Brydson RM and Gass MH *et al.* High-activity, single-site mesoporous Pd/Al<sub>2</sub>O<sub>3</sub> catalysts for selective aerobic oxidation of allylic alcohols. *Angew Chem Int Ed* 2007; **46**: 8593–6.
58. Li T, Liu F and Tang Y *et al.* Maximizing the number of interfacial sites in single-atom catalysts for the highly selective, solvent-free oxidation of primary alcohols. *Angew Chem Int Ed* 2018; **57**: 7795–9.
59. Zhang H, Watanabe T and Okumura M *et al.* Catalytically highly active top gold atom on palladium nanocluster. *Nat Mater* 2012; **11**: 49–52.
60. Xie S, Tsunoyama H and Kurashige W *et al.* Enhancement in aerobic alcohol oxidation catalysis of Au<sub>25</sub> clusters by single Pd atom doping. *ACS Catal* 2012; **2**: 1519–23.
61. Song G, Wang F and Li X. C–C, C–O and C–N bond formation via rhodium(III)-catalyzed oxidative C–H activation. *Chem Soc Rev* 2012; **41**: 3651–78.
62. Sahu S and Goldberg DP. Activation of dioxygen by iron and manganese complexes: a heme and nonheme perspective. *J Am Chem Soc* 2016; **138**: 11410–28.
63. Chandrasekhar V, Boomishankar R and Nagendran S. Recent developments in the synthesis and structure of organosilanols. *Chem Rev* 2004; **104**: 5847–910.
64. Chen Z, Zhang Q and Chen W *et al.* Single-site Au<sup>I</sup> catalyst for silane oxidation with water. *Adv Mater* 2018; **30**: 1704720.
65. Li W, Wang A and Yang X *et al.* Au/SiO<sub>2</sub> as a highly active catalyst for the selective oxidation of silanes to silanols. *Chem Commun* 2012; **48**: 9183–5.
66. Franke R, Selent D and Boörner A. Applied hydroformylation. *Chem Rev* 2012; **112**: 5675–732.
67. Evans D, Osborn JA and Wilkinson G. Hydroformylation of alkenes by use of rhodium complex catalysts. *J Chem Soc, A* 1968; 3133–42.
68. Ford ME and Premecz JE. Preparation and evaluation of ion exchange resin-immobilized rhodium-phosphine hydroformylation catalysts. *J Mol Catal* 1983; **19**: 99–112.
69. Li C, Wang W and Yan L *et al.* A mini review on strategies for heterogenization of rhodium-based hydroformylation catalysts. *Front Chem Sci Eng* 2018; **12**: 113–23.
70. Sun Q, Dai Z and Meng X *et al.* Enhancement of hydroformylation performance via increasing the phosphine ligand concentration in porous organic polymer catalysts. *Catal Today* 2017; **298**: 40–5.
71. Sun Q, Dai Z and Meng X *et al.* Task-specific design of porous polymer heterogeneous catalysts beyond homogeneous counterparts. *ACS Catal* 2015; **5**: 4556–67.
72. Jiang M, Yan L and Ding Y *et al.* Ultrastable 3V-PPh<sub>3</sub> polymers supported single Rh sites for fixed-bed hydroformylation of olefins. *J Mol Catal A: Chem* 2015; **404**: 211–7.
73. Li C, Yan L and Lu L *et al.* Single atom dispersed Rh-biphenos&PPh<sub>3</sub>@porous organic copolymers: highly efficient catalysts for continuous fixed-bed hydroformylation of propene. *Green Chem* 2016; **18**: 2995–3005.
74. Huang L and Kawi S. An active and stable Wilkinson's complex-derived SiO<sub>2</sub>-tethered catalyst via an amine ligand for cyclohexene hydroformylation. *Catal Lett* 2004; **92**: 57–62.

75. van der Veen LA, Keeven PH and Schoemaker GC *et al.* Origin of the bite angle effect on rhodium diphosphine catalyzed hydroformylation. *Organometallics* 2000; **19**: 872–83.
76. Billig E, Abatjoglou AG and Bryant DR. (Union Carbide Corp.) Bis-phosphite compounds. 1987; Eur. Pat. EP0213639.
77. Billig E, Abatjoglou AG and Bryant DR. (Union Carbide Corp.) Bis-phosphite compounds. 1988; US Pat. 4748261.
78. Li C, Sun K and Wang W *et al.* Xantphos doped Rh/POPs-PPh<sub>3</sub> catalyst for highly selective long-chain olefins hydroformylation: chemical and DFT insights into Rh location and the roles of Xantphos and PPh<sub>3</sub>. *J Catal* 2017; **353**: 123–32.
79. Liu J, Yan L and Ding Y *et al.* Promoting effect of Al on tethered ligand-modified Rh/SiO<sub>2</sub> catalysts for ethylene hydroformylation. *Appl Catal, A* 2015; **492**: 127–32.
80. Wang L, Zhang W and Wang S *et al.* Atomic-level insights in optimizing reaction paths for hydroformylation reaction over Rh/CoO single-atom catalyst. *Nat Commun* 2016; **7**: 14036.
81. Liu X, Hu B and Fujimoto K *et al.* Hydroformylation of olefins by Au/Co<sub>3</sub>O<sub>4</sub> catalysts. *Appl Catal, B* 2009; **92**: 411–21.
82. Miyaura N, Yanagi T and Suzuki A. The palladium-catalyzed cross-coupling reaction of phenylboronic acid with haloarenes in the presence of bases. *Synth Commun* 1981; **11**: 513–9.
83. Heck RF. Palladium-catalyzed vinylation of organic halides. *Org React* 1982; **27**: 345–90.
84. Stork G, Rosen P and Goldman NL. The  $\alpha$ -alkylation of enolates from the lithium-ammonia reduction of  $\alpha, \beta$ -unsaturated ketones. *J Am Chem Soc* 1961; **83**: 2965–6.
85. Zhang L, Wang A and Miller JT *et al.* Efficient and durable Au alloyed Pd single-atom catalyst for the Ullmann reaction of aryl chlorides in water. *ACS Catal* 2014; **4**: 1546–53.
86. Zhang X, Sun Z and Wang B *et al.* C-C coupling on single-atom based heterogeneous catalyst. *J Am Chem Soc* 2018; **140**: 954–62.
87. Lee EK, Park SA and Woo H *et al.* Platinum single atoms dispersed on carbon nanotubes as reusable catalyst for Suzuki coupling reaction. *J Catal* 2017; **352**: 388–93.
88. Liu Y, Zhou Y and Li J *et al.* Direct aerobic oxidative homocoupling of benzene to biphenyl over functional porous organic polymer supported atomically dispersed palladium catalyst. *Appl Catal B* 2017; **209**: 679–88.
89. Yan Z, Lin L and Liu S. Synthesis of  $\gamma$ -valerolactone by hydrogenation of biomass-derived levulinic acid over Ru/C catalyst. *Energy Fuels* 2009; **23**: 3853–8.
90. Cao W, Luo W and Ge H *et al.* UiO-66 derived Ru/ZrO<sub>2</sub>@C as a highly stable catalyst for hydrogenation of levulinic acid to  $\gamma$ -valerolactone. *Green Chem* 2017; **19**: 2201–11.
91. Ftouni J, Muñoz-Murillo A and Goryachev A *et al.* ZrO<sub>2</sub> is preferred over TiO<sub>2</sub> as support for the Ru-catalyzed hydrogenation of levulinic acid to  $\gamma$ -valerolactone. *ACS Catal* 2016; **6**: 5462–72.
92. Ji N, Zhang T and Zheng M *et al.* Direct catalytic conversion of cellulose into ethylene glycol using nickel-promoted tungsten carbide catalysts. *Angew Chem* 2008; **120**: 8638–41.
93. Pang J, Zheng M and Sun R *et al.* Synthesis of ethylene glycol and terephthalic acid from biomass for producing PET. *Green Chem* 2016; **18**: 342–59.
94. Wang A and Zhang T. One-pot conversion of cellulose to ethylene glycol with multifunctional tungsten-based catalysts. *Acc Chem Res* 2013; **46**: 1377–86.
95. Liu G, Robertson AW and Li MMJ *et al.* MoS<sub>2</sub> monolayer catalyst doped with isolated Co atoms for the hydrodeoxygenation reaction. *Nat Chem* 2017; **9**: 810–6.
96. Li C, Zhao X and Wang A *et al.* Catalytic transformation of lignin for the production of chemicals and fuels. *Chem Rev* 2015; **115**: 11559–624.
97. Yang M, Zhao X and Ren Y *et al.* Pt/Nb-WO<sub>x</sub> for the chemoselective hydrogenolysis of glycerol to 1,3-propanediol: Nb dopant pacifying the over-reduction of WO<sub>x</sub> supports. *Chin J Catal* 2018; **39**: 1027–37.

## MATERIALS SCIENCE

Special Topic: Single-Atom Catalysts

**Recent advances in the precise control of isolated single-site catalysts by chemical methods**Zhijun Li<sup>1,†</sup>, Dehua Wang<sup>3,†</sup>, Yuen Wu<sup>1,\*</sup> and Yadong Li<sup>1,2,\*</sup>**ABSTRACT**

The search for constructing high-performance catalysts is an unending topic in chemical fields. Recently, we have witnessed many breakthroughs in the synthesis of single-atom catalysts (SACs) and their applications in catalytic systems. They have shown excellent activity, selectivity, stability, efficient atom utilization and can serve as an efficient bridge between homogeneous and heterogeneous catalysis. Currently, most SACs are synthesized via a bottom-up strategy; however, drawbacks such as the difficulty in accessing high mass activity and controlling homogeneous coordination environments are inevitably encountered, restricting their potential use in the industrial area. In this regard, a novel top-down strategy has been recently developed to fabricate SACs to address these practical issues. The metal loading can be increased to 5% and the coordination environments can also be precisely controlled. This review highlights approaches to the chemical synthesis of SACs towards diverse chemical reactions, especially the recent advances in improving the mass activity and well-defined local structures of SACs. Also, challenges and opportunities for the SACs will be discussed in the later part.

**Keywords:** single-atom catalysts, bottom-up, top-down, catalytic performance**INTRODUCTION**

In the worldwide theme of exploring efficient and low-cost technologies for energy conversion and chemical transformations, substantial effort has been devoted to the development of general, practical and simple chemical approaches for catalyst preparation in past decades [1–6]. Studies have shown that ultrasmall assemblies, compared to their macroscopic counterparts [7], can exhibit essentially different physical and chemical properties. These unique properties would drastically alter their practical applications in a variety of areas, such as catalysis, biomedical research, energy and environmental fields [6]. Therefore, metal nanoparticles represent a rich resource for a variety of chemical processes, employed both in industry and in academia [8]. The maximized surface area of support, increased number of catalytic active sites, minimized catalyst loading and strong catalyst-support interaction determine the nature of nanocatalysts [2,6]. The supported metal nanoparticles are frequently employed

in heterogeneous catalysis; however, to greatly increase the turnover frequency of surface active sites and to enhance the mass activity remain the primary goals in catalysis [9,10]. In most circumstances, it has been demonstrated that the surface atoms of the nanomaterials in an unsaturated coordination environment generally act as the active sites to catalyze specific reactions [11]. Therefore, extensive studies have been devoted to rationally controlling the shapes, structures, crystal phases and compositions of nanocatalysts [3,8,12–18].

With decreasing the size of nanomaterials, the number of surface atoms is increased substantially, exposing more defects and active sites, tuning geometric and electronic properties involved in chemical reactions [10]. Nanoclusters have shown intriguing properties because of the reduced size compared to nanoparticles, exposing more uncoordinated active sites and changing molecular orbital energy levels [19,20]. Heiz and co-workers found a pronounced size effect for model catalysts of

<sup>1</sup>Department of Chemistry, iChEM (Collaborative Innovation Center of Chemistry for Energy Materials), University of Science and Technology of China, Hefei 230026, China;

<sup>2</sup>Department of Chemistry, Tsinghua University, Beijing 100084, China and

<sup>3</sup>School of Pharmaceutical and Chemical Engineering, Taizhou University, Taizhou 318000, China

\*Corresponding authors. E-mails: yuenwu@ustc.edu.cn; ydli@mail.tsinghua.edu.cn  
†Equally contributed to this work.

Received 21 March 2018; Revised 10 May 2018; Accepted 31 May 2018

size-selected  $\text{Pd}_n$  ( $n \leq 30$ ) clusters supported on  $\text{MgO}(100)$  for the cyclotrimerization of acetylene to benzene [21]. Anderson *et al.* studied size-selected palladium clusters and deposited them on the rutile phase of titanium dioxide ( $\text{TiO}_2$ ) for CO oxidation [22]. By employing X-ray photoemission spectroscopy and temperature-programmed reaction measurements, they found that the activity of these catalysts was associated with  $\text{Pd}_{3d}$  binding energy. Li *et al.* utilized a double-solvent method combined with a photoreduction process to prepare active Pd nanoclusters encapsulated inside the cage of  $\text{NH}_2\text{-Uio-66}$  [23]. The resultant catalyst showed exceptional performance for a Suzuki coupling reaction under visible-light irradiations. Nevertheless, although the sizes of the nanoclusters have been reduced, their multiple distributions of active metal sites alongside different geometric and electric structures might not be ideal for specific catalytic reactions [9,10]. The stability of nanoclusters would also be a problem for their application in heterogeneous catalysis, especially at higher operational temperatures [24].

Further downsizing nanoclusters to the atomic level, namely single atoms (SAs), maximum atom utilization and superior/distinguishing catalytic performance are supposed to be obtained [9,10]. Of note is the fact that unexpected superior catalytic performances of the single-atom catalysts (SACs) are often observed as one of the key advances of these novel catalysts versus their nanoscale counterparts. This can be ascribed to the unsaturated environments of metal active sites, quantum size effects and metal-support interactions [25–28]. Therefore, the research on SACs has rapidly progressed from their fundamental aspects to pursuing practical applications in areas of nanotechnology and materials science. A study that has attracted considerable attention since its publication in 1995 is that of Thomas *et al.*, who reported that direct grafting of organometallic complexes onto the walls of mesoporous silica gives a shape-selective high-performance catalyst with well-separated, homogeneously dispersed and high surface concentrations of active sites for the epoxidation of cyclohexenes and their derivatives [29]. Later, in 2003, Flytzani-Stephanopoulos *et al.* discovered that the water-gas shift reaction was not affected by the catalytic activity of metallic Au or Pt nanoparticles; instead, nonmetallic Au or Pt species on the ceria surface played a key role in this reaction [30]. In 2007, Lee *et al.* successfully synthesized  $\text{Pd-Al}_2\text{O}_3$  catalyst and validated that the extremely low metal loading leads to the formation of atomically isolated  $\text{Pd}^{\text{II}}$  species, which greatly contribute to the excellent selox ac-

tivity of allylic alcohols [31]. The key discovery was that the employment of homogeneously dispersed SACs generally confers a dramatic improvement in catalytic activity, selectivity and stability, or even considerably different catalytic properties than the corresponding nanoparticles and nanoclusters [32–35]. This is highly desirable and has attracted extensive scientific attention, as they might potentially act as alternatives to circumvent the problems of scarcity and high cost of the noble-metal catalysts used in large-scale catalysis applications [36]. Specifically, the active single-atom sites are well defined and atomically stabilized on the supports, and the identical geometric structure of each active site is similar to that of a homogeneous catalyst. Recently, studies have clearly demonstrated that the utility and uniqueness of these SACs have great potential to bridge the gap between homogeneous and heterogeneous catalysis [37–42]. This would solve the problems of the difficulty in separating the homogeneous catalysts from raw materials and products, as well as combining the merits of both hetero- and homogeneous catalysts. The SACs also provide a good avenue to identify the detailed structural features for the active sites and an ideal model to elucidate the structure-activity relationship [43–45]. Such catalysts have shown intriguing interests in the catalysis field [10,32,34,43,46–49]. To meet the practical demand, the most important challenges for fabricating the SACs are to increase the density of active sites and to improve their intrinsic activities [32,36,45]. The first challenge is the high propensity for aggregation of SAs once the size of the nanomaterials is greatly reduced [10]. The second challenge is the rational control of the coordination environment of the single metal atoms.

Recently, several strategies for constructing atomically dispersed metal sites on catalyst supports have been extensively studied [9,10,32,42]. These strategies include enhancing the metal-support interactions, engineering vacancy defects and voids on the supports, and modifying surface functional groups [9,42]. In most cases, the supports for isolated SACs are chosen on purpose, as they can stabilize the isolated catalytic SAs or activate nearby reactants to form intermediate species for the catalytic active sites [50–52]. For example, zeolites could provide effective voids to anchor individual metal atoms to maintain the high dispersion of the isolated metal atoms and prevent them from sintering at high temperatures under oxidative or reductive atmospheres during catalysis processes [53]. Nanoparticles and nanoclusters can also serve as supports. Through elegant studies of support materials, Sykes *et al.* showed that the isolated Pd atoms can be supported on a Cu surface and

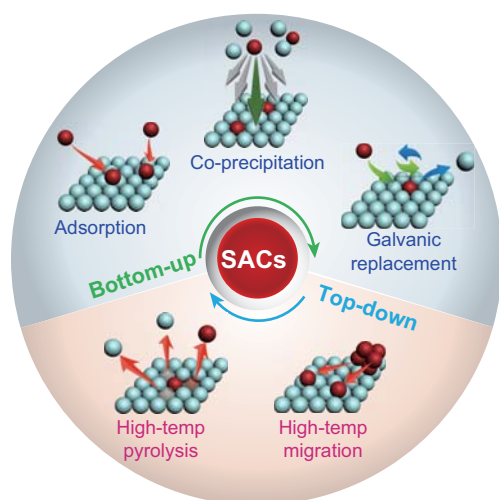


**Figure 1.** Schematic representation of the bottom-up and top-down strategies for the synthesis of SACs.

significantly lower the energy barrier to hydrogen uptake on and subsequent desorption from the nearby Cu atoms [48]. This facile hydrogen dissociation at the isolated Pd atoms and weak binding to the Cu surface together facilitate selective hydrogenation of styrene and acetylene. Toshima *et al.* described a crown-jewel concept for the construction of catalytically highly active top gold atoms on palladium nanoclusters [54]. Interestingly, the gold atoms can be controllably assembled at the top position on the cluster and exhibit high catalytic activity because of their high negative-charge density and unique structure. Recent reports have begun to document that the defects in reducible oxides (e.g.  $\text{TiO}_2$  and  $\text{CeO}_2$ ), graphene or  $\text{C}_3\text{N}_4$  also help to stabilize isolated metal atoms [32,42,55]. For example, Du *et al.* investigated the favorable role of isolated palladium and platinum atoms supported on graphitic carbon nitride ( $\text{g-C}_3\text{N}_4$ ) to act as photocatalysts for  $\text{CO}_2$  reduction [56]. Overall, an important conclusion derived from these works is that the further development of this SACs field requires a more fundamental understanding of SA formation at the atomic scale.

This review covers the preparation strategies for SACs, which can be categorized according to how their components are integrated, namely via bottom-up and top-down approaches (Fig. 1). Currently, a large majority of SACs are synthesized via a bottom-up strategy by using oxides or carbon supports to construct N or O defects to enable the deposition of metal precursors. This is followed by a chemical reduction process to generate SACs from high-oxidation-state ions to low oxidation state. However, the following drawbacks are encountered frequently: difficulty in accessing high metal loading

because of their high propensity for aggregation and the difficulty in constructing homogeneous coordination environments for the reactive sites. These drawbacks lead to limited selectivity and stability of the SACs, greatly limiting their potential use in various industrial fields. In this regard, Li and Wu proposed a top-down strategy to construct SACs by the pyrolysis of metal nodes in metal-organic frameworks (MOFs) for the first time [57]. In this case, the introduction of Zn atoms into MOFs is important and can effectively prevent the formation of Co NPs (nanoparticles) during the high-temperature pyrolysis process. The resulting Co SAC has a high metal loading close to 5% and showed exceptional chemical and thermal stability. A distinguishing feature of this strategy is not only that the metal loading can be substantially increased from 1% to 5%, which is important from practical perspectives, but it can control the coordination environments to construct high-performance SACs by exposing real active sites. This top-down strategy overcome challenges in the fabrication of SACs with a traditional bottom-up strategy and has great potential to meet the requirement for use in practical applications. In addition to the fabrication strategies, the use of these methods in different chemical reactions will also be presented. Finally, future challenges and opportunities will be discussed.

## BOTTOM-UP SYNTHETIC METHODOLOGIES FOR THE CONSTRUCTION OF SACs

The bottom-up strategy is the most common method to synthesize metal SACs, during which the metal precursors are adsorbed, reduced and confined by the vacancies or defects of the supports [9,10,32,52]. Nevertheless, how to effectively increase the SACs loading with well-defined dispersion on the supports is still challenging. First, aggregation would occur during a chemical synthesis or catalytic process when high loading of SAs is required. Second, the architectural structures of anchor sites for confining and stabilizing the metal SACs on the support remain elusive; therefore, the coordination environment for metal SAs might be inhomogeneous and poorly defined [58]. Optimization of the precursors and supports and controlling of the synthetic procedures play a key role in tuning the metal-support interaction and guaranteeing the homogeneous dispersion of SACs.

For the wet-chemistry strategy, the precursor solutions of mononuclear metal complexes are first anchored to the supports by a coordination effect

## Co-precipitation

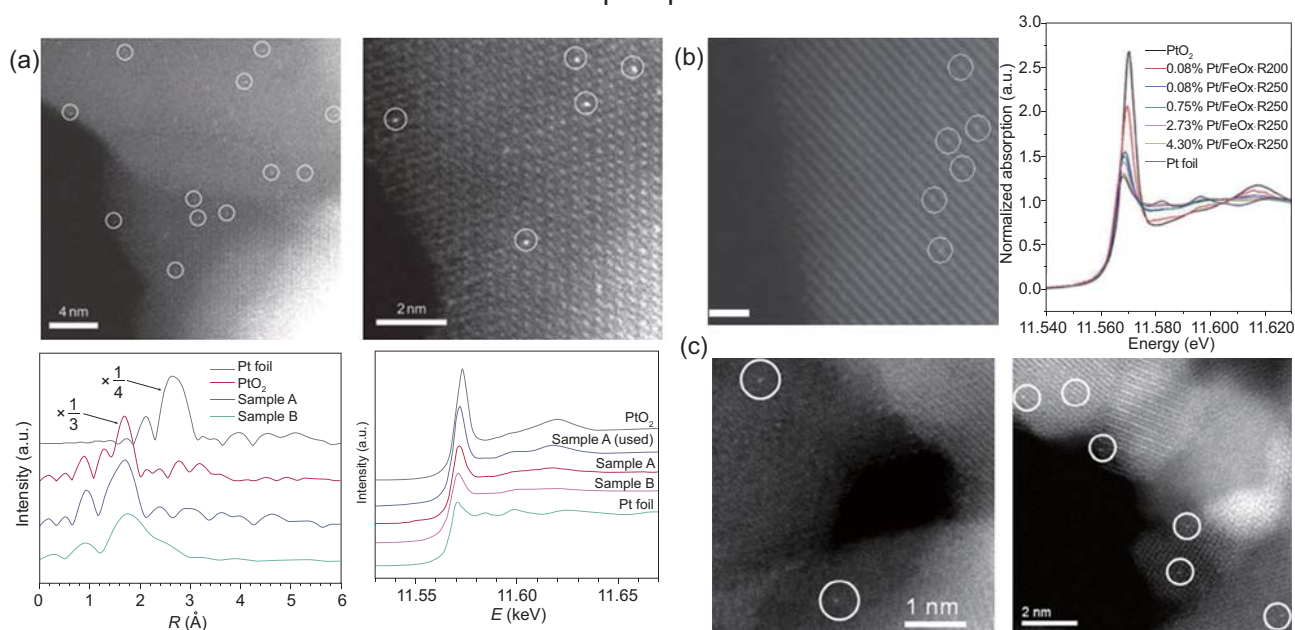


**Figure 2.** (a) HAADF-STEM images of Pt<sub>1</sub>/FeO<sub>x</sub>. Adapted with permission from [46]. (b) HAADF-STEM image of 0.08%Pt/FeO<sub>x</sub>-R200. Adapted with permission from [60]. (c) HAADF-STEM images of Ir<sub>1</sub>/FeO<sub>x</sub>. Adapted with permission from [61].

between the metal complexes and the functional groups of the support surfaces [32]. Then, the organic ligands of the metal complexes are removed by a post-treatment to expose more active sites to meet the requirement of catalytic reactions. Particularly, the advantage of wet chemistry for preparing SACs is that this method does not require specialized equipment and can be routinely practiced in any chemistry lab [59].

### Co-precipitation approach

Co-precipitation is one of the commonly employed approaches for preparing SACs, during which the substances that are normally soluble under the conditions would be precipitated. A significant advantage of this method lies in its extreme simplicity, as no additional complicated steps are involved. For a classical example, Zhang *et al.* employed this method to fabricate single Pt atoms supported on iron oxide nanocrystallites (Pt<sub>1</sub>/FeO<sub>x</sub>) [46]. The metal precursor of H<sub>2</sub>PtCl<sub>6</sub>·H<sub>2</sub>O was mixed with Fe(NO<sub>3</sub>)<sub>3</sub>·9H<sub>2</sub>O in a proper molar ratio and pH. After recovery, the precipitate was dried and calcined, resulting in the formation of Pt<sub>1</sub>/FeO<sub>x</sub>. The aberration-corrected scanning transmission electron microscopy (AC-STEM) and extended X-ray absorption fine structure (EXAFS) spectra demonstrated the individual Pt atoms were uniformly dispersed on FeO<sub>x</sub> support, with a metal loading level of 0.17 wt% (Fig. 2a). This

SAC showed extremely high atom efficiency, excellent stability and superior activity for both CO oxidation and preferential oxidation of CO in H<sub>2</sub>. They found that these merits can be attributed to the partially vacant 5d orbitals of the positively charged high-valent Pt atoms, as they can effectively reduce CO-adsorption energy and activation barriers that are required for CO oxidation. This study demonstrated the feasibility of using the defects of oxide supports to serve as anchoring sites for metal clusters and single metal atoms. Subsequently, the feasibility and efficiency of this approach were further demonstrated by the Zhang group showing that the high-performance Pt- and Ir-based SACs could also be obtained (Fig. 2b and c) for use in organic transformation [60] and water-gas shift reactions [61]. In these examples, defects in the oxide supports and the amount of metal loading were found to be critical for accessing high-performance SACs that would normally lead to aggregation.

### Adsorption approach

The adsorption method is one of the most fundamental approaches for constructing isolated metal atoms on the supports [62,63]. It is simple, direct and has been widely used in the preparation of supported metal catalysts. Generally, after the metal precursors are adsorbed on the support, the residual solution is removed and then the catalysts are dried and calcined. To ensure the SAs could be stably

anchored onto the supports with atomic dispersion, appropriate functional groups on the supports should be given consideration.

Oxides are generally employed as an efficient support for preparing catalysts. In 2013, Narula *et al.* [64] reported single Pt atoms supported on  $\theta$ -Al<sub>2</sub>O<sub>3</sub>(010) prepared by a wet-impregnation method using alumina powder and chloroplatinic acid. In this work, water was gradually evaporated before the resulting powder was transferred to an alumina crucible and subjected to a pyrolysis process. The resultant catalyst was catalytically active in its ability to oxidize CO to CO<sub>2</sub>. In addition, series of Pt/ $\theta$ -Al<sub>2</sub>O<sub>3</sub> catalysts with different metal loadings were prepared, and the results reveal that they are highly active towards NO oxidation [65].

In the same year, Tao *et al.* [66] developed an impregnation-reduction method for preparing singly dispersed Rh atoms supported on Co<sub>3</sub>O<sub>4</sub> nanorods. This method involves the impregnation of Rh<sup>3+</sup> on Co<sub>3</sub>O<sub>4</sub> nanorods followed by on-site reduction of Rh<sup>3+</sup> using NaBH<sub>4</sub>. *In situ* characterizations reveal evidence of the active sites of isolated Rh atoms in the formation of RhCo<sub>n</sub> on Co<sub>3</sub>O<sub>4</sub> nanorods, which were generated through restructuring of Rh<sub>1</sub>/Co<sub>3</sub>O<sub>4</sub> at 220°C in reactant gases. The resulting new catalytic phase exhibits a high selectivity to produce N<sub>2</sub> in the reduction of NO with H<sub>2</sub> between 180°C and 300°C.

A report by Li *et al.* demonstrated that single Pt<sub>1</sub> and Au<sub>1</sub> atoms can be stabilized by lattice oxygen on ZnO{1010} surface via an adsorption method [67]. In detail, ZnO-nanowires (nws) were dispersed in de-ionized water followed by the addition of H<sub>2</sub>PtCl<sub>6</sub>·6H<sub>2</sub>O or HAuCl<sub>4</sub> solution. After an aging process, the suspension was filtered, washed and dried to give Pt<sub>1</sub>/ZnO and Au<sub>1</sub>/ZnO catalysts. Similarly, Zhang *et al.* fabricated an Rh SAC supported on ZnO nws by introducing RhCl<sub>3</sub> solution into ZnO nws that were dispersed in de-ionized water [40]. After stirring and aging processes, the resulting precipitate was filtered, washed, dried and reduced. As the weight loading of Rh reduced from 0.03% to 0.006%, the isolated Rh SACs can be clearly observed. During the synthetic process, the Rh atoms bond with proximal Zn atoms which lose one or more O atoms. Therefore, electrons transfer from metallic Zn to Rh atoms to generate near-metallic Rh species. The results show that the as-obtained Rh<sub>1</sub>/ZnO-nws SACs exhibited comparable efficiency in the hydroformylation of several olefins to the homogeneous Wilkinson's catalyst, along with superior catalytic activity to those of the most highly reported heterogeneous nanoparticle-based catalysts.

In a more recent piece of work, Wang and co-workers described a convenient two-step synthesis of an atomically dispersed Pt catalyst supported on ceria (CeO<sub>2</sub>), with 1 wt.% metal loading, by wetness impregnation and steam treatment [68]. Chloroplatinic acid was added drop-wise to the CeO<sub>2</sub> support while being ground in a mortar and pestle. The as-obtained powder was then dried, calcined, thermal aged and steam treated to give the catalyst. The authors demonstrated that the activation of SACs on CeO<sub>2</sub> via high-temperature steam treatment can accomplish excellent low-temperature CO-oxidation activity and superior thermal stability. This is because the steam treatment can enable the formation of active surface lattice oxygen near isolated Pt atoms to considerably enhance catalytic performance. Further investigation of the nature of this active surface lattice oxygen on Pt/CeO<sub>2</sub> was supported by density functional theory (DFT) calculations and reaction kinetic analyses. They found the oxygen vacancies from the CeO<sub>2</sub> bulk can redistribute to the CeO<sub>2</sub>(111) surface when exposed to water at a high temperature. During the steam-treatment process, H<sub>2</sub>O molecules can fill out the oxygen vacancy over the atomically dispersed Pt/CeO<sub>2</sub> surface, affording two neighboring active O<sub>lattice</sub>[H] sites around Pt. This provides the significantly improved reactivity and stability.

Yan and co-workers developed a unique adsorption approach to construct Pt SACs, anchored in the internal surface of mesoporous Al<sub>2</sub>O<sub>3</sub>, by a modified sol-gel solvent vaporization self-assembly method [69], as shown in Fig. 3a. Triblock copolymers P123, C<sub>9</sub>H<sub>21</sub>AlO<sub>3</sub> and H<sub>2</sub>PtCl<sub>6</sub> were first mixed in ethanol. With continued evaporation of the solvent, the amphiphilic P123 macromolecules and C<sub>9</sub>H<sub>21</sub>AlO<sub>3</sub> assembled into a highly ordered hexagonally arranged mesoporous structure, with Pt precursor encapsulated in the matrix. The as-obtained gel was then calcined in air to decompose the P123 template. Meanwhile, the C<sub>9</sub>H<sub>21</sub>AlO<sub>3</sub> was transformed into a rigid, well-aligned mesoporous Al<sub>2</sub>O<sub>3</sub> framework. This was followed by a reducing step in 5% H<sub>2</sub>/N<sub>2</sub> to give the isolated Pt SAs stabilized by the unsaturated pentahedral Al<sup>3+</sup> centers. The authors showed that the catalyst retained its structural integrity and exceptional catalytic performance in several reactions under harsh conditions, such as hydrogenation of 1,3-butadiene after exposure to a reductive atmosphere at 200°C for 24 h, n-hexane hydroreforming at 550°C for 48 h and CO oxidation after 60 cycles between 100°C and 400°C over 1 month.

Zeolites are crystalline materials with well-defined structures and high surface area, along with more sites for robust bonding with catalytic species



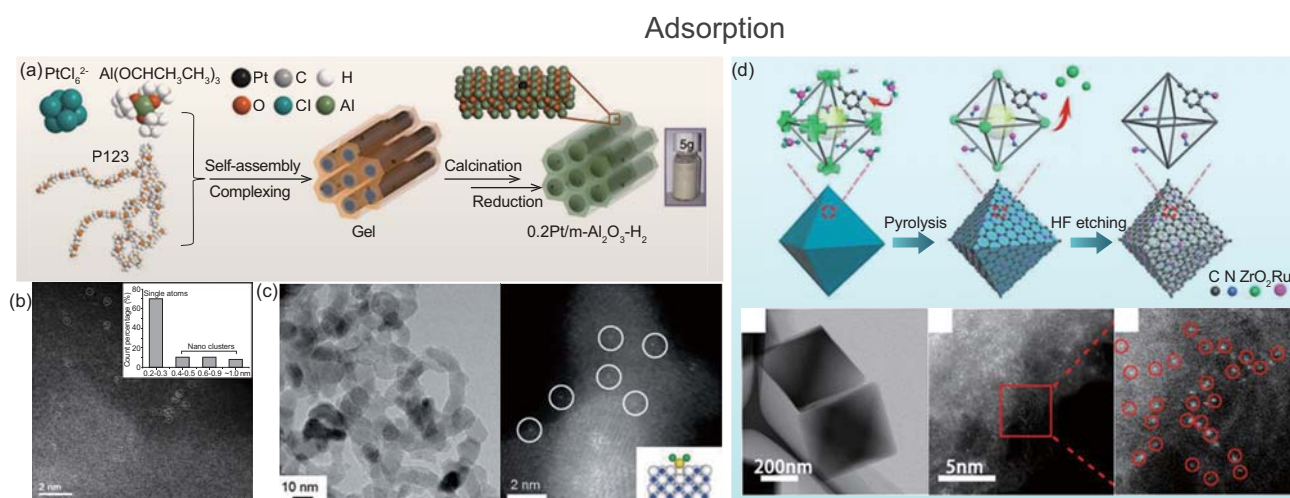


**Figure 3.** (a) Schematic illustration of the  $0.2\text{Pt}/\text{m-Al}_2\text{O}_3\text{-H}_2$  synthesis process. Adapted with permission from [69]. (b) HAADF-STEM images of the  $0.25\text{Au-Na}/[\text{Si}]\text{MCM41}$  catalyst. Adapted with permission from [72]. (c) TEM and HAADF-STEM images of  $0.35\text{ wt\% Pt}/\text{TiN}$ . Adapted with permission from [73]. (d) Scheme of proposed formation mechanisms, TEM and HAADF-STEM images for Ru SAs/N-C. Adapted with permission from [76].

[24,70]. Specifically, zeolites could provide effective voids to anchor individual metal atoms to maintain the high dispersion and prevent them from sintering at high temperatures under oxidative or reductive atmospheres during the catalysis processes [53]. In 2012, Gates *et al.* reported that atomically dispersed gold atoms catalyze with a high degree of uniformity supported on zeolite NaY [71]. The site-isolated gold complexes retained after CO-oxidation catalysis, confirming the robust stabilization effect of the zeolite channels for gold species.

The addition of alkali ions, such as sodium or potassium, on inert KLTL-zeolite and mesoporous MCM-41 silica materials could structurally stabilize the single gold sites in  $\text{Au-O}(\text{OH})_x$  ensembles (Fig. 3b), as demonstrated by Flytzani-Stephanopoulos and co-workers [72]. They have shown evidence that the active catalyst was composed of alkali ions linked to the gold atom through  $-\text{O}$  ligands, not merely on the support, making the reducible oxide supports no longer an essential requirement. The validation tests show that the single-site gold atoms were homogeneously dispersed and highly active for the industrially important low-temperature water-gas shift reaction.

In addition to metal oxides and zeolites, other supports such as nitrides and carbides have also been explored and shown promise for stabilizing SAs for use in catalysis. Lee *et al.* described a Pt SAC supported on titanium nitride (TiN) nanoparticles with the aid of chlorine ligands [73].  $\text{H}_2\text{PtCl}_6 \cdot 6\text{H}_2\text{O}$  was dissolved in anhydrous ethanol and mixed with acid-treated TiN nanoparticles before the resulting sample was dried and reduced. Transmission electron microscopy (TEM) and HAADF-STEM images of the samples are shown in Fig. 3c.

The results show that the  $0.35\text{ wt\% Pt}/\text{TiN}$  sample affords a high mass activity and a unique selectivity towards electrochemical oxygen reduction, formic acid oxidation and methanol oxidation.

Carbon nitride ( $\text{C}_3\text{N}_4$ ) has been proved as an alternative support material by virtue of their porosity and high surface area [55]. Li *et al.* used an impregnation method to access isolated Au atoms anchored on polymeric mesoporous graphitic  $\text{C}_3\text{N}_4$  (mpg- $\text{C}_3\text{N}_4$ ) [74]. The catalytically active  $\text{Au}^{\text{I}}$  atom was coordinated by three nitrogen or carbon atoms in tri-s-triazine repeating units. This coordination feature significantly prevents the Au atoms from aggregation and makes the  $\text{Au}^{\text{I}}$  surface highly active. Moreover, they demonstrated this catalyst as highly active, selective and stable for silane oxidation with water.

In 2017, Ma *et al.* developed a highly efficient catalyst consisting of isolated Pt atoms uniformly dispersed on an  $\alpha$ -molybdenum carbide ( $\alpha$ -MoC) support that can enable low-temperature, base-free hydrogen production through aqueous-phase reforming of methanol [75]. They found that the  $\alpha$ -MoC displays stronger interactions with Pt than other oxide supports or  $\beta$ - $\text{Mo}_2\text{C}$ ; therefore, atomically dispersed Pt atoms can be formed on an  $\alpha$ -MoC support following a high-temperature activation process. This generates an exceptionally high-density electron-deficient surface to stabilize Pt sites for the adsorption/activation of methanol. This catalyst affords an excellent turnover frequency and the corresponding hydrogen production greatly exceeds those of previously reported catalysts for low-temperature aqueous-phase reforming of methanol. They deduce that the unique structure of  $\alpha$ -MoC, which affects water dissociation, and the synergic

effects between Pt and  $\alpha$ -MoC together affect the activation of methanol and the subsequent reforming process.

In 2017, Wu *et al.* reported a novel synthetic approach to construct isolated single Ru atoms on nitrogen-doped porous carbon (Ru SAs/N-C) by a coordination-assisted strategy using MOFs for the hydrogenation of quinolones [76]. It is noticed that the strong coordination effect between the lone pair of nitrogen and d-orbital of Ru atoms is crucial for the formation of stable Ru SAs (Fig. 3d). Without the dangling  $-\text{NH}_2$  groups, the Ru atoms tend to aggregate into nanoclusters, even confined in the pores of MOFs. The results demonstrate the Ru SAs serve as an effective semi-homogeneous catalyst to the chemoselective catalyze hydrogenation of quinolones. This method has been shown to potentially broaden the substrate scope for the synthesis of SACs with unique properties for use in various chemical reactions.

Together, the ease of preparation for SACs using a wet-chemistry strategy envisages a promising future in the field. However, these methods have their own disadvantages. For example, some metal atoms might be buried either in the interfacial regions of the support agglomerates or within the bulk of the support when co-precipitation methods are applied [43]. In addition, when high metal loading is required for the construction of SACs, aggregation would inevitably occur [9]. This trade-off should be minimized by developing new synthesis methods.

Other methodologies have also been explored to design and synthesize SACs with varies chemical and physical functionalities and future underpinned studies in these directions. The photochemical method becomes particularly appealing to assist the effective adsorption of SAs on the supports and has been proven to be effective for the synthesis of nanocrystals, such as gold, silver, platinum, palladium, etc. [77–80]. In this process, regulating the nucleation and growth processes of nanocrystals has been a major topic. Flytzani-Stephanopoulos *et al.* constructed isolated gold atoms supported on titania with a loading of approximately 1 wt% under ultraviolet (UV) irradiation [81]. They found that the addition of ethanol can serve as a charge scavenger to facilitate the donation of electrons from gold atoms to  $-\text{OH}$  groups on the titania support. The catalytic performance was examined and the results showed that this catalyst displayed excellent activity for the low-temperature water–gas shift reaction, as well as admirable stability in long-term cool-down and startup operations.

An important study by Zheng *et al.* demonstrated a room-temperature photochemical strategy to construct atomically dispersed palladium atoms

supported on ethylene glycolate (EG)-stabilized ultrathin  $\text{TiO}_2$  nanosheets ( $\text{Pd}_1/\text{TiO}_2$  catalyst) with a Pd loading up to 1.5% [82]. Typically, two-atom-thick  $\text{TiO}_2$  nanosheets were prepared by reacting  $\text{TiCl}_4$  with EG and used as the support.  $\text{H}_2\text{PtCl}_6$  was then added to the  $\text{TiO}_2$  dispersion for adsorption of Pd species followed by irradiation by UV to give the  $\text{Pd}_1/\text{TiO}_2$  catalyst. TEM, STEM and EXAFS revealed that the isolated Pd atoms were evenly dispersed over the  $\text{TiO}_2$  support, without any observable evidence of NPs (Fig. 4a). The catalyst exhibited excellent catalytic performance in the hydrogenation of  $\text{C}=\text{C}$  bonds, outperforming those commercial Pd catalysts. In addition, there was no observable decay in the catalytic activity for 20 cycles, suggesting the robustness of the  $\text{Pd}_1/\text{TiO}_2$  catalyst. Importantly, they found this catalyst can activate  $\text{H}_2$  in a heterolytic pathway to drastically enhance its catalytic activity in the hydrogenation of aldehydes. This mechanism has been commonly observed for homogeneous catalysts, such as Au, Pd and Ru complexes; however, there is no report for heterogeneous Pd catalysts. This study set a good example using atomically dispersed metal catalysts for bridging the gap between heterogeneous and homogeneous catalysis.

Very recent work by Wu and co-workers showed a novel synthetic approach to accessing atomically dispersed platinum species on mesoporous carbon via iced-photochemical reduction of frozen chloroplatinic acid solution (Fig. 4b) [83]. In this report,  $\text{H}_2\text{PtCl}_6$  solution was first frozen by liquid nitrogen followed by irradiation using a UV lamp. The  $\text{H}_2\text{PtCl}_6$  ice was kept overnight in dark conditions at room temperature to give a clear aqueous Pt single-atom solution. Then mesoporous carbon solution and Pt single-atom solution were mixed, filtered, and dried at room temperature. Finally, the ice lattice naturally confines the dispersed ions and atoms to affect the photochemical reduction products and further prevent the aggregation of atoms. To test the generality of this concept, they also fabricated isolated Pt atoms deposited on different supports, including mesoporous carbon, graphene, carbon nanotubes,  $\text{TiO}_2$  nanoparticles and zinc oxide nanowires. Among them, the isolated Pt atoms supported on mesoporous carbon exhibited exceptional catalytic performance for hydrogen evolution reaction, as well as an excellent long-time durability, outperforming the commonly employed Pt/carbon catalyst. This iced-photochemical reduction approach provides a promising avenue for the green synthesis of SAs and sub-nanometer clusters, and opens up possibilities for fine-tuning the nucleation and growth of nanocrystals in wet chemistry.

## Other techniques-assisted adsorption

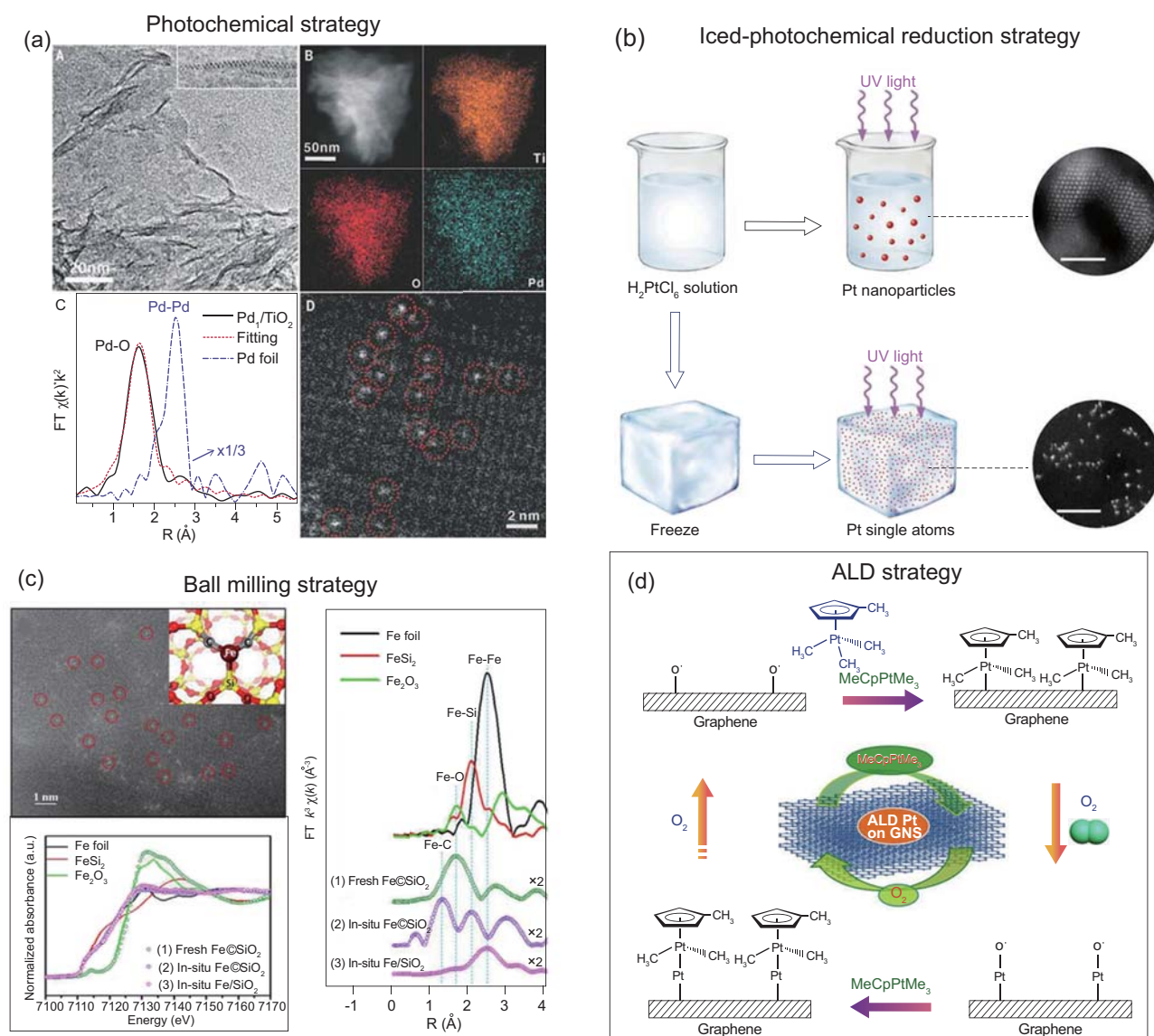


**Figure 4.** (a) Structural characterizations of Pd<sub>1</sub>/TiO<sub>2</sub> catalyst. Adapted with permission from [82]. (b) Schematic illustration of the iced-photochemical process compared with the conventional photochemical reduction of H<sub>2</sub>PtCl<sub>6</sub> aqueous solution. Adapted with permission from [83]. (c) Structural features of 0.5% Fe@SiO<sub>2</sub>. Adapted with permission from [39]. (d) Schematic illustrations of the Pt ALD mechanism on graphene nanosheets. Adapted with permission from [86].

Recently, high-energy bottom-up ball-milling synthesis has been proved as a powerful method to break and reconstruct chemical bonds of materials with high efficiency. Such an approach was taken by Bao *et al.*, who reported a lattice-confined single iron site catalyst embedded within a silica matrix by a solid fusion method. Briefly, commercial SiO<sub>2</sub> and Fe<sub>2</sub>SiO<sub>4</sub> were mixed and subjected to ball milling under argon and fused in the air [39]. As expected, the unsaturated single Fe sites served as active centers (Fig. 4c) to efficiently enable the direct, non-oxidative conversion

of methane, exclusively to ethylene and aromatics. The presence of single Fe sites effectively prevented catalytic C-C coupling, oligomerization and coke deposition. In addition, this catalyst showed extremely stable performance, with no deactivation observed during long-term testing, and the selectivity for total carbon of the three products was retained. Subsequently, the group used the same method to construct single-atom iron sites by embedding highly dispersed FeN<sub>4</sub> centers in graphene matrix via high-energy ball milling of iron phthalocyanine and graphene nanosheets [84]. In this

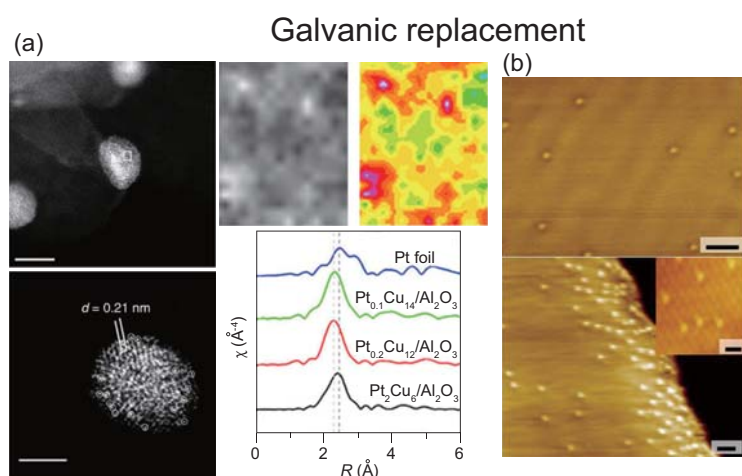


**Figure 5.** (a) Characterization of Pt/Cu SAA NPs. Adapted with permission from [50]. (b) Scanning tunneling microscope image of a 0.01 ML Pt/Cu(111) SAA surface. Adapted with permission from [90].

system, the FeN<sub>4</sub> center is highly dispersed and well stabilized by the graphene matrix. The formation of the Fe = O intermediate is important in promoting the conversion of benzene to phenol. Remarkably, this reaction can proceed efficiently at mild conditions such as room temperature or even as low as 0°C. DFT calculations confirm that the catalytic activity stems from the confined iron sites, along with moderate activation barriers for the reaction that proceeded at room temperature. Both studies clearly show the potential of the highly efficient ball-milling method for the fabrication of SACs for use in catalysis areas.

The atomic layer deposition (ALD) technique is a gas-phase chemical process and commonly used to deposit a thin layer of film in a bottom-up fashion with near-atomic precision on the substrate by repeated exposure of separate precursors [85]. This technique offers the feasibility of precise control of the catalyst size from a single-atom, subnanometer cluster to the nanoparticle. It is expected that ALD would potentially provide a powerful approach for the construction of intriguing SACs. This approach was first demonstrated by Sun *et al.* in 2013, who reported a practical synthesis of isolated single Pt atoms on graphene nanosheets using the ALD technique (Fig. 4d) [86]. In this work, Pt was deposited on graphene supports by the ALD method using MeCpPtMe<sub>3</sub> and oxygen as precursors and nitrogen as a purge gas. The resulting Pt SAC showed improved catalytic activity compared with the commercial Pt/C catalyst. X-ray absorption fine structure (XAFS) analyses show that the low-coordination and partially unoccupied 5d orbital of Pt atoms are responsible for the excellent catalytic performance.

In 2015, Lu *et al.* described a single-atom Pd<sub>1</sub>/graphene catalyst prepared by the ALD method with excellent performance in the selective hydrogenation of 1,3-butadiene [87]. First, the anchor sites were created by an oxidation process on pristine graphene nanosheets, followed by a reduction process via thermal de-oxygenation to control the surface oxygen functional groups. After an annealing step, phenolic oxygen was observed to be the dominated oxygen species on the graphene support. ALD was then performed on the reduced graphene to give a single-atom Pd catalyst by alternately exposing Pd(hfac)<sub>2</sub> and formalin. This catalyst showed superior catalytic performance in the selective hydrogenation of 1,3-butadiene, affording nearly 100% butenes selectivity, and ~70% selectivity for 1-butene at a conversion ratio of 95% under mild conditions. They speculate that both the mono- $\pi$ -adsorption mode of 1,3-butadiene and the enhanced steric effect induced by 1,3-butadiene adsorption on the isolated Pd atoms contribute to the improved selectivity of butenes. In addition, the Pd<sub>1</sub>/graphene showed remarkable durability against deactivation via either metal atom aggregation or coking during a 100-h reaction time on stream.

Using the same strategy, Sun and co-workers described the preparation of isolated single Pt atoms and clusters on nitrogen-doped graphene nanosheets (NGNs) [88]. Here, Pt was first deposited on the NGNs by the ALD technique using MeCpPtMe<sub>3</sub> and O<sub>2</sub> as precursors and N<sub>2</sub> as a purging gas and a carrier gas. The size, density and distribution of the Pt atoms on the NGNs or graphene nanosheets (GNs) can be precisely controlled by the ALD cycles. As expected, the isolated Pt atoms and clusters on the NGNs have been demonstrated to show superior catalytic activity and stability for the hydrogen evolution reaction (HER) compared with the conventional Pt NP catalysts. This can be explained by the small size and the special electronic structure of the adsorbed single Pt atoms on NGNs. Together, the use of the ALD technique has shown great promise for large-scale synthesis of highly active and stable single-atom and cluster catalysts.

### The galvanic-replacement method

Galvanic replacement is a highly versatile and effective approach for the construction of a variety of nanostructures, with the ability to control the size and shape, composition, internal structure and morphology [24,57,89]. It is an electrochemical process that consists of oxidation of one metal, termed as a sacrificial template, by other metal ions that have a higher reduction potential. When they are exposed

to each other in solution, the sacrificial metal template will be preferably oxidized and dissolved into the solution, while the ions of the second metal will be reduced and deposited onto the template surface.

In 2015, Sykes *et al.* demonstrated that low concentrations of isolated Pt atoms in the Cu(111) surface (Fig. 5a) can be prepared by galvanic replacement on pre-reduced Cu NPs to catalyse the butadiene hydrogenation with remarkable activity and high selectivity to butenes [50]. In this case, Cu NPs were first prepared and supported on  $\gamma$ -Al<sub>2</sub>O<sub>3</sub> followed by calcination in air. The galvanic-replacement reaction was then carried out in an aqueous solution under nitrogen protection with constant stirring and refluxing. A desired amount of Pt precursor was introduced to a suspension of Cu NPs in an aqueous solution containing HCl. The resulting material was filtered, washed and dried to yield the catalyst. They notice that, at low Pt loadings, the isolated Pt atoms can substitute into the Cu(111) surface to activate the dissociation and spillover of H to Cu. The weak binding between butadiene and Cu would facilitate the highly selective hydrogenation reaction to butenes, without decomposition or poisoning of the catalysts. This catalyst, with less than one Pt atom per 100 copper atoms, also binds CO more weakly than metallic Pt, which is particularly important for use in many Pt-catalysed chemical reactions.

In a follow-up report, the Sykes group used the same approach to construct Pt/Cu single-atom alloys (SAAs) to examine C–H activation in different systems, including methyl groups, methane and butane [90]. They observed that the Pt atoms were distributed over the Cu surface and across both terraces and at regions near step edges (Fig. 5b). The results show the Pt/Cu SAAs activate C–H bonds more efficiently than Cu, along with superior stability under realistic operating conditions, effectively avoiding the coking problem that typically occurred with Pt. Both pieces of work from the Sykes group demonstrated how SAs can be deposited on alloys—an important future direction for this field.

Though a variety of SACs have been developed by the bottom-up strategy, the downside of the methods described here is that it is still challenging to access SACs with high metal loading and a homogeneous coordination environment for the active sites used in the catalytic process. This would lead to limited selectivity and stability of the SACs for their practical use in various industrial fields. In addition, although ground-breaking, some of these methods do require specific/sophisticated preparation procedures that might not be compatible with all kinds of SACs and ideal from practical perspectives.

## TOP-DOWN SYNTHETIC METHODOLOGIES FOR THE CONSTRUCTION OF SACS

The top-down strategy is based on the dissolution of ordered nanostructures into smaller pieces to give desired properties and intriguing performances [59,91]. Extensive research efforts have pursued this strategy with the overarching aim of synthesizing SACs with unprecedented chemical and physical properties and understanding the complex mechanisms for catalysis that occur at the atomic level. This strategy has proven particularly useful in the formation of SACs with accurate control over the micro- or nanostructures [92]. The precise structure (such as coordination number, dispersion tendencies and binding mode) of metal SAs synthesized by the top-down methods has shown great promise in industrially important applications [9,89,93,94]. Efforts to further understand the underlying features and mechanisms are required for the development of new methods for the construction of SACs and represent a fertile area for future studies.

### The high-temperature pyrolysis method

High-temperature pyrolysis has become one of the fascinating methods for synthesizing nanomaterials on different supports. Particularly, the development of a template-sacrificial approach via acid leaching or oxidative calcination has offered an alternative way to generate SACs. Of note is that an appropriate pyrolysis temperature is critically important to give the desired properties.

MOFs and zeolitic imidazolate frameworks (ZIFs) have interconnected 3D molecular-scale cages that make them highly accessible through small apertures. Importantly, they can serve as templates to obtain nitrogen-doped porous carbon with abundant active nitrogen sites. Very recently, Wu *et al.* took advantage of the MOFs and originally developed an effective strategy for accessing single Co atoms supported on nitrogen-doped porous carbon with a particularly high metal loading of over 4 wt% via the pyrolysis of bimetallic Zn/Co MOFs [57]. This is pioneering work in this field and the strategy is particularly applicable to access high-loading metal SACs that would otherwise be difficult to produce. It should be noted that the enhancement of metal loading for preparing SACs in the present study is a significant breakthrough in this area, highlighting the specific requirement of SACs for practical applications. Importantly, the introduction of Zn atoms into MOFs is critical and acts as an elegant approach to efficiently manipulate the adjacent spatial distance between Co atoms,

## High-temperature pyrolysis

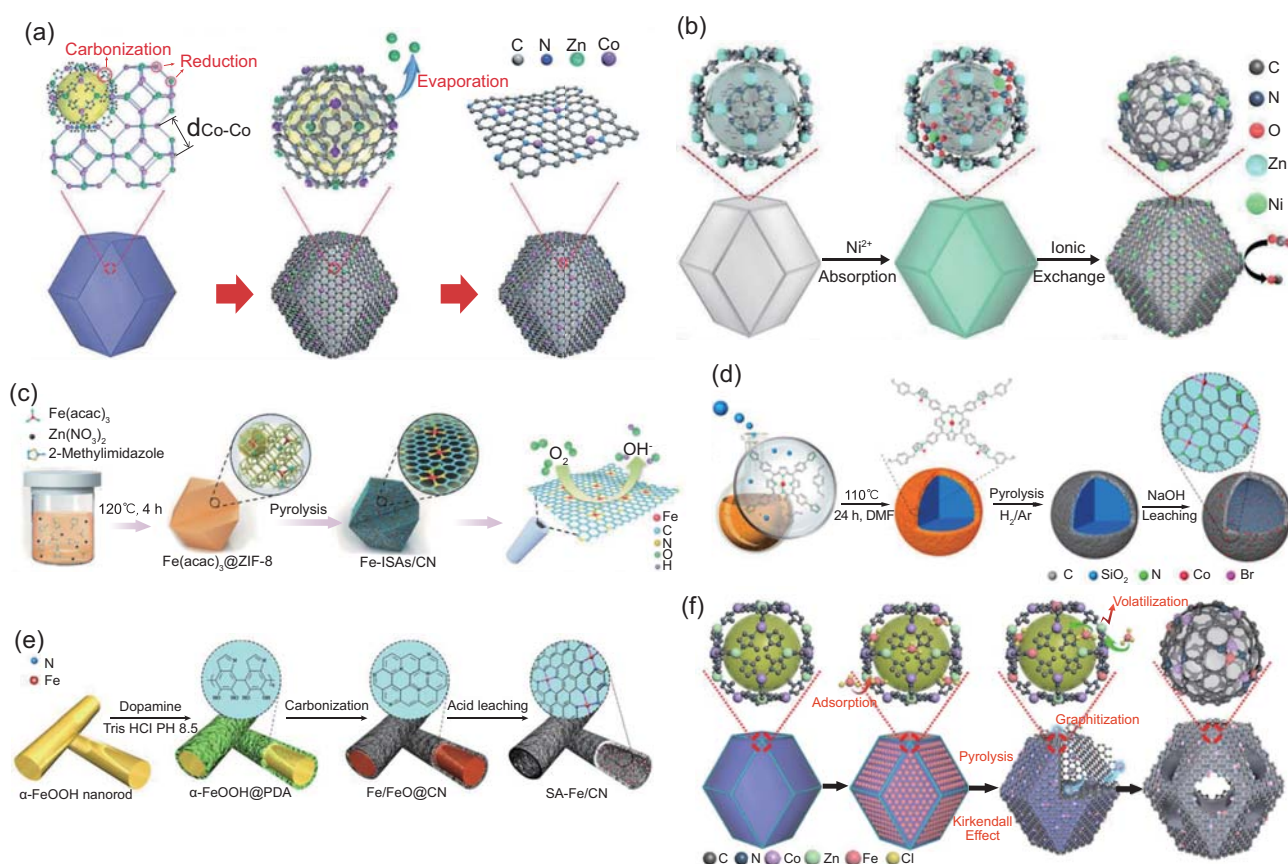


**Figure 6.** (a) Schematic illustration of the construction of Co SAs/N-C. Adapted with permission from [57]. (b) Schematic illustration of the construction of Ni SAs/N-C. Adapted with permission from [95]. (c) Schematic illustrations of the construction of Fe-ISAs/CN. Adapted with permission from [97]. (d) Schematic illustration of the construction of ISAS-Co/HNCS. Adapted with permission from [99]. (e) Schematic illustration of the construction of SA-Fe/CN. Adapted with permission from [103]. (f) Schematic illustration of the construction of (Fe, Co)/N-C. Adapted with permission from [104].

thereby effectively preventing the formation of Co NPs (Fig. 6a). The Zn atoms, with a low boiling point of  $907^{\circ}\text{C}$ , can be evaporated in the high-temperature pyrolysis process, providing abundant N sites. The Co nodes can be reduced *in situ* by carbonization of the organic linkers in MOFs and anchored on the as-obtained N-doped porous carbon support. Assuming the MOF as an integrated system, using this high-temperature pyrolysis of MOF to access unsaturated SAs anchored on the N-doped porous carbon support can be categorized into the top-down approach. Control testing demonstrated that the aggregated Co atoms were formed for Co-containing MOF (ZIF-67) after a pyrolysis treatment. HAADF-STEM and EXAFS verified the presence of isolated Co atoms dispersed on the N-doped porous carbon support. The resulting Co SAC shows exceptional oxygen-reduction reaction (ORR) catalytic performance with a half-wave potential more positive than the commercial Pt/C and most of the reported non-precious metal

catalysts. Robust chemical stability during electrocatalysis and thermal stability that resists sintering at a high temperature of  $900^{\circ}\text{C}$  have also been confirmed, as little evidence of catalyst degradation was observed during the catalytic cycles. This work has underlined the significant importance of employing MOFs as an ideal carbon support for stabilizing single metal atoms at the atomic scale.

Subsequently, an ionic exchange strategy was developed by the Wu group to assist in the construction of a single Ni atom catalyst (Fig. 6b) between Zn nodes and adsorbed Ni ions within the cavities of the MOF [95]. In this case, ZIF-8 was first dispersed in n-hexane under ultrasound until a homogeneous solution was formed. Then a small amount of  $\text{Ni}(\text{NO}_3)_2$  aqueous solution was introduced, and the mixed solution was vigorously stirred to cause the Ni ions to be absorbed completely. Then the sample was centrifuged and dried, followed by a high-temperature heating process in an argon atmosphere to yield Ni SAC. This Ni SAC, with a

metal weight loading of 1.53 wt%, delivered an excellent turnover frequency for CO<sub>2</sub> electroreduction of 5273 h<sup>-1</sup>, along with a maximum Faradaic efficiency for CO production of 71.9% and a high current density of 10.48 mA cm<sup>-2</sup>. This work, for the first time, demonstrates the great potential of using MOF-based materials to access SACs for use in CO<sub>2</sub> electroreduction.

To investigate the relationship between coordination numbers and CO<sub>2</sub> electroreduction catalytic performance, the Wu group sequentially prepared a series of Co SACs with different N coordination environments treated at different temperatures [96]. Bimetallic Co/Zn ZIFs were treated by a pyrolysis process, during which the Zn was evaporated away and the Co was reduced by carbonized organic linkers, generating isolated Co atoms stabilized on nitrogen-doped carbon. By controlling the pyrolysis temperatures, three Co SACs with different Co–N coordination numbers were obtained, being Co–N<sub>4</sub> (800°C), Co–N<sub>3</sub> (900°C), and Co–N<sub>2</sub> (1000°C), respectively. The catalytic performance of these samples was examined, and the results show that the isolated Co atom with two coordinated nitrogen atoms (prepared at 1000°C) can afford significantly higher selectivity and superior activity, resulting in a CO formation Faradaic efficiency of 94% and a current density of 18.1 mA cm<sup>-2</sup> at an overpotential of 520 mV. Importantly, this catalyst achieved a turnover frequency for CO formation of 18 200 h<sup>-1</sup>, outperforming most of the reported metal-based catalysts under comparable conditions. DFT calculation reveals that the decreased N coordination environment leads to more unoccupied 3d orbitals for Co atoms, thereby facilitating adsorption of CO<sub>2</sub><sup>•-</sup> and increasing CO<sub>2</sub> electroreduction performance. This study demonstrates the significant effect of N coordination environments on SACs for catalytic performance.

The above studies further confirm the great potential of high-temperature pyrolysis of MOFs as a promising strategy to access SACs for different demanding industrial applications.

With these attractive features, Li and co-workers prepared a highly stable isolated Fe atom catalyst, with Fe loading up to 2.16 wt%, that showed excellent ORR reactivity via a cage-encapsulated precursor pyrolysis approach [97]. This method is highly effective to access SACs because the precursors can be encapsulated inside the ZIF pores, thereby preventing them from aggregating into nanoparticles (Fig. 6c). In this study, Fe(acac)<sub>3</sub> was mixed with ZIF-8, and the molecular-scale cages were formed with the assembly of Zn<sup>2+</sup> and 2-methylimidazole, with one Fe(acac)<sub>3</sub> molecule trapped in one cage.

After a pyrolysis step, the ZIF-8 was transformed into nitrogen-doped porous carbon, whereas the Fe(acac)<sub>3</sub> within the cage was reduced by carbonization of the organic linker, resulting in the formation of isolated iron atoms anchored on nitrogen species. The catalyst has been demonstrated to show exceptional ORR catalytic activity, good methanol tolerance and impressive stability. Importantly, the ORR catalytic activity of this SAC outperforms those of recently reported Fe-bases materials and other non-precious metal materials. Experimental results and DFT calculations reveal the excellent ORR performance stems from the formation of atomically isolated iron atoms coordinated with four N atoms and one O<sub>2</sub> molecule adsorbed end-on.

Using a similar approach, Li *et al.* described the synthesis of atomically dispersed Ru<sub>3</sub> clusters via a cage-separated precursor pre-selection and pyrolysis strategy [98]. Generally, two steps are involved: (i) encapsulation and separation of preselected metal cluster precursors followed by (ii) a pyrolysis treatment. The resulting catalyst was characterized by HAADF-STEM and XAFS, and the catalytic performance was tested for the oxidation of 2-amino-benzyl alcohol. The results show that this Ru<sub>3</sub>/nitrogen-doped carbon (CN) catalyst possesses 100% conversion, 100% selectivity and an unexpectedly high turnover frequency (TOF), outperforming those of Ru SACs and small-sized Ru particle catalysts.

An alternative approach to the thermal treatment of MOFs for achieving SACs has been employed by Li *et al.*, who used SiO<sub>2</sub> as a template to access a hollow N-doped carbon sphere with isolated Co atomic sites (Fig. 6d) [99]. Briefly, the SiO<sub>2</sub> template was dispersed in Co–TIPP/TIPP solution before introducing another monomer. The collected powder was thermally treated under a flowing H<sub>2</sub>/Ar and then etched with sodium hydroxide to remove the SiO<sub>2</sub> template to yield the Co SAC. Its ORR performance was investigated and the results demonstrate that exceptional catalytic activity was originated from the single Co sites that can significantly facilitate the proton and charge transfer to the adsorbed \*OH species. Using the same approach, a Mo SAC was prepared by the Li group using sodium molybdate and chitosan as precursors and showed excellent HER performance [100]. Further studies of the structure of the catalyst were supported by AC-STEM and XAFS, which confirmed that the Mo atom was anchored with one nitrogen atom and two carbon atoms (Mo<sub>1</sub>N<sub>1</sub>C<sub>2</sub>).

In 2016, Zhang *et al.* described a similar template-sacrificial approach to create a self-supporting Co–N–C catalyst with single-atom dispersion and showed excellent catalytic activity for the

chemoselective hydrogenation of nitroarenes to yield azo compounds under mild conditions [101]. In this study, the  $\text{Co}(\text{phen})_2(\text{OAc})_2$  complex was supported on  $\text{Mg}(\text{OH})_2$  and then subjected to a pyrolysis process. This was followed by the removal of the  $\text{MgO}$  support by an acid-leaching treatment. The merit of employing  $\text{Mg}(\text{OH})_2$  is that it can essentially prevent the aggregation of cobalt atoms. This is because of the moderate interaction between  $\text{Mg}(\text{OH})_2$  and the Co species, as well as its inertness towards the reaction with Co during the pyrolysis process. After the acid-leaching step, the support material was removed to give a self-supporting Co–N–C material. X-ray absorption spectroscopy was tested and the exact structure of the catalyst was confirmed to be  $\text{CoN}_4\text{C}_8\text{-1-2O}_2$ . Specifically, the Co single atom was coordinated with four pyridinic nitrogen atoms on the graphitic layer, along with oxygen atoms weakly adsorbed on the Co atoms perpendicular to the Co– $\text{N}_4$  plane.

Using the same approach, Zhang *et al.* prepared an atomically dispersed Fe–N–C catalyst, which exhibited exceptional activity and excellent reusability for the selective oxidation of the C–H bond, along with tolerance for a wide scope of substrates [102]. Briefly, the  $\text{Fe}(\text{phen})_x$  complex supported on the nano- $\text{MgO}$  template was pyrolysed at different temperatures under  $\text{N}_2$  atmosphere, followed by an acid-leaching step to remove the  $\text{MgO}$  template. They observed that the properties of the Fe species were dependent on the pyrolysis temperature, with more metallic Fe particles formed at higher temperatures. The critical role of the Fe– $\text{N}_x$  sites in catalysis was further confirmed by potassium thiocyanate titration experiments and Mössbauer spectroscopy.

An effective core–shell strategy has been introduced by the Li group using metal hydroxides or oxides coated with polymers followed by high-temperature pyrolysis and acid-leaching steps, to synthesize single metal atoms anchored on the inner wall of hollow CN materials [103]. By employing different metal precursors or polymers, they have successfully synthesized a series of metal SAs dispersed on CN materials (Fig. 6e). In detail,  $\alpha$ - $\text{FeOOH}$  nanorods were first prepared by a hydrothermal method, followed by self-polymerizing dopamine monomers to generate  $\alpha$ - $\text{FeOOH}@$ PDA. Then it was thermally treated under an inert atmosphere, during which the polydopamine (PDA) layers were converted into the CN shell and  $\alpha$ - $\text{FeOOH}$  was reduced to iron, giving rise to the strong interaction between the Fe atoms and the CN shell. Finally, acid leaching was carried out to generate Fe SAs on the inner wall of the CN materials. The obtained SA-Fe/CN catalyst

showed a high conversion of 45% and an excellent selectivity of 94% for the hydroxylation of benzene to phenol, outperforming Fe nanoparticles/CN.

Notably, in a most recent research, Wu *et al.* originally developed a host–guest strategy based on MOFs to construct a Fe–Co dual-sites catalyst embedded in N-doped porous carbon support [104]. It involves binding between Co nodes and adsorbed Fe ions within the confined space of MOFs (Fig. 6f). Specifically, Zn/Co bimetallic MOF was employed as a host to encapsulate  $\text{FeCl}_3$  within the cavities by a double-solvents method. The  $\text{Fe}^{3+}$  species were reduced by the as-generated carbon and bond with the neighboring Co atoms. Meanwhile, the adsorbed  $\text{Fe}^{3+}$  species can accelerate the decomposition of metal–imidazolate–metal linkages and generate voids inside the MOF. EXAFS and Mössbauer spectroscopic analyses were performed to investigate the coordination environment of the Fe–Co dual sites. The experimental results show that  $\text{FeCoN}_6$  is the active site for the (Fe, Co)/N–C catalyst and has been demonstrated to endow excellent ORR performance in an acidic electrolyte, along with comparable onset potential and half-wave potential to those of the commercial Pt/C. DFT calculation reveals that the activation of O–O is favored on the dual sites, which is important for the four-electron oxygen-reduction process. The fuel cell testing revealed that this catalyst outperforms most of the reported Pt-free catalysts in  $\text{H}_2/\text{O}_2$  and  $\text{H}_2/\text{air}$  conditions. In addition, this cathode catalyst is rather robust in long-term operation for electrode measurement and  $\text{H}_2/\text{air}$  single cell testing. Of note is that, despite the fact that SACs generally confer greater activity than the corresponding nanoparticles, it is still important to be aware of the potential aggregation pathways available to them. This is especially crucial in cases where higher operational temperatures were applied. Therefore, the superior catalytic activity, selectivity, stability and the ease of fabrication of the dual-sites Fe–Co catalyst make this type of SAC truly remarkable. Importantly, the main advantages of this host–guest strategy include the ability to incorporate different metal atoms and to permit the catalyst to be operated in a wider dynamic range. This study is expected to provide avenues for the synthesis of high-performance dual-sites catalysts with unique properties for use in chemical transformations.

Overall, these studies have shown that the high-temperature pyrolysis method is capable of producing SACs with precisely controlled structures and morphologies. Additionally, this unique approach has been seen as a significant opportunity to enable the efficient construction of high-performance SACs for use in various reactions.



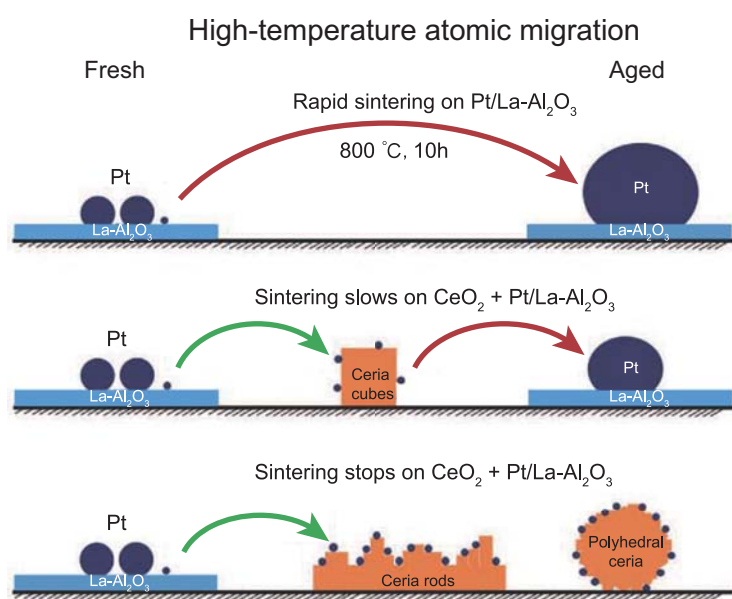


**Figure 7.** Schematic illustration of Pt nanoparticle sintering, showing how ceria can trap the mobile Pt to suppress sintering. Adapted with permission from [105].

### The high-temperature atomic-migration method

High temperatures are generally detrimental to catalysts' activities. Although the SAs are homogeneously dispersed on the support materials, they have a high propensity to move and aggregate into nanoparticles when heated at high temperatures. Datye and co-workers take advantage of the phenomenon that metal nanoparticles can emit mobile species to prepare atomically dispersed metal catalysts [105]. In this study, a Pt/La-Al<sub>2</sub>O<sub>3</sub> catalyst was physically mixed with different types of ceria powders followed by a thermal treatment in flowing air. Because of the strong interaction between PtO<sub>2</sub> and ceria powders, the Pt species emitted from the alumina were trapped on the CeO<sub>2</sub>, forming thermally stable Pt<sub>1</sub>/CeO<sub>2</sub> SACs (Fig. 7). The performance of the resulting SAC was tested for CO oxidation, and the results suggest that it can serve as a highly effective sintering-resistant CO-oxidation catalyst at high temperature. They believe that this atom-trapping approach is potentially applicable and might provide exciting possibilities to access a variety of high-performance SACs. This work represents a novel strategy and has been demonstrated as being particularly effective in fabricating SACs and connecting the relationship between the nanoparticles and SAs.

### CONCLUSIONS AND PERSPECTIVE

Over just a few years, there has been remarkable progress in the development of various methods for

the synthesis of SACs. In this review, we summarize the progress, bring new insights from recent years and pointed the way to the synthesis of SACs.

Currently, two general approaches have been employed for accessing SACs: bottom-up and top-down. Though still being developed, SACs have emerged as an exceptional advancement in the development of highly efficient heterogeneous catalysts. The researchers have shown evidence that the size of the nanomaterials does affect catalytic efficiency in the catalysis process. A noteworthy result is that, by reducing the size of nanostructures from the nano- to the sub-nano scale and finally to SAs in atomic dimensions, catalytic performance has been observed to change drastically. This results from the low-coordination environment, quantum size effect and enhanced metal-support interactions. Moreover, the homogeneously and isolated metal active sites can maximize metal utilization, giving rise to the impressively enhanced catalytic performance.

Recent experimental and theoretical progress has unambiguously validated the strong evidence for the high activity, selectivity and stability of the high-performance SACs. These intriguing properties of SACs are believed to endow great potential for applications in heterogeneous catalysis. Importantly, SACs can act as an ideal platform to serve as a bridge to connect hetero- and homogeneous catalysis. Thus, SACs are thought to have the potential to overcome the difficulty encountered in homogeneous catalysis.

As discussed previously, a major limiting factor in the development of SACs is the lack of general methods to directly and efficiently access high-performance SACs. The construction of SACs for use in catalysis represents an important challenge, highlighting the need for more fundamental research into detailed mechanisms. Along with the emergence of new characterization and computational modeling techniques, single-atom active sites can be investigated further. More advanced, direct and effective *in situ* spectroscopic and microscopic techniques become particularly important to offer new insights into the chemical reactions involved in SACs. Elucidating the important role of metal precursors, support materials and experimental conditions and understanding the prerequisites for catalytic activity of a given catalytic system are crucial for developing effective strategies for the synthesis of SACs. Several aspects should also be given enough attention: first, the development of novel, controllable and facile synthesis methods for access high-loading SACs with finely and densely dispersed single atoms; second, the construction of single metal atoms with robust stabilization on the support for use in practical conditions; third,

detailed experimental and theoretical work should be done to comprehensively understand SACs-support effects. The top-down strategy has shown great promise and significantly contributed to the simplified synthesis routes for SACs with exceptional activity and stability. Moreover, the metal loading can be markedly increased from 1% to 5%, and the coordination environments can be elaborately controlled. This will definitely facilitate the development of general protocols for accessing SACs and underpin the exploration of other intriguing applications.

Together, the field of SAs is expansive and rapidly developing towards different applied research fields. The continued development of SACs represents an important advancement in heterogeneous catalysis and will surely be the important focus of extensive research efforts and a thriving field for various applications for years to come.

## FUNDING

This work was supported by the National Key R&D Program of China (2017YFA0208300) and the National Natural Science Foundation of China (21522107, 21671180, 21521091, 21390393, U1463202).

## REFERENCES

1. Kärkäs MD, Verho O and Johnston EV *et al.* Artificial photosynthesis: molecular systems for catalytic water oxidation. *Chem Rev* 2014; **114**: 11863–2001.
2. Tao F and Crozier PA. Atomic-scale observations of catalyst structures under reaction conditions and during catalysis. *Chem Rev* 2016; **116**: 3487–539.
3. Gilroy KD, Ruditskiy A and Peng HC *et al.* Bimetallic nanocrystals: syntheses, properties, and applications. *Chem Rev* 2016; **116**: 10414–72.
4. Blakemore JD, Crabtree RH and Brudvig GW. Molecular catalysts for water oxidation. *Chem Rev* 2015; **115**: 12974–3005.
5. Wang X, Ruditskiy A and Xia Y. Rational design and synthesis of noble-metal nanoframes for catalytic and photonic applications. *Nat Sci Rev* 2016; **3**: 520–33.
6. Seh ZW, Kibsgaard J and Dickens CF *et al.* Combining theory and experiment in electrocatalysis: insights into materials design. *Science* 2017; **355**: 6321–32.
7. Vajda S and White MG. Catalysis applications of size-selected cluster deposition. *ACS Catal* 2015; **5**: 7152–76.
8. Gawande MB, Goswami A and Felpin FX *et al.* Cu and Cu-based nanoparticles: synthesis and applications in catalysis. *Chem Rev* 2016; **116**: 3722–811.
9. Liu J. Catalysis by supported single metal atoms. *ACS Catal* 2017; **7**: 34–59.
10. Yang XF, Wang A and Qiao B *et al.* Single-atom catalysts: a new frontier in heterogeneous catalysis. *Acc Chem Res* 2013; **46**: 1740–8.
11. Boles MA, Ling D and Hyeon T *et al.* The surface science of nanocrystals. *Nat Mater* 2016; **15**: 141–53.
12. Xia BY, Wu HB and Wang X *et al.* One-pot synthesis of cubic PtCu<sub>3</sub> nanocages with enhanced electrocatalytic activity for the methanol oxidation reaction. *J Am Chem Soc* 2012; **134**: 13934–7.
13. Christopher P, Xin H and Linic S. Visible-light-enhanced catalytic oxidation reactions on plasmonic silver nanostructures. *Nat Chem* 2011; **3**: 467–72.
14. Wu Y, Wang D and Li Y. Nanocrystals from solutions: catalysts. *Chem Soc Rev* 2014; **43**: 2112–24.
15. Lu Q, Wang AL and Gong Y *et al.* Crystal phase-based epitaxial growth of hybrid noble metal nanostructures on 4H/fcc Au nanowires. *Nat Chem* 2018; **10**: 456–61.
16. Fan Z and Zhang H. Crystal phase-controlled synthesis, properties and applications of noble metal nanomaterials. *Chem Soc Rev* 2016; **45**: 63–82.
17. Chen Y, Fan Z and Luo Z *et al.* High-yield synthesis of crystal-phase-heterostructured 4H/fcc Au@Pd core-shell nanorods for electrocatalytic ethanol oxidation. *Adv Mater* 2017; **29**: 1701331–5.
18. Fan Z and Zhang H. Template synthesis of noble metal nanocrystals with unusual crystal structures and their catalytic applications. *Acc Chem Res* 2016; **49**: 2841–50.
19. Liu P, Qin R and Fu G *et al.* Surface coordination chemistry of metal nanomaterials. *J Am Chem Soc* 2017; **139**: 2122–31.
20. Boronat M, Leyva-pérez A and Corma A. Theoretical and experimental insights into the origin of the catalytic activity of subnanometric gold clusters: attempts to predict reactivity with clusters and nanoparticles of gold. *Acc Chem Res* 2014; **47**: 834–44.
21. Abbet S, Sanchez A and Heiz U *et al.* Acetylene cyclotrimerization on supported size-selected Pd<sub>n</sub> clusters (1 ≤ n ≤ 30): one atom is enough! *J Am Chem Soc* 2000; **122**: 3453–7.
22. Kaden WE, Wu T and Kunkel WA *et al.* Electronic structure controls reactivity of size-selected Pd clusters adsorbed on TiO<sub>2</sub> surfaces. *Science* 2009; **326**: 826–9.
23. Sun D and Li Z. Double-solvent method to Pd nanoclusters encapsulated inside the cavity of NH<sub>2</sub> UiO-66(Zr) for efficient visible-light-promoted Suzuki coupling reaction. *J Phys Chem C* 2016; **120**: 19744–50.
24. Liu L, Diaz U and Arenal R *et al.* Generation of subnanometric platinum with high stability during transformation of a 2D zeolite into 3D. *Nat Mater* 2017; **16**: 132–8.
25. Chakraborty I and Pradeep T. Atomically precise clusters of noble metals: emerging link between atoms and nanoparticles. *Chem Rev* 2017; **117**: 8208–71.
26. Jin R, Zeng C and Zhou M *et al.* Atomically precise colloidal metal nanoclusters and nanoparticles: fundamentals and opportunities. *Chem Rev* 2016; **116**: 10346–413.
27. Fortea-Pérez FR, Mon M and Ferrando-Soria J *et al.* The MOF-driven synthesis of supported palladium clusters with catalytic activity for carbene-mediated chemistry. *Nat Mater* 2017; **16**: 760–6.

28. Yao S, Zhang X and Zhou W *et al.* Atomic-layered Au clusters on  $\alpha$ -MoC as catalysts for the low-temperature water-gas shift reaction. *Science* 2017; **357**: 389–93.
29. Maschmeyer T, Rey F and Sankar G *et al.* Heterogeneous catalysts obtained by grafting metallocene complexes onto mesoporous silica. *Nat Catal* 1995; **378**: 159–62.
30. Fu Q, Saltsburg H and Flytzani-Stephanopoulos M. Active nonmetallic Au and Pt species on ceria-based water-gas shift catalysts. *Science* 2003; **301**: 935–8.
31. Hackett SFJ, Brydson RM and Gass MH *et al.* High-activity, single-site mesoporous Pd/Al<sub>2</sub>O<sub>3</sub> catalysts for selective aerobic oxidation of allylic alcohols. *Angew Chem* 2007; **119**: 8747–50.
32. Zhu C, Fu S and Shi Q *et al.* Single-atom electrocatalysts. *Angew Chem Int Ed* 2017; **56**: 13944–60.
33. Zheng Y, Jiao Y and Zhu Y *et al.* Molecule-level g-C<sub>3</sub>N<sub>4</sub> coordinated transition metals as a new class of electrocatalysts for oxygen electrode reactions. *J Am Chem Soc* 2017; **139**: 3336–9.
34. Zhang H, Hwang S and Wang M *et al.* Single atomic iron catalysts for oxygen reduction in acidic media: particle size control and thermal activation. *J Am Chem Soc* 2017; **139**: 14143–9.
35. Ma XL, Liu JC and Xiao H *et al.* Surface single-cluster catalyst for N<sub>2</sub>-to-NH<sub>3</sub> thermal conversion. *J Am Chem Soc* 2018; **140**: 46–9.
36. Zhang W and Zheng W. Single atom excels as the smallest functional material. *Adv Funct Mater* 2016; **26**: 2988–93.
37. Wang D and Astruc D. The golden age of transfer hydrogenation. *Chem Rev* 2015; **115**: 6621–86.
38. Zhang X, Sun Z and Wang B *et al.* C–C coupling on single-atom-based heterogeneous catalyst. *J Am Chem Soc* 2018; **140**: 954–62.
39. Guo X, Fang G and Li G *et al.* Direct, nonoxidative conversion of methane to ethylene, aromatics, and hydrogen. *Science* 2014; **344**: 616–9.
40. Lang R, Li T and Matsumura D *et al.* Hydroformylation of olefins by a rhodium single-atom catalyst with activity comparable to RhCl(PPh<sub>3</sub>)<sub>3</sub>. *Angew Chem Int Ed* 2016; **55**: 16054–8.
41. Fei H, Dong J and Arellano-Jimenez MJ *et al.* Atomic cobalt on nitrogen-doped graphene for hydrogen generation. *Nat Commun* 2015; **6**: 8668–75.
42. Liang S, Hao C and Shi Y. The power of single-atom catalysis. *ChemCatChem* 2015; **7**: 2559–67.
43. Chen Y, Huang Z and Ma Z *et al.* Fabrication, characterization, and stability of supported single-atom catalysts. *Catal Sci Technol* 2017; **7**: 4250–8.
44. Fei H, Dong J and Feng Y *et al.* General synthesis and definitive structural identification of Mn<sub>4</sub>C<sub>4</sub> single-atom catalysts with tunable electrocatalytic activities. *Nat Catal* 2018; **1**: 63–72.
45. Xu H, Cheng D and Cao D *et al.* A universal principle for a rational design of single-atom electrocatalysts. *Nat Catal* 2018; doi: 10.1038/s41929-018-0063-z.
46. Qiao B, Wang A and Yang X *et al.* Single-atom catalysis of CO oxidation using Pt<sub>1</sub>/FeO<sub>x</sub>. *Nat Chem* 2011; **3**: 634–41.
47. Yang S and Lee H. Atomically dispersed platinum on gold nano-octahedra with high catalytic activity on formic acid oxidation. *ACS Catal* 2013; **3**: 437–43.
48. Kyriakou G, Boucher MB and Jewell AD *et al.* Isolated metal atom geometries as a strategy for selective heterogeneous hydrogenations. *Science* 2012; **335**: 1209–12.
49. Shi Y, Zhao C and Wei H *et al.* Single-atom catalysis in mesoporous photovoltaics: the principle of utility maximization. *Adv Mater* 2014; **26**: 8147–53.
50. Lucci FR, Liu J and Marcinkowski MD *et al.* Selective hydrogenation of 1,3-butadiene on platinum-copper alloys at the single-atom limit. *Nat Commun* 2015; **6**: 8550–7.
51. Serna P and Gates BC. Molecular metal catalysts on supports: organometallic chemistry meets surface science. *Acc Chem Res* 2014; **47**: 2612–20.
52. Thomas JM. The concept, reality and utility of single-site heterogeneous catalysts (SSHCs). *Phys Chem Chem Phys* 2014; **16**: 7647–61.
53. Choi CH, Kim M and Kwon HC *et al.* Tuning selectivity of electrochemical reactions by atomically dispersed platinum catalyst. *Nat Commun* 2016; **7**: 10922–30.
54. Zhang H, Watanabe T and Okumura M *et al.* Catalytically highly active top gold atom on palladium nanocluster. *Nat Mater* 2012; **11**: 49–52.
55. Wang X, Maeda K and Thomas A *et al.* A metal-free polymeric photocatalyst for hydrogen production from water under visible light. *Nat Mater* 2009; **8**: 76–80.
56. Li X, Bi W and Chen M *et al.* Exclusive Ni-N<sub>4</sub> sites realize near-unity CO selectivity for electrochemical CO<sub>2</sub> reduction. *J Am Chem Soc* 2017; **139**: 14889–92.
57. Yin P, Yao T and Wu Y *et al.* Single cobalt atoms with precise N-coordination as superior oxygen reduction reaction catalysts. *Angew Chem Int Ed* 2016; **55**: 10800–5.
58. Chung HT, Cullen DA and Higgins D *et al.* Direct atomic-level insight into the active sites of a high-performance PGM-free ORR catalyst. *Science* 2017; **357**: 479–84.
59. Wu Y, Wang D and Li Y. Understanding of the major reactions in solution synthesis of functional nanomaterials. *Sci China Mater* 2016; **59**: 938–96.
60. Wei H, Liu X and Wang A *et al.* FeO<sub>x</sub>-supported platinum single-atom and pseudo-single-atom catalysts for chemoselective hydrogenation of functionalized nitroarenes. *Nat Commun* 2014; **5**: 5634–41.
61. Lin J, Wang A and Qiao B *et al.* Remarkable performance of Ir<sub>1</sub>/FeO<sub>x</sub> single-atom catalyst in water gas shift reaction. *J Am Chem Soc* 2013; **135**: 15314–7.
62. Zhang C, Oliaee SN and Hwang SY *et al.* A generic wet impregnation method for preparing substrate-supported platinum group metal and alloy nanoparticles with controlled particle morphology. *Nano Lett* 2016; **16**: 164–9.
63. Iqbal S, Kondrat SA and Jones DR *et al.* Ruthenium nanoparticles supported on carbon: an active catalyst for the hydrogenation of lactic acid to 1,2-propanediol. *ACS Catal* 2015; **5**: 5047–59.
64. Moses-DeBusk M, Yoon M and Allard LF *et al.* CO oxidation on supported single Pt atoms: experimental and ab initio density functional studies of CO interaction with Pt atom on  $\theta$ -Al<sub>2</sub>O<sub>3</sub>(010) surface. *J Am Chem Soc* 2013; **135**: 12634–45.
65. Narula CK, Allard LF and Stocks GM *et al.* Remarkable NO oxidation on single supported platinum atoms. *Sci Rep* 2015; **4**: 7238–43.
66. Wang L, Zhang S and Zhu Y *et al.* Catalysis and in situ studies of Rh<sub>1</sub>/Co<sub>3</sub>O<sub>4</sub> nanorods in reduction of NO with H<sub>2</sub>. *ACS Catal* 2013; **3**: 1011–9.
67. Gu XK, Qiao B and Huang CQ *et al.* Supported single Pt<sub>1</sub>/Au<sub>1</sub> atoms for methanol steam reforming. *ACS Catal* 2014; **4**: 3886–90.
68. Nie L, Mei D and Xiong H *et al.* Activation of surface lattice oxygen in single-atom Pt/CeO<sub>2</sub> for low-temperature CO oxidation. *Science* 2017; **358**: 1419–23.
69. Zhang Z, Zhu Y and Asakura H *et al.* Thermally stable single atom Pt/m-Al<sub>2</sub>O<sub>3</sub> for selective hydrogenation and CO oxidation. *Nat Commun* 2017; **8**: 16100–9.
70. Moliner M, Gabay JE and Kliewer CE *et al.* Reversible transformation of Pt nanoparticles into single atoms inside high-silica chabazite zeolite. *J Am Chem Soc* 2016; **138**: 15743–50.
71. Lu J, Aydin C and Browning ND *et al.* Imaging isolated gold atom catalytic sites in zeolite NaY. *Angew Chem Int Ed* 2012; **51**: 5842–6.

72. Yang M, Li S and Wang Y *et al.* Catalytically active Au-O(OH)<sub>x</sub> species stabilized by alkali ions on zeolites and mesoporous oxides. *Science* 2014; **346**: 1498–501.
73. Yang S, Kim J and Tak YJ *et al.* Single-atom catalyst of platinum supported on titanium nitride for selective electrochemical reactions. *Angew Chem Int Ed* 2016; **55**: 2058–62.
74. Chen Z, Zhang Q and Chen W *et al.* Single-site Au<sup>1</sup> catalyst for silane oxidation with water. *Adv Mater* 2018; **30**: 1704720–7.
75. Lin L, Zhou W and Gao R *et al.* Low-temperature hydrogen production from water and methanol using Pt/ $\alpha$ -MoC catalysts. *Nature* 2017; **544**: 80–3.
76. Wang X, Chen W and Zhang L *et al.* Uncoordinated amine groups of metal-organic frameworks to anchor single Ru sites as chemoselective catalysts toward the hydrogenation of quinoline. *J Am Chem Soc* 2017; **139**: 9419–22.
77. Tjoa V, Chua J and Pramana SS *et al.* Facile photochemical synthesis of graphene-Pt nanoparticle composite for counter electrode in dye sensitized solar cell. *ACS Appl Mater Interfaces* 2012; **4**: 3447–52.
78. Xu D, Diao P and Jin T *et al.* Iridium oxide nanoparticles and iridium/iridium oxide nanocomposites: photochemical fabrication and application in catalytic reduction of 4-nitrophenol. *ACS Appl Mater Interfaces* 2015; **7**: 16738–49.
79. Zhan WW, Zhu QL and Dang S *et al.* Synthesis of highly active sub-nanometer Pt@Rh core-shell nanocatalyst via a photochemical route: porous titania nanoplates as a superior photoactive support. *Small* 2017; **13**: 1603879–84.
80. Fageria P, Uppala S and Nazir R *et al.* Synthesis of monometallic (Au and Pd) and bimetallic (AuPd) nanoparticles using carbon nitride (C<sub>3</sub>N<sub>4</sub>) quantum dots via the photochemical route for nitrophenol reduction. *Langmuir* 2016; **32**: 10054–64.
81. Yang M, Allard LF and Flytzani-Stephanopoulos M. Atomically dispersed Au-(OH)<sub>x</sub> species bound on titania catalyze the low-temperature water-gas shift reaction. *J Am Chem Soc* 2013; **135**: 3768–71.
82. Liu P, Zhao Y and Qin R *et al.* Photochemical route for synthesizing atomically dispersed palladium catalysts. *Science* 2016; **352**: 797–800.
83. Wei H, Huang K and Wang D *et al.* Iced photochemical reduction to synthesize atomically dispersed metals by suppressing nanocrystal growth. *Nat Commun* 2017; **8**: 1490–7.
84. Deng D, Chen X and Yu L *et al.* A single iron site confined in a graphene matrix for the catalytic oxidation of benzene at room temperature. *Sci Adv* 2015; **1**: e1500462.
85. O'Neill BJ, Jackson DHK and Lee J *et al.* Catalyst design with atomic layer deposition. *ACS Catal* 2015; **5**: 1804–25.
86. Sun S, Zhang G and Gauquelin N *et al.* Single-atom catalysis using Pt/graphene achieved through atomic layer deposition. *Sci Rep* 2013; **3**: 1775–83.
87. Yan H, Cheng H and Yi H *et al.* Single-atom Pd<sub>1</sub>/graphene catalyst achieved by atomic layer deposition: remarkable performance in selective hydrogenation of 1,3-butadiene. *J Am Chem Soc* 2015; **137**: 10484–7.
88. Cheng N, Stambula S and Wang D *et al.* Platinum single-atom and cluster catalysis of the hydrogen evolution reaction. *Nat Commun* 2016; **7**: 13638–46.
89. Ren Q, Wang H and Lu XF *et al.* Recent progress on MOF-derived heteroatom-doped carbon-based electrocatalysts for oxygen reduction reaction. *Adv Sci* 2018; **5**: 1700515–35.
90. Marcinkowski MD, Darby MT and Liu J *et al.* Pt/Cu single-atom alloys as coke-resistant catalysts for efficient C–H activation. *Nat Chem* 2018; doi: 10.1038/NCHEM.2915.
91. Wu Y, Wang D and Zhou G *et al.* Sophisticated construction of Au islands on Pt-Ni: an ideal trimetallic nanoframe catalyst. *J Am Chem Soc* 2014; **136**: 11594–7.
92. Qin R, Liu P and Fu G *et al.* Strategies for stabilizing atomically dispersed metal catalysts. *Small Methods* 2018; **2**: 1700286–306.
93. Jiao L, Wang Y and Jiang HL *et al.* Metal-organic frameworks as platforms for catalytic applications. *Adv Mater* 2017; doi: 10.1002/adma.201703663.
94. Liang Z, Qu C and Guo W *et al.* Pristine metal-organic frameworks and their composites for energy storage and conversion. *Adv Mater* 2017; doi: 10.1002/adma.201702891.
95. Zhao C, Dai X and Yao T *et al.* Ionic exchange of metal-organic frameworks to access single nickel sites for efficient electroreduction of CO<sub>2</sub>. *J Am Chem Soc* 2017; **139**: 8078–81.
96. Wang X, Chen Z and Zhao X *et al.* Regulation of coordination number over single Co sites triggers the efficient electroreduction of CO<sub>2</sub>. *Angew Chem Int Ed* 2018; **57**:1–6.
97. Chen Y, Ji S and Wang Y *et al.* Isolated single iron atoms anchored on N-doped porous carbon as an efficient electrocatalyst for the oxygen reduction reaction. *Angew Chem Int Ed* 2017; **56**: 6937–41.
98. Ji S, Chen Y and Fu Q *et al.* Confined pyrolysis within metal-organic frameworks to form uniform Ru<sub>3</sub> clusters for efficient oxidation of alcohols. *J Am Chem Soc* 2017; **139**: 9795–8.
99. Han Y, Wang YG and Chen W *et al.* Hollow N-doped carbon spheres with isolated cobalt single atomic sites: superior electrocatalysts for oxygen reduction. *J Am Chem Soc* 2017; **139**: 17269–72.
100. Chen W, Pei J and He CT *et al.* Rational design of single molybdenum atoms anchored on N-doped carbon for effective hydrogen evolution reaction. *Angew Chem Int Ed* 2017; **56**: 16086–90.
101. Liu W, Zhang L and Yan W *et al.* Single-atom dispersed Co–N–C catalyst: structure identification and performance for hydrogenative coupling of nitroarenes. *Chem Sci* 2016; **7**: 5758–64.
102. Liu W, Zhang L and Liu X *et al.* Discriminating catalytically active FeNx species of atomically dispersed Fe–N–C catalyst for selective oxidation of the C–H bond. *J Am Chem Soc* 2017; **139**: 10790–8.
103. Zhang M, Wang YG and Chen W *et al.* Metal (Hydr)oxides@Polymer core-shell strategy to metal single-atom materials. *J Am Chem Soc* 2017; **139**: 10976–9.
104. Wang J, Huang Z and Liu W *et al.* Design of N-coordinated dual-metal sites: a stable and active Pt-free catalyst for acidic oxygen reduction reaction. *J Am Chem Soc* 2017; **139**: 17281–4.
105. Jones J, Xiong H and DeLaRiva AT *et al.* Thermally stable single-atom platinum-on-ceria catalysts via atom trapping. *Science* 2016; **353**: 150–4.

Special Topic: Single-Atom Catalysts

## Single-atom catalysis: a new field that learns from tradition

By Philip Ball

Much of industrial chemical processing (in the petrochemicals industry, for example), and a great deal of laboratory chemical synthesis, involves catalysts that both lower the energy barrier to reaction and may help steer a reaction along a particular path. Traditionally, catalysts have come in two classes: heterogeneous, typically meaning that the catalyst is an extended solid; and homogeneous, where the catalyst is a small molecule that shares a solvent with the reactants. In heterogeneous catalysis, the reaction generally takes place on a surface, involving molecules attached there by covalent bonds. Homogeneous catalysts are often organometallic compounds, in which a metal atom or small cluster of atoms supplies the active site for reaction.

In recent years, these distinctions have become somewhat blurred thanks to the advent of single-atom catalysis, where the catalytic site consists of a single atom (as in many homogeneous catalysts) attached to or embedded in a surface. The emergence of this field might be regarded as the logical conclusion of the use of ‘supported metal clusters’—small metal particles of nanometer scale and below, containing perhaps hundreds, tens or just a few atoms. It has become clear that such clusters can sometimes provide greater product selectivity and activity than macro-sized particles or powders of the same metal, partly because the active sites might be atoms at particular locations (such as edges and corners) in the nanoscale particles. By reducing their scale down to the level of single atoms, one can optimize these properties. At the same time, the potential uniformity of the atoms’ environments makes such catalysts more amenable to rational design and modeling to understand mechanism.

This field represents an appealing blend of fundamental chemistry and physics—from the quantum-mechanical level upwards—and applied research aimed at producing many of the products vital to society, such as fuels and materials. Researchers in China have been strongly active in this field in recent years (see, for example, refs [1–5]). Jean-Marie Basset of the King Abdullah University of Science and Technology in Thuwal, Saudi Arabia, is one of the leading practitioners in the area, and National Science Review spoke to him about the development and prospects of the field.

**NSR:** When was it first appreciated that catalysis by supported metals could involve single atoms?

**Basset:** In work that my team and I published in 1998 [6] we discovered that when we fully characterize a platinum particle modified with tin deposited by the surface organometallic chemistry (SOMC) technique, we found that each Pt atoms is surrounded by tin atoms, and this increased the selectivity of the surface for catalysing dehydrogenation of isobutane to almost 100%. At that time we said that this increase in selectivity could be explained by a ‘site isolation effect’—that the important factor was that the platinum atoms were individually isolated.

At about the same time, we discovered that a single zirconium atom attached to a silica surface by a triple bond to a Si-O- group could achieve low-temperature hydrogenolysis (splitting of the carbon backbone using hydrogen) of alkanes. The method we used to prepare the lone Zr atoms started with an organometallic alkyl precursor, and created Zr atoms with a hydrogen attached [7]. Hydrogenolysis of alkane was a known reaction in heterogeneous catalysis (for example, on nickel particles) but here the temperature was much lower (close to room temperature) than in heterogeneous catalysis (above 200°C). Besides that, the mechanism could be unambiguously determined, and shown to occur on a single Zr atom—it was



Jean-Marie Basset, distinguished professor at King Abdullah University of Science and Technology, Saudi Arabia. (Courtesy of Prof. Basset)

no longer necessary to invoke any ‘ensemble effect’, a common notion in heterogeneous catalysis on small metal particles.

**NSR:** I understand that one of the difficulties with supported metal nanoparticles is that they are often inhomogeneous. Is one of the attractions of single-atom catalysis that homogeneity becomes possible again?

**Basset:** That’s the right question, and the answer is yes. With single atoms, we can have a situation where all the active

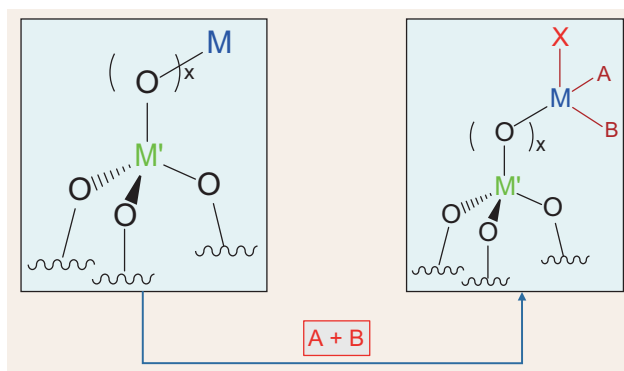
sites are almost identical. The discovery of low-temperature hydrogenolysis of alkanes was part of the origin of surface organometallic chemistry. Since then, a huge variety of metal atoms have been attached homogeneously on the surfaces of oxides, with the same structure for each atom. SOMC is not particularly familiar within the heterogeneous catalysis community, but has led to the discovery of new catalytic reactions such as Ziegler-Natta depolymerization [8], alkane metathesis [9], non-oxidative coupling of methane [10] and cyclo-alkane metathesis [11]. Furthermore it has improved the activity, selectivity or lifetime of known reactions such as alkene metathesis and epoxidation, and imine metathesis. In these cases, the majority if not all of the active sites are identical. Because the structure of these grafted atoms are known at the atomic and molecular level, we can use the familiar concepts of molecular chemistry (organic, organometallic, coordination chemistry) to explain how bonds can be broken and reformed. The reactivity of surface organometallic fragments (SOMF) or surface coordination fragments (SCF) is pivotal to the outcomes.

**NSR:** In your own work, you have promoted the idea of SOMC, which seems to aim at applying the concepts of homogeneous organometallic chemistry to surface-bound species. Can you explain more about what this entails? What advantages does a surface provide, relative to homogeneous catalysts?

**Basset:** As I said earlier, SOMC is not really an extension of homogeneous catalysis. Rather, it is a new discipline of heterogeneous catalysis. It uses organometallic compounds to prepare well-defined heterogeneous catalysts in which a single atom is linked to a surface. It is quite distinct from homogeneous catalysis, in which typically the catalysts are metal atoms with ligands attached, because here the 'ligand' is a rigid surface, which creates completely different reactivity. The concept is actually much closer to heterogeneous catalysis, because it is like a supported metal on an oxide. Or one might better say, it is closest to the concept of surface-active catalysts (SAC).

You can see the strong difference with classical homogeneous catalysis, and the consequent benefits, in the way that many new reactions which do not exist in homogeneous catalysis (or for that matter in heterogeneous catalysis) can be achieved in SOMC.

Here's a simple way of picturing the comparison between a heterogeneous SOMF used in SOMC and a surface-active catalyst:



The comparison between SOMF and SAC.

The image on the left shows a SAC where a metal atom  $M'$  is linked to an oxide. On the right is a SOMF. In SOMC we have a 'preconceived' mechanism, and the fragments are just possible intermediates in the catalytic cycle. In SAC it is intuitively assumed that the metal will, under the influence of the reagents  $A$  and  $B$ , adopt the right coordination sphere. But in SOMC the fragments  $A$  and  $B$  are components of the SOMF, already attached to the metal atom before grafting. Another difference between SOMC and SAC is the presence of a predetermined spectator ligand  $X$  in the former to tune the coordination number, the electron density and ultimately the steric control around the metal atom. The concepts of molecular chemistry are used to determine  $A$ ,  $B$  and  $X$ , as in homogeneous catalysis—but the surface acts as a ligand that brings rigidity, pincer properties, acid-base and redox properties.

**NSR:** How easy is it to prepare and characterize well-defined catalysts of this type? How much do we know, and not know, about the precise environment of the metal atoms?

**Basset:** The preparation of SOMC is becoming ever easier. We have improved the methods. At the beginning it was necessary to use fragile organometallic components under a well controlled atmosphere, but now there are techniques to adsorb simple coordination complexes on oxides, as was done in many cases in classical heterogeneous catalysis (for example,  $WCl_6$  and  $TiCl_4$  on silica) and then to alkylate (say) *in situ* to achieve the right coordination sphere.

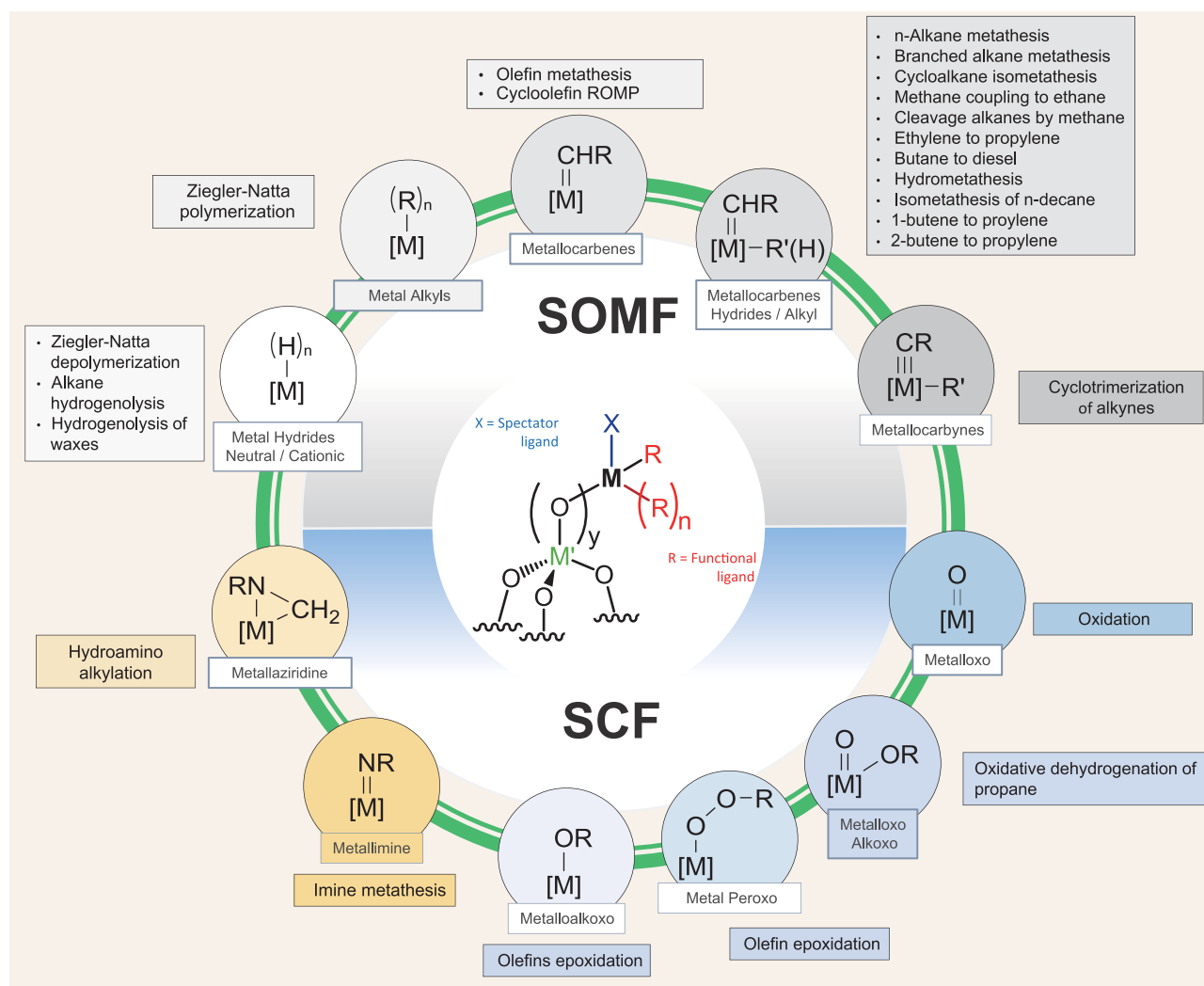
The characterization is becoming easier, because the sites are mostly identical. The classical techniques can be applied, such as surface microanalysis, IR and UV spectroscopy, extended X-ray absorption fine structure spectroscopy (EXAFS), X-ray absorption near-edge structure (XANES) and density functional theory for calculations. The most useful method is solid-state NMR, which has played a decisive role in identifying the SOMFs with the accuracy of molecular chemistry. When we write a formula on a surface, it is no longer a cartoon but is very close to the real structure of most of the sites.

**NSR:** That single metal atoms can be important and versatile catalytic centers is of course a well-established idea in bioinorganic chemistry too. Is there any overlap with this field in terms of an understanding of the mechanisms involved?

**Basset:** SOMC can let us create well-defined SOMFs, thanks to the conceptual overlap with organometallic chemistry. But it can also lead to well-defined surface coordination compounds thanks to the overlap with bioinorganic chemistry, inorganic and coordination chemistry. This is the direction in which we are currently obtaining the most spectacular results—unpublished as yet!

**NSR:** What kinds of reactions can be catalysed by these surface organometallic single-atom systems? What are some of the most useful and/or important?

**Basset:** See the scheme below. Some recent advances include using  $CO_2$  to make cyclic carbonates, alkane metathesis, converting methane to ethane and hydrogen and to aromatics, oxidation chemistry of epoxides and aldehydes, and direct transformation of ethylene to propylene. The case of alkane metathesis is particularly important. When we discovered this reaction the

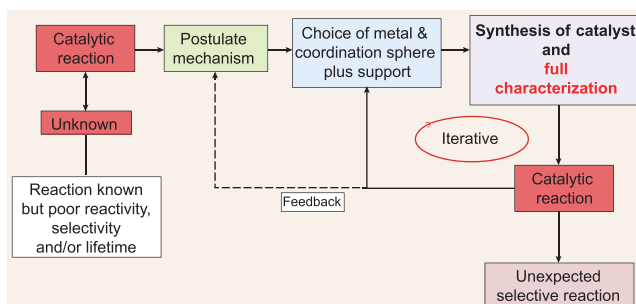


Reactions catalysed by surface organometallic single-atom systems.

turnover number [number of times the catalyst can repeat the reaction] was 60 using hydrogenated tantalum atoms. Now we can reach turnover numbers of 20 000 with bimetallic systems (tungsten/titanium) [12]. Our target is 100 000, which is what we need for such a process to become commercial.

**NSR:** How predictable and amenable to rational design are these systems? Do we have the computational methods that we need?

**Basset:** We use the scheme below to do ‘catalysis by design’ and discover new reactions or to improve existing ones. The most



Catalysis by design.

important aspect is to transfer the elementary steps known in organic, organometallic and coordination chemistry to write a priori a catalytic cycle. Based on these elementary steps, we choose the metal, the support and the ligands X, A and B as mentioned earlier, and fully characterize the coordination sphere.

**NSR:** How did your own interest in this field evolve?

**Basset:** My first experiment in this area was to chemisorb an iron carbonyl complex  $Fe_3(CO)_{12}$  on alumina in order to make iron nanoparticles. We were surprised to find formation of the species  $[HFe_3(CO)_{11}]^- Al^+$  [13]. This was a shock for us. It seemed that a new kind of chemistry was emerging from the overlap between organometallic and surface chemistry. We progressively developed this chemistry in many directions, with many metals and diverse supports: porous, non-porous, acidic, redox and so on. Then we discovered that this field could also apply to nanoparticles of zero-valent metals and we adapted the tools to characterize such materials.

The first catalytic reaction was also a second shock: the low-temperature hydrogenolysis of alkanes with atomic Zr on hydrogenated silica, which I mentioned earlier. This opened the way to predict Ziegler-Natta depolymerization. Moving from

“

This area has a fantastic future because it allows us to get out of the ‘black box’.

—Jean-Marie Basset

”

Zr to Ta, we discovered how to conduct metathesis of alkanes [7] and plenty of new reactions too. Density functional theory was a crucial tool to understand what was going on, in particular using the tools developed by Luigi Cavallo here at KAUST. The strategy to develop new catalytic reactions slowly emerged, and the concepts are still evolving as we discover new catalytic reactions.

**NSR:** There seems to be a strong interest in this topic in China. From where do you think the most important results are emerging in China? Do you feel they are building on a strong tradition of inorganic chemistry in China?

**Basset:** Catalysis requires diversified approaches. I’m not sure that the SOMC concept has yet been so much explored in China. But Xuxu Wang from Fuzhou, one of my former students in Lyon, has made big impact in photocatalysis via SOMC. Nevertheless, there have been some great advances in catalysis in China in the last 20 years or so. Many impressive homogeneous and heterogeneous systems have been developed: heterogeneous by Tao Zhang, Can Li, Xinhe Bao, Yuhuan Sun, Wei Wei and others; homogeneous by Xiaoming Feng, Kuiling Ding, Zhenfeng Xi, Qilin Zhou, Zhangjie Shi, Aiwen Lei, Guosheng Liu, Shuli You, Zhixiang Yu and many others. However, I’d like to see more emphasis given to fundamental understanding at the molecular level. For example, studies on the reactivities of organometallic species seem less popular, but they build the basis for catalytic applications. There is, however, very good work in this area from people like Zuowei Xie, Shaowu Wang, Yaofeng Chen, Ming-Hua Zeng and many others.

**NSR:** Where do you feel the field is now heading? Are there potential types of analytical/characterization techniques that would make a big difference to our fundamental understanding of the processes involved?

**Basset:** I feel that this area has a fantastic future because it allows us to get out of the so-called ‘black box’. This is due to the fact that we have the conceptual and experimental tools to predict any reaction, just by transferring concepts from molecular chemistry to surfaces. The science of molecular chemistry, whether it is inorganic, organometallic or organic, teaches us how to create or cleave bonds. Then the choice of metals, ligands, surfaces and so on is becoming more understood. We have some spectacular

new results that will explain my optimism when we publish them in the near future.

**NSR:** Do you think that this is one area of chemistry in which the links between fundamental research and industrial applications are particularly strong?

**Basset:** I believe that CO<sub>2</sub> chemistry, photocatalytic dissociation of water, CH<sub>4</sub> and alkane chemistry, and oxidation are the areas where industry will benefit most from SOMC.

**NSR:** Who were your own key influences in your early career, and why?

**Basset:** When I was in France, I recruited Yves Chauvin when he retired from the French Petroleum Institute [where he worked from 1960 to 1995]. Nine years later he was awarded the Nobel Prize in chemistry. Not only was he a friend but I learned a lot from his broad knowledge of homogeneous catalysis and industrial processes. I want to mention his strong influence on me, and I will always be thankful to him: he was a modest, curious but fantastic scientist.

Besides Yves Chauvin, I would like to mention Renato Ugo from Milan, who in the 1980s was developing analogies between homogeneous and heterogeneous catalysis; Paolo Chini, also from Milan, who made me dream about large clusters; Bob Grubbs from Caltech for his work on olefin metathesis; Wolfgang Herrmann for collaboration on SOMC; and all the community in homogeneous and heterogeneous catalysis, from whom I have learnt a lot in two disciplines that have tended to develop their own concepts separately.

Philip Ball writes for NSR from London.

## REFERENCES

1. Qiao B, Wang A and Yang X *et al.* *Nat Chem* 2011; **3**: 634–41.
2. Wang X, Chen Z and Zhao X *et al.* *Angew Chem Int Ed* 2018; **57**: 1944–8.
3. Guo X, Fang G and Li G *et al.* *Science* 2014; **344**: 616–9.
4. Liu P, Zhao Y and Qin R *et al.* *Science* 2016; **352**: 797–800.
5. Cao Y, Chen S and Luo Q *et al.* *Angew Chem Int Ed* 2017; **56**: 12191–6.
6. Humblot F, Candy JP and Peltier FL *et al.* *J Catal* 1998; **179**: 459–68.
7. Corker J, Lefebvre F and Lecuyer C *et al.* *Science* 1996; **271**: 966–9.
8. Dufaud V and Basset JM. *Angew Chem Int Ed* 1998; **37**: 806–10.
9. Vidal VV, Theolier A and Thivolle-Cazat J *et al.* *Science* 1997; **276**: 99–102.
10. Soulivong D, Norsic S and Taoufik M *et al.* *J Am Chem Soc* 2008; **130**: 5044–5.
11. Riache N, Callens E and Samantaray MK *et al.* *Chem Eur J* 2014; **20**: 15089–94.
12. Samantaray MK, Kavitate S and Morlanés N *et al.* *J Am Chem Soc* 2017; **139**: 3522–7.
13. Hugues F, Basset JM and Taarit YB *et al.* *J Am Chem Soc* 1982; **104**: 7020–4.